VOID FRACTION MEASUREMENT IN A TWO-PHASE FLOW SYSTEM WITH IMPEDANCE PROBE TECHNIQUE

A THESIS SUBMITTED TO
THE GRADUATE SCHOOL OF NATURAL AND APPLIED SCIENCES
OF
THE MIDDLE EAST TECHNICAL UNIVERSITY

BY

TUFAN HOSANOĞLU

IN PARTIAL FULFILLMENT OF THE REQUIREMENTS FOR THE DEGREE OF
MASTER OF SCIENCE
IN
THE DEPARTMENT OF MECHANICAL ENGINEERING

JANUARY 2002

Approval of the Graduate School of Natural and Applied Sciences

Prof. Dr. Tayfur ÖZTÜRK
Director

I certify that this thesis satisfies all the requirements as a thesis for the degree of Master of Science.

Prof. Dr. Ilres SÖYLEMEZ
Head of Department

This is to certify that we have read this thesis and that in our opinion it is fully adequate, in scope and quality, as a thesis for the degree of Master of Science.

Prof. Dr. Orhan YEŞİN
Supervisor

Examining Committee Members

Chairperson : Prof. Dr. Ediz PAYKOÇ

Supervisor : Prof. Dr. Orhan YEŞİN

Member : Prof. Dr. Cahit ERALP

Member : Prof. Dr. Rüyal ERGÜL (EE)

Member : Dr. Abdullah ULAŞ

ABSTRACT

VOID FRACTION MEASUREMENT IN A TWO-PHASE FLOW SYSTEM WITH IMPEDANCE PROBE TECHNIQUE

Hosanoğlu, Tufan

M.S., Department of Mechanical Engineering

Supervisor: Prof. Dr. Orhan Yeşin

January 2002, 183 pages

The objective of this experimental study is to measure the void fraction of a two-phase flow system with impedance probe technique. A Two-Phase Flow Test facility was constructed in the Mechanical Engineering Department of Middle East Technical University for a Joint Research Project.

Impedance probe technique which has a potential advantage from an economical standpoint in comparison to the other void fraction measurement techniques, is based on the significant difference in the electrical properties such as capacitance and resistance, between liquid and gas phases.

To relate the changes in capacitance and resistance of two-phase mixture flowing between the probe's electrodes to the void fraction, several prototypes of analog signal conditioner circuit for each impedance probe were designed and manufactured which is necessary for PC based data acquisition system. Ultimately, depending on the characteristics of each impedance probe, the

satisfactory version of analog signal conditioner circuit was developed and manufactured.

Some parameters affecting the measurement of void fraction namely water temperature, moisture, flow regime, and also the pre-resistance value and frequency of the analog signal conditioner circuit are investigated.

In the calibration tests of impedance probes, different void fraction values, between 0 and 1, based on homogenous two-phase flow model, are obtained by changing the ratio of volume flow rates of water and air. Five impedance probes which have two different inner diameters (25.4 mm and 34.5 mm) are calibrated at their own inclination (0^o, 180^o, 216^o, 288^o, 324^o).

During calibration tests of the impedance probes, various flow regimes which change by void fraction were observed and recorded with video camera.

At the end of the calibration tests of the probes, a graph of non-dimensional voltage output of analog signal conditioner circuit versus void fraction values was plotted for each impedance probe.

Calibration tests cover a range of water volume flow rate of 0 to 0.00183 m^3/s, air volume flow rate of 0 to 0.00185 m^3/s, water temperature of 21.2 to 25.6 ^oC, air temperature of 21.5 to 26 ^oC.

Keywords: Two-phase Flow, Void Fraction, Volume Flow Rate, Impedance Probe, Homogenous Two-Phase Flow Model, Analog Signal Conditioner Circuit.

ÖZ

İKİ FAZLI AKIŞ SİSTEMİNDE HAVA HACİM ORANININ EMPEDANS PROB TEKNİĞİYLE ÖLÇÜLMESİ

Hosanoğlu, Tufan
Yüksek Lisans, Makina Mühendisliği Bölümü
Tez Yöneticisi: Prof. Dr. Orhan Yeşin

Ocak 2002, 183 sayfa

Bir Ortak Araştırma Projesi için, Ortadoğu Teknik Üniversitesi Makina Mühendisliği Bölümünde kurulmuş olan İki Fazlı Akış Test Düzeneğinde yapılan bu deneysel çalışmanın amacı, iki fazlı akış sisteminde empedans prob tekniğiyle hava hacim oranının ölçülmesidir.

Diğer hava hacim oranı ölçme tekniklerine göre ekonomik bakımdan avantajlı olan empedans prob tekniği, iki faz arasındaki kapasite ve direnç gibi elektriksel özelliklerdeki önemli farklılıklara dayanır.

Prob electrodları arasında akan iki fazlı karışımın kapasite ve direnç değişimleriyle hava hacim oranı arasında bağlantı kurmak amacıyla; bilgisayar tabanlı veri toplama sistemi için gerekli olan empedans probların analog sinyal işleme devreleri için birkaç prototip tasarlandı. Sonunda, herbir empedans probun karakteristik özelliklerine uygun olan prototip analog sinyal işleme devresi geliştirildi ve üretildi.

Su sıcaklığı, nem, akış rejimi, analog sinyal işleme devresine ait öndirenç ve frekans gibi hava hacim oranı ölçümlerine etki eden bazı parametreler incelendi.

Empedans problarının kalibrasyon testlerinde, homojen iki fazlı akış modeline göre, 0 ile 1 arasındaki değişik hava hacim oranları; suyun ve havanın farklı hacimsel debi oranlarında karıştırılmasıyla elde edildi. İki farklı iç çaptaki (25.4 mm ve 34.5 mm) beş empedans prob kendi açısal pozisyonlarında kalibre edildi (0^o, 180^o, 216^o, 288^o, 324^o).

Probların kalibrasyon testleri esnasında, hava hacim oranındaki farklılıklardan dolayı, farklı akış rejimleri gözlendi ve video kamerayla kayıt edildi.

Prob calibrasyon testlerinin sonucunda; herbir empedans probu için, hava hacim oranı değerlerine karşılık gelen analog sinyal işleme devresinin boyutsuz voltaj çıkış değerlerinin grafiği çizildi.

Kalibrasyon test aralığı, 0-0.00183 m^3/s arasındaki suyun hacimsel debisini, 0-0.00185 m^3/s arasındaki havanın hacimsel debisini, 21.1-25.6 ^oC arasındaki su sıcaklıklarını, 21.5-26 ^oC arasındaki hava sıcaklıklarını kapsamaktadır.

Anahtar Kelimeler: İki Fazlı Akış, Hava Hacim Oranı, Hacimsel Debi, Empedans Prob, Homojen İki Fazlı Akış Modeli, Analog Sinyal İşleme Devresi.

ACKNOWLEDGEMENTS

I would like to express my sincere appreciation to my supervisor Prof. Dr. Orhan Yeşin for his invaluable guidance and insight throughout this study. Thanks go to my colleague Mr. Barış Kaya for his intelligent suggestions and worthy contributions, to Mr. Okan Demirel for his invaluable comments and ideas and to Mr. İbrahim Özdemir for his skilful technical assistance. I also would like to thank to Atomic Energy of Canada Limited and Turkish Atomic Energy Authority which supplied most of the equipment of the experimental test facility. Finally I would like to thank to my family for their lovely support during my whole life.

TABLE OF CONTENTS

LIST OF TABLES

TABLE

LIST OF FIGURES

FIGURE

NOMENCLATURE

A	Area (m^2)
C	Capacitance (F)
d	Diameter, Separation (m)
D	Diode
DP	Dip-Switch
f	Excitation Frequency (Hz)
G	Conductance (S)
I	Total Current Flowing in the Circuit (A)
IC	Integrated Circuit
K	Conductivity (μS/cm)
m	Mass (kg)
$\dot{m}$	Total Mass Flow Rate of Two-phase Mixture (kg/s)
P	Potentiometer
Q	Volume Flow Rate of Mixture (m^3/s)
Q_A	Volume Flow Rate of Air (m^3/s)
Q_W	Volume Flow Rate of Water (m^3/s)
r	Radius (m)
R	Resistance (Ω)
R_m	Internal Resistance of Measuring Instrument(Ω)
R_p	Pre-resistance (Ω)
R^2	Correlation Coefficient
s	Slip Ratio
S	Standard Deviation

t	Time (s)
T	Period (s)
U	Average Velocity (m/s)
v	Specific Volume (m^3/kg)
V	Volume (m^3)
V	Voltage (V)
V_{exc}	Excitation Voltage (V)
V_{OW}	Voltage Output in all Water medium (V)
V_{OA}	Voltage Output in all Air medium (V)
V_Z	Voltage drop across the probe (V)
$\overline{V}$	Non-dimensional Voltage
V_m	Average Voltage (V)
w	Angular Velocity (radian/s)
x	Quality
X_C	Capacitive Reactance (Ω)
Z	Impedance (Ω)
Z_A	Probe Impedance in all Air Medium (Ω)
Z_W	Probe Impedance in all Water Medium (Ω)
Z_{probe}	Probe Impedance (Ω)
Z_T	Total Impedance (Ω)
α	Void Fraction
β	Volume Flow Ratio
ρ	Density (kg/m^3)
ρ_m	Mean Density (kg/m^3)
ε	Permittivity of Medium (F/m)
ε_o	Permittivity of Vacuum ($8.85*10^{-12}$ F/m)
ε_r	Relative Permittivity of Medium

Subscripts

g	gas
f	liquid

CHAPTER 1

INTRODUCTION

1.1 DEFINITION

Two-phase flow is apparent in a whole range of industrial applications. Systems involving gas-liquid flows are found widely in the process, chemical, petroleum industries and also in thermal and nuclear power plants.

In the process, chemical, petroleum and related industries, problems exist in the transport of gas-liquid mixtures in pipelines and also in the design of equipment such as boilers, condensers, distillation towers, absorption towers.

Void fraction is one of the fundamental properties necessary to describe the flow characteristics of a two-phase mixture.

The void fraction of a gas-liquid mixture is defined as;

$$\alpha = \frac{\text{volume of gas in mixture}}{\text{total volume of mixture}}$$

The measurement of void fraction is required in many engineering applications, such as in nuclear power plants, in heat transfer systems (heat exchanger etc.) and in studying the characteristics of two-phase flow.

In nuclear power plants, the coolant flowing around the fuel rod bundles of a pressurized water nuclear reactor may boil, thus creating two-phase flow. The vapour distribution in a nuclear reactor core determines its thermal behaviour under normal and off-normal operating conditions. A knowledge of vapour volume is needed for the determination of mean fluid density and acceleration for the establishment of two-phase flow frictional pressure drop correlations.

In heat transfer systems; for example in a heat exchanger, prediction of the void fraction as a function of the design and operating parameters of the heat exchanger (geometry, working pressure, fluid flow rate, flow pattern, thermodynamic and transport properties of two phase, etc.) is of considerable importance.

In any of these cases the analysis of fluid flow requires the prediction of the void fraction which is the key variable for calculating pressure losses, phase velocities, heat transfer rate and flow stability conditions.

1.2 VOID FRACTION MEASUREMENT TECHNIQUES

Most commonly used techniques for void fraction measurement are;

-Radiation Techniques

  γ, X, β, α Rays

  Neutron Moderation

-Ultrasonic Methods

-Optical Methods

-Photographic Methods

-Hot Wire or Hot Film Anemometer

-Quick Closing Valves

-Electrical Methods

-Capacitance Probes

-Conductance Probes

-Impedance Probes

Generally a radiation measurement system consists of a radioactive source (emitter), collimators, shielding materials and detectors. Emitters and detecting sensors may take the form of (1) a point emitting the rays radially in all directions, (2) a rod emitting radially from a line or (3) an array consisting of several point emitters in a row. Any combination of point (rod) array emitter with point/rod/array detector is possible.

From a source standpoint , only the X-ray system does not require a nuclear or radioisotopic source. X-rays are generated in a vacuum tube, where a high potential is applied between a target of a specific material and a heated filament. Nowadays, X-ray image forming techniques are being used in void fraction measurements. The advantage of using X-rays lies in the lack of bulky source and the repeatability and long term stability of the source length. The disadvantages lie in the short-term unsteadiness in the source, due to the alternating portion of applied voltage [1,2].

Gamma rays are obtained from nuclear disintegration, The degree of attenuation of γ-rays depends on the density of substance through which the rays travel. This means that for gas-liquid mixtures the attenuation is high, if only liquid is in the control volume under investigation, and it decreases with increasing gas content therefore with void fraction. It has, however, to be taken into account that the radiation is also attenuated in tube wall. The spheric waves originating from the γ source first hit lead plate in which a narrow slot or a small hole is placed. This forms thin, well-bundled rays which penetrate the two-phase flow channel. That lead plate is called collimator. Behind the flow channel

another collimator is placed, then rays enter into the detector. Special care has to be taken that during this movement the collimators and detector are always made exactly straight along one line because small deviations in the alignment may cause serious misreadings. The source strength is time-dependent. Thus, the half-life of the source material is an important consideration as the strength of the beam. The movement of the γ-rays perpendicular to the flow channel takes much time, therefore, several arrangements are proposed using more than one γ-ray penetrating the channel at the same time in different directions. The advantages of gamma sources over x-rays are principally in cost, short-term stability and simplicity. In addition, high-voltage supplies and regulating systems are not required [3,4].

Specifically, β-rays are really made up of a stream of electrons emitted at high energy from a radioisotope. The basic method of attenuation for electrons is different from that for photons. Attenuation of X-ray and γ ray is caused by photoelectric effects, where X-rays are completely absorbed by ejecting electrons from the absorbing material and Compton or recoil scattering, where only partial energy loss of a photon occurs with the electron ejection and a new photon of longer wavelength is emitted. There are two major advantages in using β-rays for void fraction measurements where complete absorption does not occur. First, the sensitivity is greater, in addition shielding is not a major obstacle, since β-rays are absorbed readily in most dense materials. However, a major disadvantage stems from the advantage of high sensitivity. That is, owing to the high attenuation rates, massive sources are required to obtain event rates at a test detector that would allow accurate transients to be measured [1].

Neutron moderation technique uses a radioactive neutron source and a neutron counter. Fast neutrons emitted from the source are slowed down by hydrogen nuclei in the water, forming a cloud whose density is related to the void fraction [1,5].

Mainly, γ or X-rays are widely used in void fraction measurement because of their stronger penetration ability compared to α or β rays. Generally, the non-invasive nature of radiation techniques in using a source and detector systems outside the pipes and tanks is particularly attractive. However, they are expensive and because of obvious dangers associated with using radiation sources, very strict safety regulations have to be satisfied when applying these techniques.

The principle of ultrasonic beam technique is based on that energy from an ultrasonic source located around the pipe is detected with the ultrasonic energy detector. There are eight different types of ultrasonic flow measurement principles. Two methods are possible with ultrasonic devices for void fraction measurements. The pulse echo method and transmission methods are used primarily for film thickness and void fraction measurements. Ultrasonic techniques have the inherent advantage of being a non-invasive technique but temperature compensation is essential because the velocity of ultrasound is particularly affected by temperature changes [6,7,8].

The optical methods rely on the principle that the intensity of light scattered by a particle depends on the intensity of the illuminating radiation, the diameter and refractive index of the particles, the wavelength of the light and the direction of illumination. Optical probe system theoretically gives an on-off signal corresponding to phase change due to the passage of an interface, the only requirement being a sufficient difference between the indices of refraction of the liquid and gaseous states. Depending upon the refractive indices of the surrounding material and of the probe material, transmitted light beam to the probe emerges from the probe or is reflected back. The light beams reflected back pass into the phototransistor that conducts the electric current according to the light intensity. In literature, generally three types of optical probe configurations are used. These are glass rod type, fiber bundle type and U-shaped fiber type [9,10].

Photographic methods have been employed extensively to give size and distribution of phase content in two-phase flow. For photographic methods to be applicable, the flow field must be illuminated. Two important considerations should be kept in mind when selecting the means of illumination; namely, the illumination intensity / particle size / velocity relationships and the angular variation of scattered light [11].

The principle of void fraction measurement by the hot wire and hot film anemometer technique is to monitor the different rates of heat dissipation from the probe in vapour and liquid phases. The fraction of time during which the probe detects the vapour phase can be considered as the local void fraction [12]. This technique has a rapid response and is expected to give good quantitative information on local vapour fraction.

Quick closing valves which are electrically triggered simultaneously, trap the two-phase fluid inside pipe between two valves and provide an exact void fraction measurement. This method may be used for calibrating the other methods. The main disadvantage of this technique is stopping fluid flow process [13].

The principle of a capacitance probe technique is based on the difference in the dielectric constant of two phases flowing between two electrodes. This method has the following advantages; it is the most economical technique and the electrodes may be external to the flow, it is applicable to fast transient phenomena (up to a few micro seconds), and it has a disadvantage that it is sensitive to the moisture and flow regime [14].

The principle of two-phase flow measurements by conductance probe is based upon the difference in electrical conductance between the gaseous and liquid phases. Electrical conductance is the reciprocal of electrical resistance. A potential difference is created between two electrodes immersed in a two-phase mixture; so that the electric current flow is directly proportional to the

conductance of fluid between the two electrodes. The changes in the electric current caused by the passage of different phases at or around the sensor tip is interpreted as a measure of void fraction. This method has the same advantages and disadvantages of those of capacitance probe technique [15].

The impedance probe measurement techniques is based on the significant difference in the electrical properties between two phases such as resistance and capacitance. The choice of excitation frequency of probes determines the dominance of one over the other [16].

1.3 SCOPE OF THESIS

The studies carried out in this thesis are part of a Joint Research Project which is being performed with the contributions of Middle East Technical University (METU), Turkish Atomic Energy Authority (TAEK), and Atomic Energy of Canada Limited (AECL).

Some information about CANDU-6 Header will be helpful to understand the goals of this project. CANDU-6 reactor is fuelled with natural uranium fuel that is distributed among 380 fuel channels. The fuel channels are housed in a cylindrical tank that contains cool heavy water (D_2O) moderator at low pressure. The CANDU Heat Transport System (HTS) circulates pressurized D_2O coolant through the fuel channels to remove the heat produced by fission. Two parallel HTS coolant loops are provided in a CANDU-6 reactor. Each of them has one inlet and one outlet Header at each end of the reactor core. D_2O is fed to each of the fuel channels through individual Feeder pipes from the Inlet Headers and is returned from each channel through the Outlet Headers (Figure 1.1).

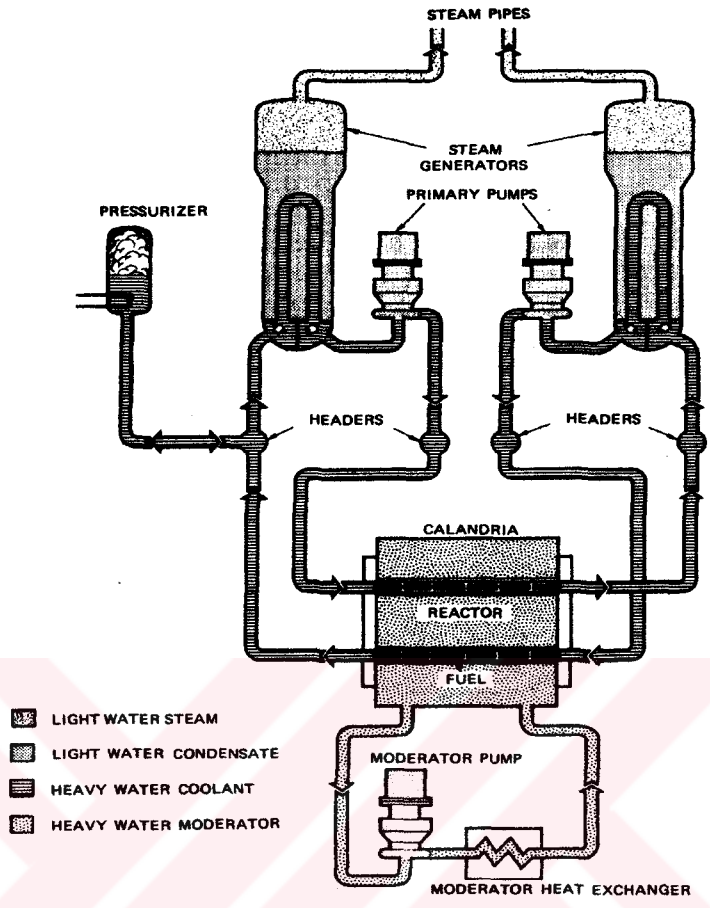

Figure 1.1: Simplified flow diagram of Candu 6 reactor.

In CANDU-6 reactors, the ability of the coolant to remove heat from the fuel channel is influenced by how the Header distributes the steam and water phases to the Feeders. Therefore in the event of some loss of coolant accidents, the effectiveness of the decay heat removal depends on the phenomena occurring in the Headers. Understanding of the Headers' behaviour is more important due to complexity of the phase distribution in this type of geometry. Void fraction which is the key parameter for determination of flow distribution and the mass flow rate in the Feeders are two crucial parameters. In addition unwanted flow oscillations and flow reversal may occur within the Feeders and their affects should be observed closely.

To investigate these behaviours qualitatively and quantitatively, Two-Phase Flow Test Facility (TPFTF) which consists of a transparent scaled model of Inlet Header and five Feeders which are connected to the Header from different positions and inclinations was constructed in D block of Mechanical Engineering Department of METU. A globe valve is placed in each Feeder to simulate flow resistance of the fuel channel and to obtain the required flow distribution in the Feeders. The rest of the facility includes a water–circulating pump, a water-storage tank, an air compressor, air storage tanks, a mixer, connecting piping, and pressure, temperature, flow rate and void fraction measuring devices. Air-water mixture is used to represent water and its vapour in the test facility. Detailed description of TPFTF is explained in Chapter 4.

The subject of this thesis is to investigate the measurement of average void fraction (α) of water-air mixture flows by means of an impedance probe technique.

To achieve this goal; an analog signal conditioner circuit for each impedance probe was designed, tested and developed which will be presented in chapter 5. Some system parameters such as pre-resistance, excitation frequency, water temperature, flow regimes, moisture, affecting the void fraction measurements were investigated. The results will be presented in chapter 6. Detailed explanation about the calibration procedure and the performed tests of impedance probes will be given in chapter 7.

CHAPTER 2

BASIC PRINCIPLES OF IMPEDANCE PROBE TECHNIQUE

2.1 DEFINITION OF VOID FRACTION

Void fraction (α) is defined as;

$$\alpha = \frac{\text{Volume of gas in mixture}}{\text{Total volume of gas - liquid mixture}}$$

In engineering applications it is customary to describe flow conditions in terms of cross sectional averages taken across the channel flow cross section (Figure 2.1).

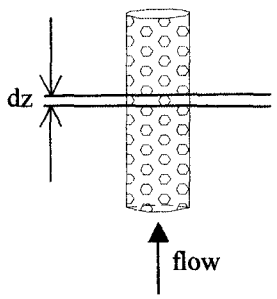

Figure 2.1: Two-phase flow in a vertical channel.

In figure 2.1, a control volume of an infinitesimally small length is considered in which the void fraction can be taken constant;

$$\alpha = \frac{A_g}{A_g + A_f} \tag{2.1}$$

where A_g and A_f are the cross sectional areas occupied by the gas phase and liquid phase respectively and perpendicular to flow direction.

The quality (x) of a vapour-liquid mixture in a non-flow system, or where no gross relative motion between the vapour and liquid phases exists is defined as;

$$x = \frac{\text{Mass of gas in mixture}}{\text{Total mass of mixture}}$$

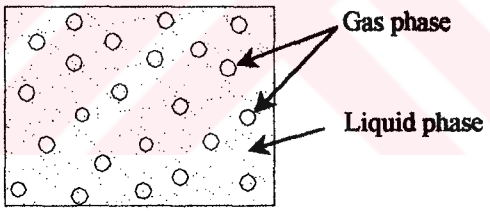

Figure 2.2: Mixture of liquid and vapour in a non-flow system.

The relation between x and α in a non-flow system can be obtained by assuming a certain volume containing 1 kg of mixture in thermal equilibrium (Figure 2.2).

That volume will be equal to $(v_f + x.v_{fg})$ m^3, where v is the specific volume (m^3/ kg).

In an equilibrium mixture, two phases are saturated liquid and saturated vapour and the volume of vapour present is equal to its mass, x.1 kg, times its specific volume v_g. α is thus given by

$$\alpha = \frac{x.v_g}{v_f + x.v_{fg}}$$

This equation can also be written in the following form;

$$\alpha = \frac{1}{1 + \left(\frac{1-x}{x}\right).\left(\frac{v_f}{v_g}\right)} \tag{2.2}$$

However, in case of two-phase flow, say up-flow in a vertical direction, the gas phase because of buoyancy, has a tendency to slip past the liquid, i.e., move at a higher velocity than that of the liquid phase.

Slip ratio (s) is defined as the ratio of the average velocity of the vapour U_g to that of the liquid U_f:

$$s = \frac{U_g}{U_f} \tag{2.3}$$

The relationship between void fraction and quality is modified by taking slip ratio into consideration [17, 18, 19]. In a flow system, the quality at any one cross section is defined by

$$x = \frac{\text{Mass flow rate of gas phase}}{\text{Mass flow rate of mixture}}$$

In an equilibrium mixture, two phases are saturated liquid and saturated vapour and the volume of vapour present is equal to its mass, x.1 kg, times its specific volume v_g. Void fraction , α, is thus given by:

$$\alpha = \frac{x.v_g}{v_f + x.v_{fg}}$$

This equation can also be written in the following form;

$$\alpha = \frac{1}{1 + \left(\frac{1-x}{x}\right)\left(\frac{v_f}{v_g}\right)} \tag{2.2}$$

However, in case of two-phase flow, say up-flow in a vertical direction, the gas phase because of buoyancy, has a tendency to slip past the liquid, i.e., move at a higher velocity than that of the liquid phase.

Slip ratio (s) is defined as the ratio of the average velocity of the vapour U_g to that of the liquid U_f:

$$s = \frac{U_g}{U_f} \tag{2.3}$$

The relationship between void fraction and quality is modified by taking slip ratio into consideration [17, 18, 19]. In a flow system, the quality at any one cross section is defined by

$$x = \frac{\text{Mass flow rate of gas phase}}{\text{Mass flow rate of mixture}}$$

Thus if the total mass flow rate of mixture is $\dot{m}$, the mass flow rate of gas phase is $x.\dot{m}$ and the mass flow rate of liquid phase is $(1-x).\dot{m}$. Applying the continuity equation, the velocities of gas and liquid phases are given by:

$$U_g = \frac{\dot{m}}{\rho_g . A_g} . x \tag{2.4}$$

$$U_f = \frac{(1-x).\dot{m}}{\rho_f . A_f} \tag{2.5}$$

combining the equations 2.3, 2.4 and 2.5:

$$s = \frac{U_g}{U_f} = \frac{x}{1-x} . \frac{A_f}{A_g} . \frac{\rho_f}{\rho_g} \tag{2.6}$$

Since equation 2.1 gives:

$$\frac{A_f}{A_g} = \frac{1-\alpha}{\alpha}$$

Equation 2.6 becomes:

$$s = \frac{x}{1-x} . \frac{1-\alpha}{\alpha} . \frac{\rho_f}{\rho_g}$$

This equation can be rearranged to give a relationship between α and x, including the effect of slip ratio, as

$$\alpha=\frac{1}{1+\left(\frac{1-x}{x}\right).\left(\frac{\rho_g}{\rho_f}\right).s} \tag{2.7}$$

On the other hand, volume flow ratio (β) of a two-phase flow system is defined as;

$$\beta=\frac{\text{Volume flow rate of gas phase}}{\text{Total volume flow rate of mixture}}=\frac{Q_g(m^3/s)}{Q(m^3/s)}$$

$$\beta=\frac{\frac{x.m}{\rho_g}}{\frac{x.m}{\rho_g}+\frac{(1-x).m}{\rho_f}}=\frac{1}{1+\left(\frac{1-x}{x}\right).\left(\frac{\rho_g}{\rho_f}\right)} \tag{2.8}$$

Pressure drop in two-phase flow is closely related to the flow pattern as defined by its void fraction and phase distribution. Various analytical models of two-phase flow models have been established. These are homogenous flow model, separated flow model and drift flux model [17]. In this work the homogenous flow model is used for the calibration procedure of the impedance probes.

Homogeneous flow model is based on the assumptions of equal average velocities of vapour and liquid phases (s=1), the existence of thermodynamic equilibrium between the phases, treating the two-phase mixture as a single phase fluid with weighted average properties.

For example, the mean density (ρ_m) can be expressed in terms of void fraction;

$$\rho_m=\alpha\rho_g+(1-\alpha).\rho_f$$

In homogenous model, for s=1 and from equation 2.7 and 2.8;

$\alpha=\beta$

In 1946 Armand [Appendix H] correlated the data for the void fraction of air-water flow in a horizontal and vertical pipes at pressures close to atmospheric by plotting α against β. Detailed explanation of Armand's studies and that of other authors are given in Appendix H.

Void fraction (α) is also used in the calculation of frictional pressure drop, accelerational pressure drop, elevational pressure drop and pressure drop due to the abrupt changes in flow cross-sectional area (expansion, contraction, bends, t-junctions, etc.)[18].

2.2 FLOW PATTERNS IN TWO-PHASE FLOW

For a liquid-gas mixture flow through a pipe, some well defined flow patterns are formed depending on the operating conditions, flow rate of two individual phases, geometry, diameter and the inclination of the pipe [19].

Vertical two-phase flow is normally divided into 4 basic flow regimes (Figure 2.3) and characterised as follows;

- Bubbly Flow in which small, discrete bubbles, which are normally distorted spheres, are surrounded by liquid.

- Slug Flow in which slugs of liquid and bubbles are separated by regions of high vapour content (plug) which appears as large, spherical-capped bubbles and followed by a collection of smaller voids in bubbly form.

- Churn Flow which is formed by the breakdown of the large vapour bubbles in slug flow and results in an oscillatory or time varying flow

with gas or vapour passing in a more or less chaotic manner through the liquid.

- Annular Flow in which the gas is flowing in the center of the tube and liquid partially as a film along the walls and partially as droplets in the central gas core.

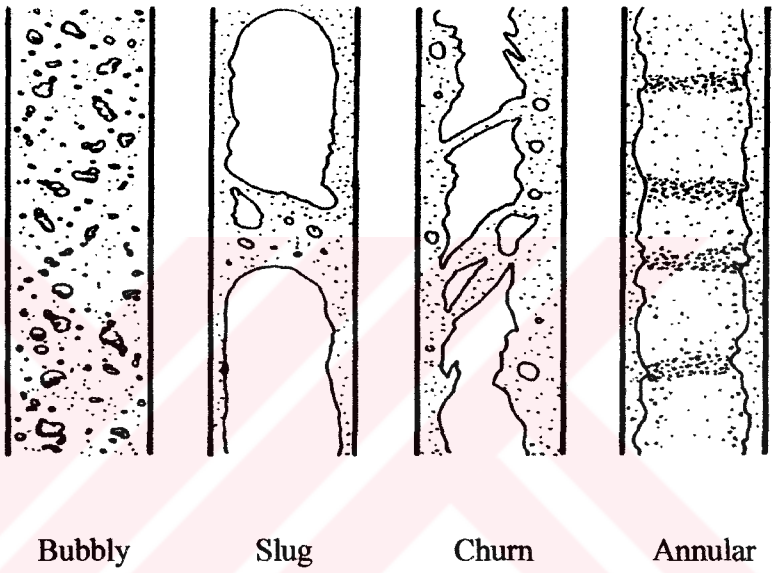

Figure 2.3: Schematics view of flow patterns in two-phase upward flow in a vertical channel

The flow patterns observed in co-current two-phase flow in horizontal and inclined tubular channels are complicated by asymmetry of the phases resulting from the influence of gravity. The generally accepted flow patterns are (Figure 2.4) [19];

- Bubbly Flow: This flow pattern is similar to that in vertical flow except that the vapour bubbles tend to travel in the upper half of the pipe. At

cross-section contains bubbles whilst at still higher velocities a flow pattern equivalent to the wispy-annular pattern is entered.

- Plug Flow: This is similar to slug flow in the vertical direction. Again the gas bubbles tend to travel in the upper half of the pipe.

- Stratified Flow: This pattern only occurs at very low liquid and vapour velocities. The two phases flow separately with a relatively smooth interface.

- Wavy Flow: As the vapour velocity is increased, the interface becomes disturbed by waves travelling in the direction of flow.

- Slug Flow: A further increase in vapour velocity causes the waves at the interface to be picked up to form a frothy slug which is propagated along the channel at a high velocity. The upper surface of the tube behind the wave is wetted by a residual film which drains into the bulk of the liquid.

- Annular Flow: A still higher vapour velocity will result in the formation of a gas core with a liquid film around the periphery of the pipe. This film may or may not be continuous around the entire circumference but it will, of course, be thicker at the base of the pipe.

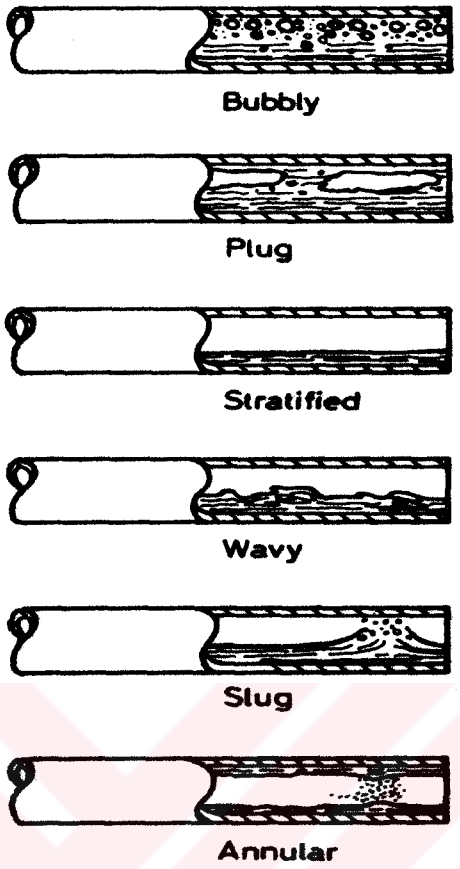

Figure 2.4: Schematic view of flow patterns in horizontal channel

2.3 THEORY OF IMPEDANCE PROBE TECHNIQUE

The electrical impedance of a flowing fluid consists of resistive and capacitive components.

A schematic diagram of an impedance probe in form of two parallel plate type electrodes inserted in a two-phase mixture can be described as shown in figure 2.5. Impedance (Z) of flowing medium measured by electrodes can be shown equivalent to resistive and capacitive components in parallel.

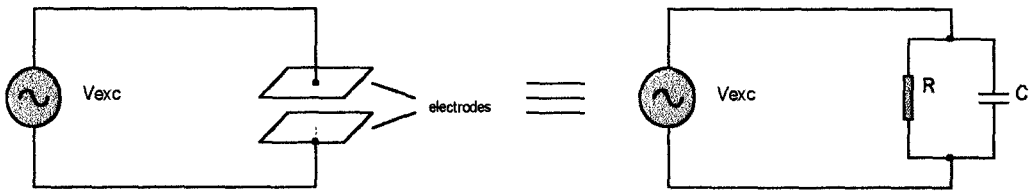

Figure 2.5: Schematic diagram of a parallel plate impedance probe

where R is the resistance corresponding to inverse of the conductance between the electrodes and C is the capacitance formed between two electrodes which are influenced by the void fraction, void distribution (flow regime), temperature of the flowing medium and the excitation frequency of the applied voltage (V_{exc}).

The conductance (G) of a solution is the inverse of its resistance and reflects its ability to conduct electricity. The unit of conductance is siemen (S) which is too large for analytical purposes where either the microsiemen (μS) or millisiemen (mS) are usually used. Since the results depend not only on the nature of the solution, but also on the cross-sectional area, A(cm^2) and physical separation of the plates (d), as well as the temperature, conductance alone has little meaning. To provide a value which can be referenced and manipulated a reading of conductance is converted into a conductivity (K) using the following relationship:

$$K=G\frac{d}{A}\ (\mu S/cm)$$

Physically, a capacitor consists of two thin metal plates separated by an insulating (or dielectric) material. For a parallel plate type capacitor as shown in figure 2.6, the value of its capacitance (C) depends upon the area of each plate

(A), the separation distance between the plates (d), and a property called permittivity of medium (ε) between the plates.

$$C = \varepsilon \frac{A}{d}$$

where C(F), ε(F/m)

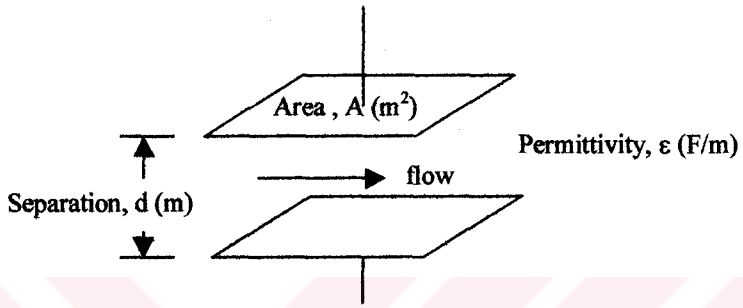

Figure 2.6: Schematic representation of a capacitor.

The dielectric constant of the medium (relative permittivity), ε_r, is directly proportional to ε. The dielectric constant is defined as the ratio of permittivity of the medium, ε, to that of vacuum ($\varepsilon_0 = 8.85 \times 10^{-12}$ F/m).

$$\varepsilon_r = \frac{\varepsilon}{\varepsilon_0}$$

Capacitance change in impedance term is based upon the fact that both liquid and gas phases have different dielectric constants.

Dielectric constant, ε_r, of gases which include steam and other liquid vapours is close to 1, whereas the dielectric constants of liquids range from 2 to 100.

Analytically, the impedance of the flowing medium between the electrodes can be expressed as (Figure 2.5);

$$\frac{1}{|Z|} = \frac{1}{R} + \frac{1}{|X_C|} \tag{2.9}$$

where X_C is defined as the capacitive reactance of the unit Ω (ohms)[Appendix F];

$$X_C = -\frac{1}{w.C}$$

where – sign states that since the voltage across the capacitor lags behind the capacitor current by exactly 90° . There is phase angle of 90° between the R and X_C and w is the angular velocity of the rotating vector in radians per second. Since there are 2π radians in one cycle so it is defined as [20];

$$w = 2.\pi.f \text{ (rad/s)}$$

where f is defined as the frequency which gives the number of cycles per second. It is the reciprocal of the period (T) of the function and a cycle per second is referred to as Hertz (abbreviated Hz).

$$f = \frac{1}{T} \text{ (Hz)}$$

If we arrange the equation 2.9, the following equation is obtained for the absolute value of the impedance (Z):

$$\frac{1}{|Z|}=\frac{1}{R}+\frac{1}{|X_C|}=\frac{R+|X_C|}{R.|X_C|}=\frac{\sqrt{R^2+\frac{1}{w^2.C^2}}}{R.\frac{1}{wC}}$$

$$|Z|=\frac{R}{\sqrt{(1+R^2.w^2.C^2)}}=\frac{R}{\sqrt{(1+(4.R^2.\pi^2.f^2.C^2))}} \qquad (2.10)$$

In a typical measurement circuit (Figure 2.7); the excitation is assured by a DC or AC voltage source. Direct voltage excitation is the easiest and least expensive technique to use but also it has some disadvantages such as polarisation effect and electrochemical attack.

To eliminate these problems; AC voltage source is generally used. The excitation frequency determines the characteristics (resistive and capacitive) of a measured impedance.

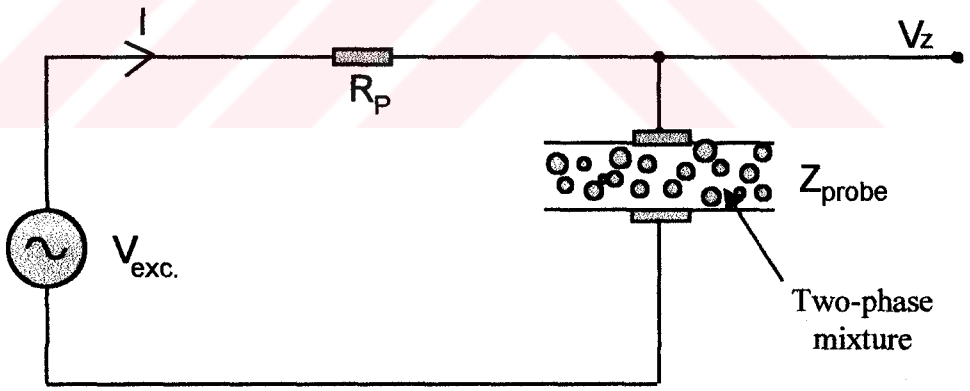

Figure 2.7: Typical measurement circuit for impedance probe.

The electric current (I), which is proportional to the impedance of a two-phase mixture (Z_{probe}) can be expressed by;

$$I = \frac{V_{exc.}}{Z_T} = \frac{|V_{exc.}|}{|Z_{probe}| + R_p}$$

where R_p is a pre-determined value of the resistance installed in the electric circuit of a signal processing. Output detected voltage drop across the probe (V_z) is directly influenced by the impedance between two electrodes and provides information on the void fraction of a two-phase flow.

$$V_z = I.Z_{probe} = \frac{V_{exc}.|Z_{probe}|}{|Z_{probe} + R_p|}$$

2.3.1 Resistive Term

When the fluid conductivity is large, the measurement of a capacitance (C) requires a high frequency in order to minimise the role of resistance and eliminate the parasitic capacitance caused by a polarisation near electrodes as well as to avoid a significant effect of external disturbances on the measurement system. Thus for overcoming these problems, it is usually decided to measure the resistance, by keeping the excitation frequency in the range of much less than 1MHz.

If the excitation frequency is zero (f=0), then the impedance term becomes purely resistive. Equation 2.10 becomes;

$Z=R$

When the excitation frequency is low enough especially under 1 MHz. depending on the probe geometry, the impedance of the probe is still resistive (Equation 2.10).

$$\frac{1}{R} >> \frac{1}{|X_C|}$$

2.3.2 Capacitive Term

Increasing the excitation frequency high enough (f>1MHz) results in decreasing the value of resistance term and approaching the value of capacitive term to the resistive term depending on the probes geometry.

$$\frac{1}{R} \approx \frac{1}{|X_C|}$$

At that point it is better to measure capacitance (C) instead of impedance of the flowing medium since the range of impedance change of probe becomes smaller compared to that of low excitation frequencies.

CHAPTER 3

LITERATURE SURVEY

This chapter will be devoted to the summary of previous impedance probe configurations used in void fraction measurements, their signal conditioner circuits and calibration methods.

In 1975, V.I. SUBBOTIN, YU.E. POKHVLOL, L.E. MIKHAILOV, I.V.KRONIN, V.A. LEONOV [21] used a coaxial probe constructed from a medical needle-capillary tube 0.8 mm in diameter for local void fraction measurement. Arranged concentrically in the capillary tube was the constantan wire central electrode 0.1mm in diameter. It was insulated from the tube by an epoxide barrier. The central electrode (point) projected 0.5 mm out of the insulation. The probe was traversed across the flow by a micrometer screw (Figure 3.1).

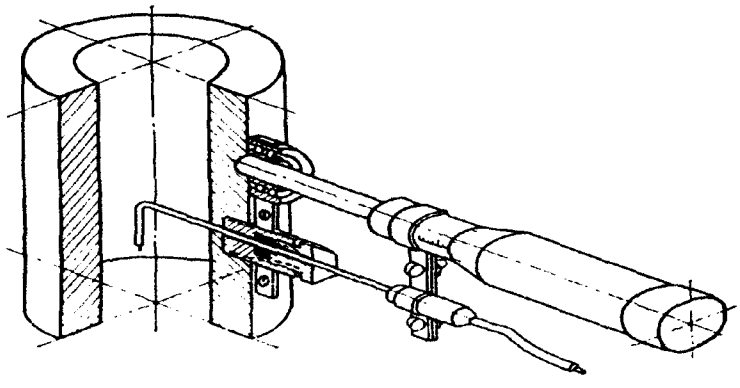

Figure 3.1 : Detailed view of the conductive probe.

The localized probe was included in a resistive bridge circuit with active resistances (Figure 3.2). Power was supplied by a GZ-33 audio oscillator when the probe needle was in liquid, the bridge was balanced by the elements R3 and C1 in such a way that at point A, the voltage was zero. If a bubble "bumped into" the needle the bridge was brought out of equilibrium and a signal appeared at point A with a frequency of 10 kHz, modulated by the instantaneous gas content (in the zone of the probe needle). The signal was transmitted through a "Topaz 1" amplifier to the counter (PST 100). The number of pulses registered during the interval T makes it possible to determine the local gas content.

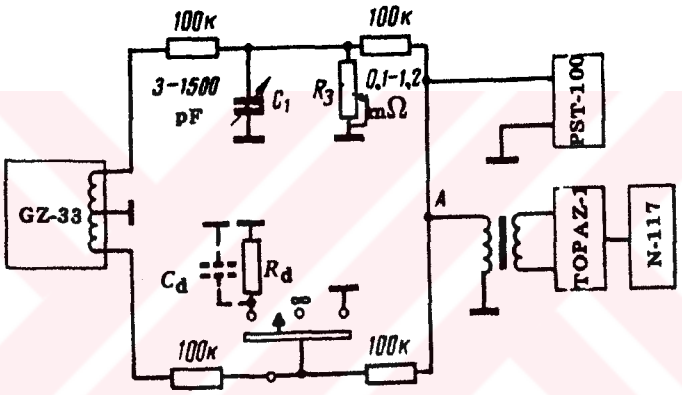

Figure 3.2 : Measuring circuit of conductivity probe.

In 1976, M.MERILO, R.L.DECHERE and W.M.CICHOWLAS [22] used a conductance gauge with a rotating electric field for measuring the void fraction. Previous attempts to utilise conductance measurements for this purpose have generally been plagued by two problems. If the electrodes are mounted flush on the tube wall to minimise the flow disturbance, the electric field is not uniform and the conductance becomes dependent on the void distribution.

On the other hand, if the electrodes are designed to distribute the field either by using parallel plates, concentric cylindrical plates or wire grids, a considerable disturbance can be introduced to the flow. These disturbances produce

accelerations in the flow field which, by changing the relative vapour and liquid velocities affect the void fraction. In their design the electrodes formed a part of the tube wall to eliminate disturbance to the flow. Further the electric field, which was perpendicular to the flow was rotated electronically to distribute it throughout the sensor volume (Figure 3.3).

The sensors consisted of 6 stainless steel electrodes separated by ceramic insulators. These electrodes and insulators formed the inside perimeter of the sensor flow area.Infact, by curving the electrodes and insulators this disturbance could be eliminated.

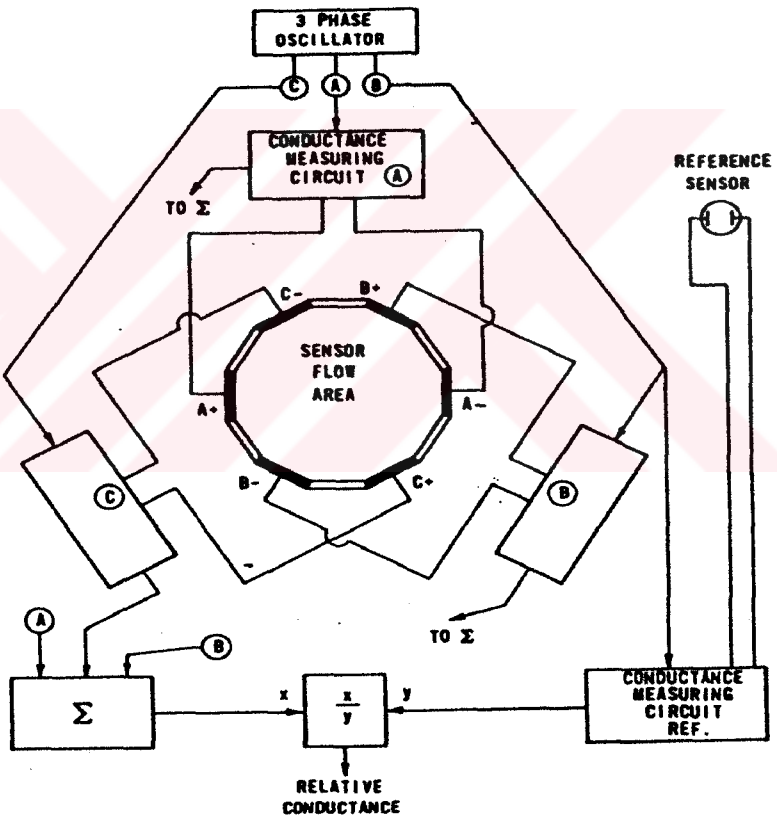

Figure 3.3 : Schematic diagram of the conductor monitor.

Six electrodes formed three sets of opposing parallel plates uniformly spaced around the circumference. Three electrode pairs were excited at a frequency of 5 kHz by a 10V three-phase signal such that the signal for each pair was 120° out of phase with the others.

Three identical conductance measurement circuits were also connected to the electrode pairs, and the absolute values of the signals from these circuits were summed. The resulting signal was proportional to the conductivity of the single phase liquid, could be used to compensate for changes in conduction of the liquid due to variations in its temperature and concentration of impurities. The final output was then simply the relative conductivity of the two-phase mixture with respect to the liquid phase (Figure 3.3).

To calibrate the probe they used the quick-closing valves in the system.

Finally they found that the rotating field conductance gauge provided a useful and versatile, relatively simple technique for void fraction measurement and flow pattern discrimination.

In 1982, J.E.HARDY and J.O.HYLTON [23] developed and used impedance probes which consisted of a pair of stainless steel electrodes strung back and forth across a rectangular stainless steel frame (Figure 3.4).

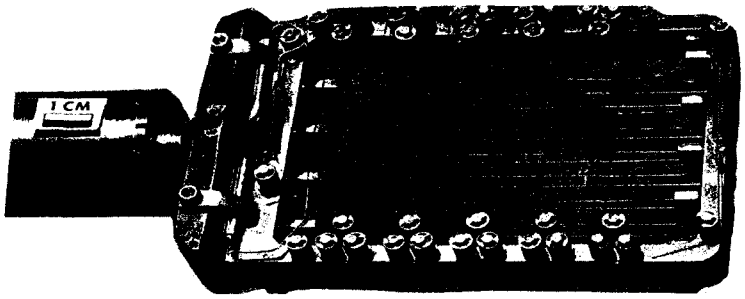

Figure 3.4: Photograph of a string probe with cermet insulator

The measured impedance could be used to determine the local void fraction

A calibration of the void fraction method was accomplished by comparing the output of string probe to the measured values of void fraction which were determined by a low-energy gamma densitometer.

In 1983, R.VAN DER WELLE [24] performed his experiments in atmospheric vertical air-water flows, for void fractions between 0.25 and 0.75 and superficial liquid velocities of 1.3, 1.7 and 2.1 m/s. Local values of void fraction and bubble velocity as well as the bubble diameter were measured by means of a conductivity probe.

The conductivity probe consisted of two tips, each having a platinum wire of about 30 μm in diameter, insulated by glass except at the front end. The tip of the probe has to be sharp in order to achieve immediate piercing with little deformation of bubble at the moment of contact. As the contact area consisted only of the cross section of the wire, rapid dewetting occured as the bubble was touched (Figure 3.5).

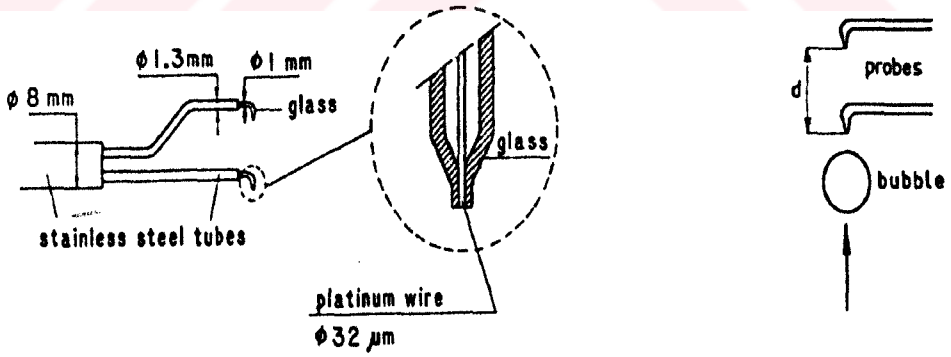

Figure 3.5: Geometry of conductivity probe.

They did the experiments for variable liquid velocities from 0.9-2.5 m/s

The void fraction measurements by conductivity probe were checked by comparison with the void fraction obtained by a γ-photon attenuation technique.

In 1985, A. TOURNAIRE [25] compared the instantaneous response of an impedance probe which has its electrodes mounted flush in the tube wall to avoid disturbing the two-phase flow in a vertical pipe.

The geometry of the probe was defined by the width and number of electrodes, characterized by the angle θ_0 and on the position of the ball, characterized by its cylindrical coordinates (Figure 3.6).

Three different probes (θ_0=22.5^0, 45^0, 85^0) and also two and four electrode probe had been tested.

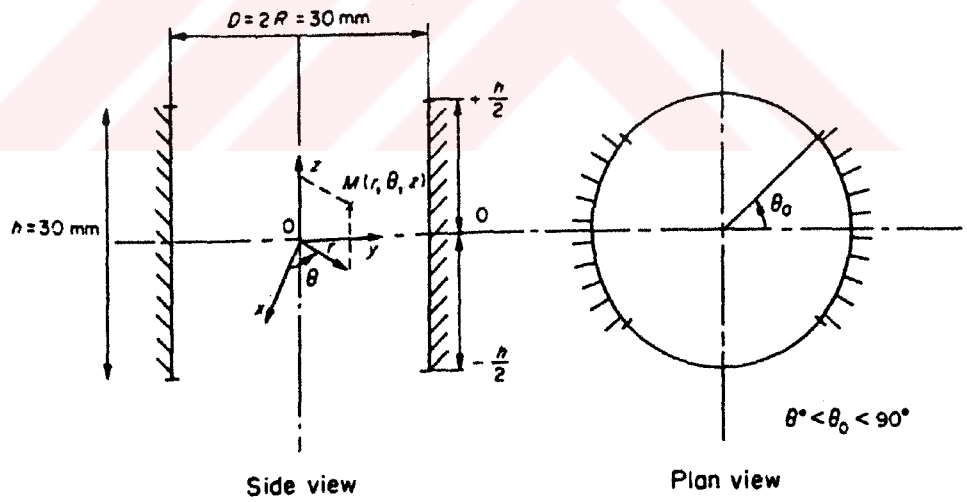

Figure 3.6: Scheme of a two-electrode probe.

In comparing the two electrodes with 45^0 with four electrode whatever the connections were (Figure 3.7), the electric field was not as evenly distributed as

with the two-electrode probe(θ_0=45^0). Increasing the number of electrodes didn't not improve the performance of the probe.

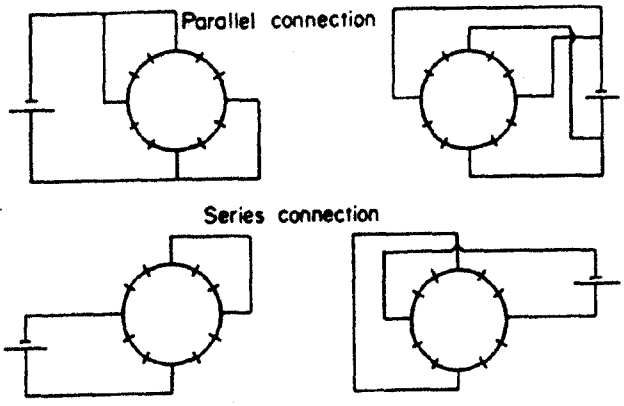

Figure 3.7: Different kinds of connection of two couples of electrodes

As he compared the two-electrode probe with 45^0 width with rotating electric field impedance probe [7], he saw that, in a pipe of circular cross-section, the rotating electric field technique yielded results which were less sensitive to the void distribution than those obtained with a classical technique. The number of electrodes of the rotating electric field impedance probe could be increased to have measurements less influenced by the void distribution. However, from a technical point of view (greater number of phases) it would be more difficult to build such a probe.

In 1987, A.TEYSSEDOU, A.TAPUCU and M.LORTIE [26] developed a conductivity probe for local void measurement system. The system had been calibrated under air-water two-phase flow conditions using the quick-closing valve technique. Comparison of the void profiles obtained with the conductivity probe with those obtained using an optical probe confirms the applicability of this system for two-phase (air-water) flows.

The sensor and its traversing mechanism are illustrated in figure 3.8.

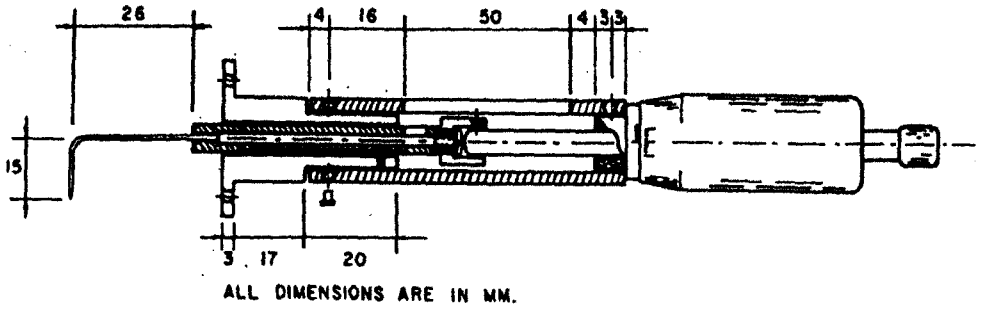

Figure 3.8: The sensor and its traversing mechanism.

Block diagram of the electronic circuit is shown in figure 3.9. Major components of the circuit are: a bridge, a 10 kHz excitation source , an instrumentation amplifier, a demodulator, a notchfilter, a comparator, a gate and an integrator.

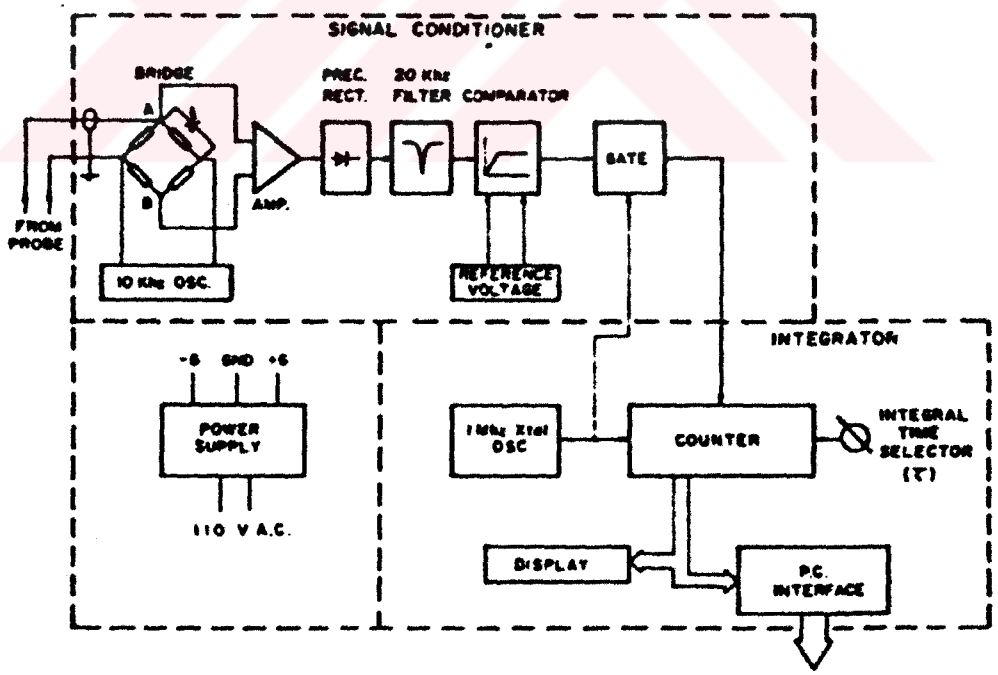

Figure 3.9: Block diagram of the signal conditioner circuit.

They also investigated the sensor tip geometry of the two species. Long tip and short tip at the bubbly and annular flow conditions (Figure 3.10). As a result; they suggested that short-tip sensor seemed to give better results when the probe was close to the tube walls.

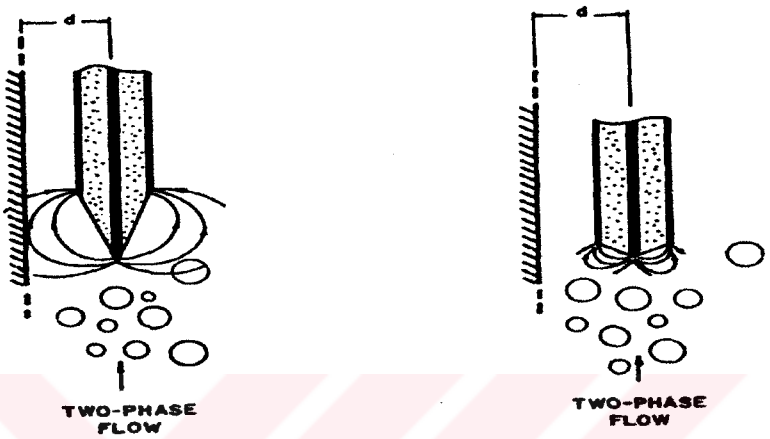

Figure 3.10: Electric field lines around long-tip and short-tip probes.

In 1987, P.ANDREUSSI, A.DI. DONFRANCESCO and M.MESSIA [27] developed a liquid hold-up gauge based on the measurement of the electrical impedance for application in gas-liquid pipe flow. The gauge consists of two ring electrodes mounted flush at the pipe wall (Figure 3.11).

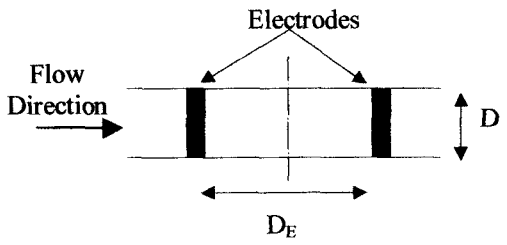

Figure 3.11: Scheme of flush mounted electrodes.

The impedance (capacitance or conductance) sensed by the electrodes depends on the distance between them and on the liquid hold up. For distances above three tube diameters (D), the impedance was independent of the flow configuration for all separated flow patterns and, with good approximation also for intermittent flows. Moreover, capacitance or conductance was linearly related to the liquid hold-up.

The distance between the electrodes could be chosen in the range 1.5-2.5D in order to have a good compromise between the conflicting requirements of a localized measurement and a reading independent of the flow configuration. When D_E >2.5 D, the hold up was linearly related to the conductance both for stratified and annular configuration. The impedance under bubbly flow conditions closely followed the theoretical predictions due to Maxwell [28]. Also for the other flow conditions (annular, stratified, intermittent) the results of static and/or dynamic calibration agreed closely with theoretical models [28].

The use of a third electrode allowed a more precise characterization of the various flow regimes and determination of the velocity at which disturbance waves or slugs travel along the tube (Figure 3.12). The third ring electrode was also used with one of the first two rings to obtain volume average void fraction information. The separation of the second and third rings should be large. This improves the linearity of the device but it inherently averages the void fraction.

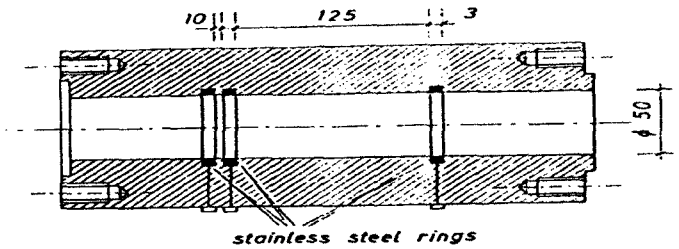

Figure 3.12: Ring electrodes for hold-up measurement in a 50 mm ID pipe

In 1994, RAMKRISHNA DAS and S. PATTANAYAK [29] investigated a method of void fraction measurement based on a technique of pulse width modulation in response to the changing electrical impedance of a gas-liquid mixture flowing through vertical narrow tubes. The test section is made of an acrylic tube of inner diameter of 11mm and length of 2.9 m Air and water mixture is injected into the base of the test section. There are three pairs of electrodes located in the test section (Figure 3.13). First electrode is made of stainless steel. The second and the third are also made of stainless steel wire and coated with teflon except the tip.

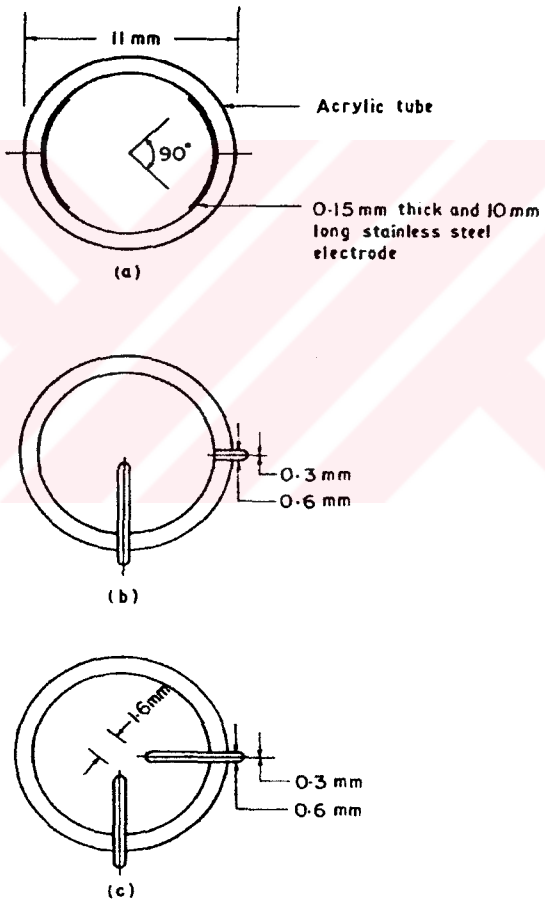

Figure 3.13 : Electrode configurations. (a) Arc-type electrodes; (b) wide-gap electrode; (c) narrow-gap electrodes.

First configuration was used for measuring the average void fraction between 0 and 100 %. The second and third pairs of electrodes were used for local void fraction values.

The electronic circuit they used basically converted the void fraction signal of two-phase mixture into a series of square pulses of varying width. The calibration of time averaged pulse width against void fraction showed that their characteristics were different in different flow regimes. Further calibrations obtained with superficial liquid velocities (U_{LS}=1.16, 0.65 and 0.16 m/s) in slug and churn flow showed their sensitivity to U_{LS}. No such effect was observed in bubbly and annular flow regimes. These effects of flow regimes and U_{LS} could be specified in terms of the number and position of the peaks of the probability distribution function (PDF) of pulse width data. For a given system, these recorded PDF data help in determining the calibrations uniquely in all unknown flow regimes and void fractions ranging from 0.1 to 100%.

In 1996, G.COSTIGAN and P.B.WHALLEY [30] developed and tested a conductivity probe for the measurement of void fraction (Figure 3.14).

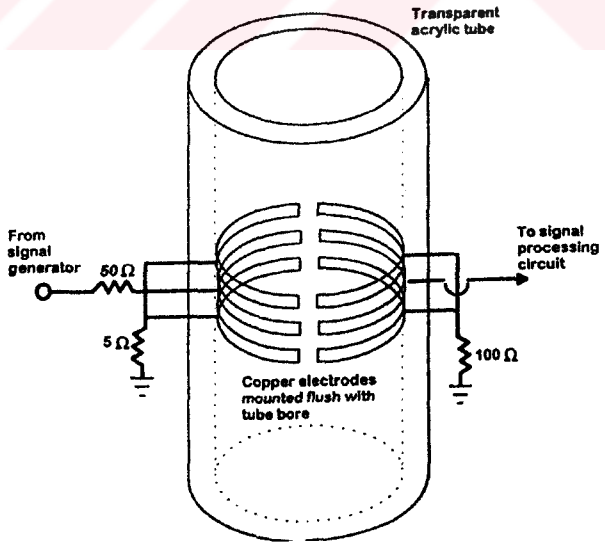

Figure 3.14: Void fraction conductivity probe arrangement

The probes' outputs were taken to the signal processing circuits, whose outputs could be either displayed on an oscilloscope or recorded using a high speed data logger. Computer modelling of the probe's response to different void distributions supported the calibration results.

In 1997, Chul-Hwa SONG , Moon Ki CHUNG , Hee Cheon NO [31] developed a multi-channel conductance void meter to investigate the structural developments of bubbly flow and the propagation of void waves in a flow channel.The sensor was designed to be flush-mounted to the inner wall of the test section to avoid the flow disturbances (Figure 3.15).

It is emphasized that the guard electrodes are electrically shielded in order not to affect the measurements of two-phase mixture conductance , but to make the electric fields evenly distributed in a measuring volume.

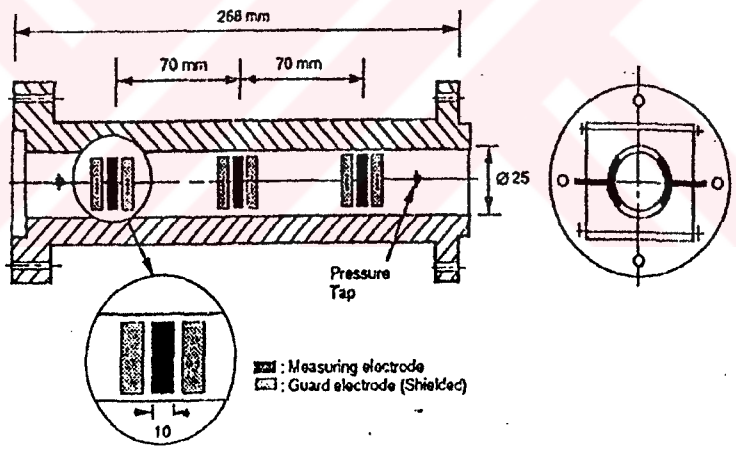

Figure 3.15: Cross section of the main sensor.

It was found out that void meter had good dynamic resolution which was required to investigate the structural developments of bubbly flow and the propagation of void waves in a flow channel. Over-estimation of void fraction could be avoided and apparent sensitivity of void meter response to void

distribution could be minimized by adopting the guard electrodes of the void meter and electrically shielding them.

In 1999, E. KREPPER, A. K. KRUSSENBERG, H.M. PRASSER and A. SCHAFFRATH [32] presented a new device for measuring the void fraction and void distribution with a high resolution (242 measuring points in a cross section area, measuring approximately 1 kHz) in vertical pipes. The sensor consisted of two electrode grids with 16 electrodes each, placed on an axial distance of 1.5 mm behind each other (Figure 3.16).

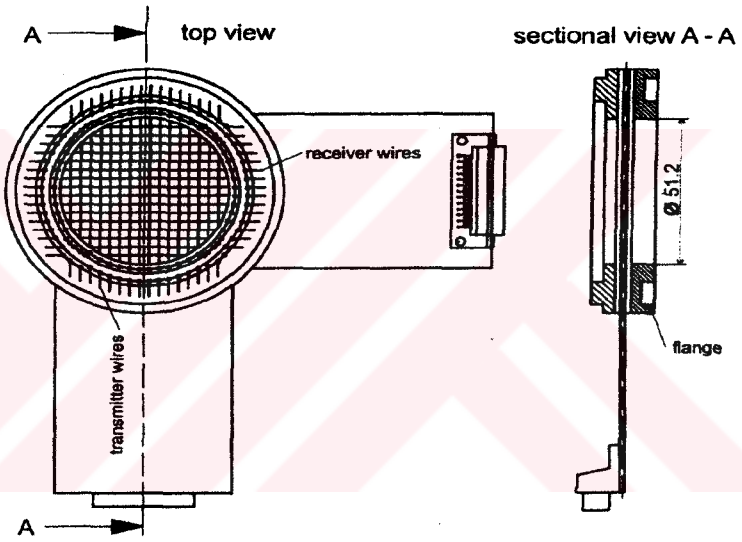

Figure 3.16: Schematic view of wire-mesh sensor (2×16 electrode wires)

The conductivity was measured at the crossing points of the wires of the two grids. The time resolution achieved by the signal processing unit is 1024 frames per second. For the conductivity measurement, one plane of electrode wires was used as transmitter, the other as receiver plane. During the measuring cycle, the transmitter electrodes were activated by a multiplex circuit in a successive order, as illustrated in figure 3.17 for example of 2×4 wires. The measurement for one row was started by closing one of the switches S1-S4. The currents arriving at the

receiver wires were transformed into the voltages by operational amplifiers and sampled by individual sample/hold circuits. After an analog/digital conversion the signals were recorded by a data acquisition computer and stored for each receiver electrode separately. This procedure was repeated for all transmitter electrodes.

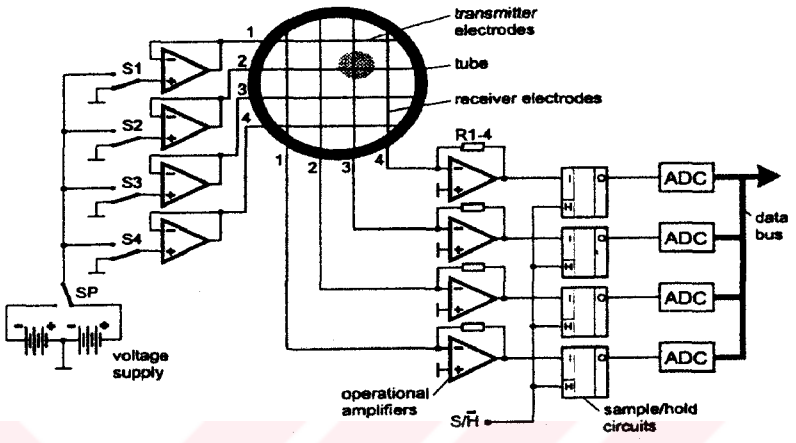

Figure 3.17: Simplified scheme of a 2×4 wire-mesh sensor with signal acquisition system.

CHAPTER 4

EXPERIMENTAL TEST FACILITY

4.1 DESCRIPTION OF EXPERIMENTAL TEST FACILITY

The specification of instruments used in the test facility may be found in Appendix A, and each of them is referred as A1,A2,..etc. The test facility is composed of scaled model of Inlet Header, 5 Feeders that are connected to the lower half of the header through nozzles, an air-water mixer placed just before the inlet nozzle of Header, a water tank, a water circulating pump [A1], three air tanks [A2], air compressor [A2] and connecting pipings (Figure 4.1). Test facility components are made of plastic or copper. Transparent acrylic is used from the mixer to each of the 5 globe valves in the individual Feeders.

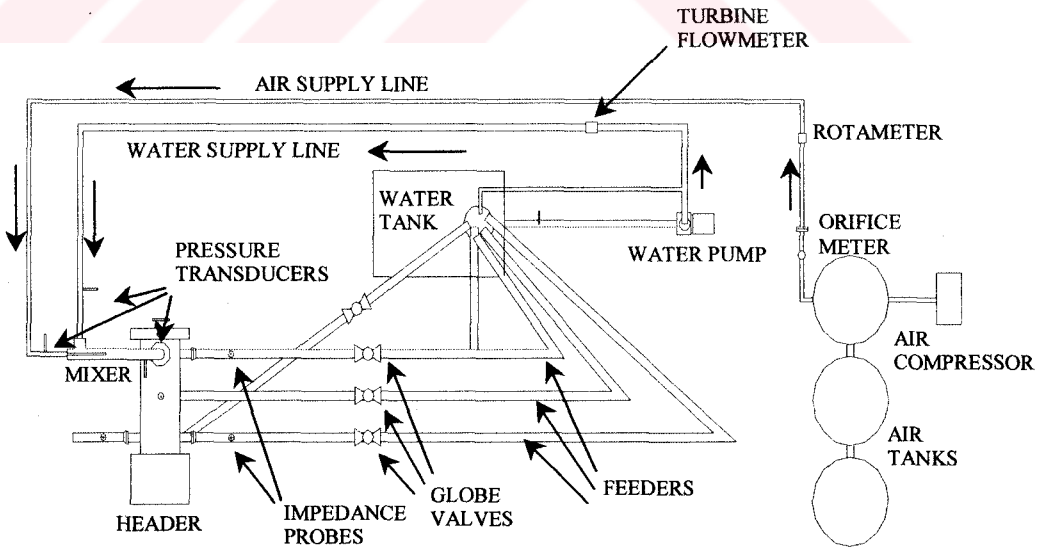

Figure 4.1: Top-view of the test facility.

4.1.1 Water Supply Line

Distilled water is used in the system and it is stored in a plastic tank. A water-circulating pump is connected to the bottom of this reservoir tank with the supply line (Figure 4.2). After the water circulating pump, there is a by-pass line with a relief valve placed on it. This line is used to direct water to the water holding tank to arrange volume flow rate of water and the relief valve prevents high pressures and ensures the safety of the test facility. In addition there are also a pressure gage [A4] to see the gage pressure and a temperature gage [A5] to see the water temperature in the water line. Volume flow rate of water is measured by a turbine type flow meter [A6] which was calibrated by B.Kaya [33]. Just before the mixer on the water line, there is a pressure transducer [A7] which shows the gage pressure and it has an output range from 0 to 5 volt corresponding to 0-100 psig (0-6.89 bar) (Figure 4.2).

4.1.2 Air Supply Line

There are three air storage tanks connected to air compressor. The stored air is supplied to the system with a regulator valve. There is a pressure gage and a temperature gage in the air line. Volume flow rate of air is measured by the help of an orifice plate [33]. The pressure tappings are connected to a differential pressure transmitter [A8](Figure 4.3). There is also a rotameter connected to the orifice in series.

Before mixer, there is a pressure transducer [A7] that shows the gage pressure and a check valve after it to prevent water from escaping into the air side (Figure 4.4).

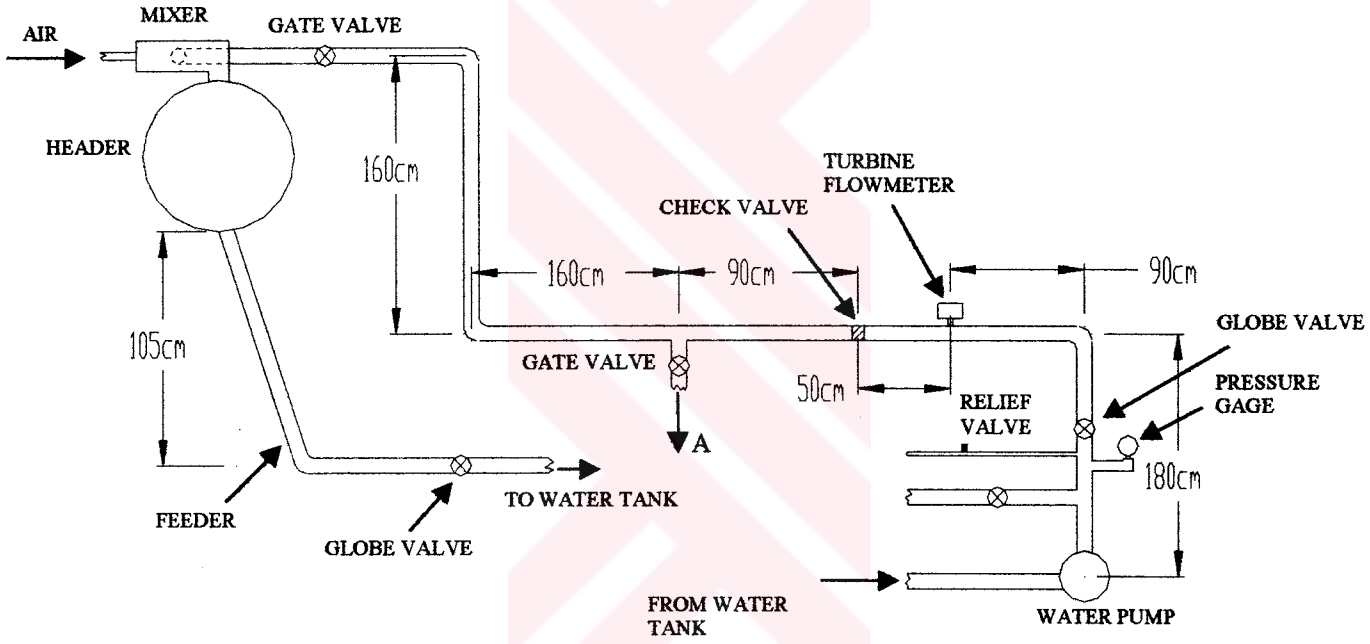

Figure 4.2: Schematic view of water supply line.

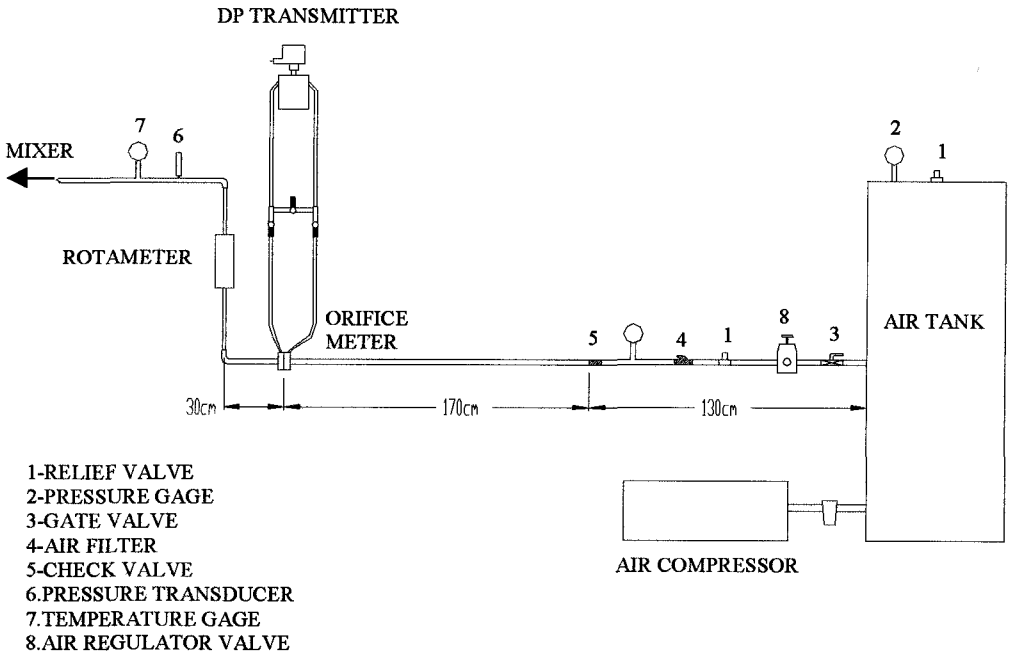

Figure 4.3: Schematic view of the air supply line.

4.1.3 Mixer

Mixer is used to mix the water and air phases before the inlet nozzle of the Header. It is made of PVC. Air supply line is ended with a perforated copper pipe. This pipe is the main component of the mixer (Figure 4.4).

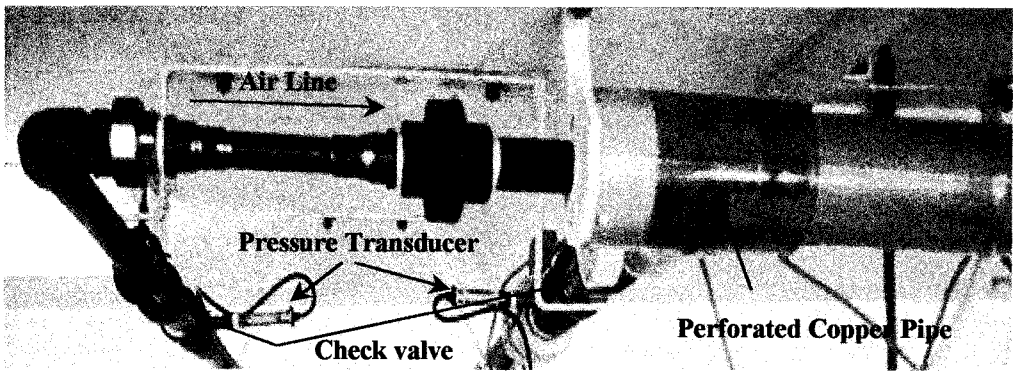

Figure 4.4: A view of mixer

4.1.4 Scaled Model of Inlet Header

Scaled model of Inlet Header has a cylindrical shape with a diameter of 193.675 mm and length of 1200 mm. It's function is to distribute the flow to % Feeders. A relief valve is placed and adjusted to 4 bar for ensuring safety (Figure 4.5). There are 5 impedance probes with ring electrodes flush mounted onto the inner surface of the header for liquid level indication.

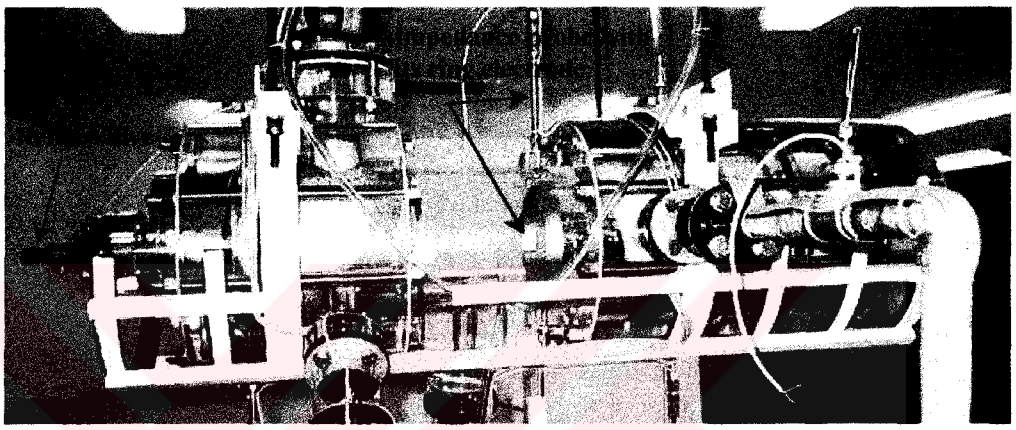

Figure 4.5: A view of scaled model of Inlet Header

4.1.5 Feeders

5 Feeders are connected to the lower half of the Header through nozzles at different angles. Two of them are symmetric to each other and parallel to the horizontal axis (0^o, 180^0), the inclination of the other two Feeders are 216^o, 314^o which are symmetric according to the y axis and the fifth one is at 288^o (Figure 4.6). Two of the Feeders have 34.5 mm inner dimeter and the others have 25.4 mm inner dimeter. On each feeder, there is an impedance probe to measure the average void fraction. There is also a globe valve to simulate the flow resistance of the fuel channel as well as to arrange the required mass flow rates in the Feeders (Figure 4.7). The pressure difference between the upstream and

downstream of the globe valve is measured by a differential pressure transmitter [A9] (Figure 4.7).

All the Feeders discharge into the water-storage tank for re-circulation of water.

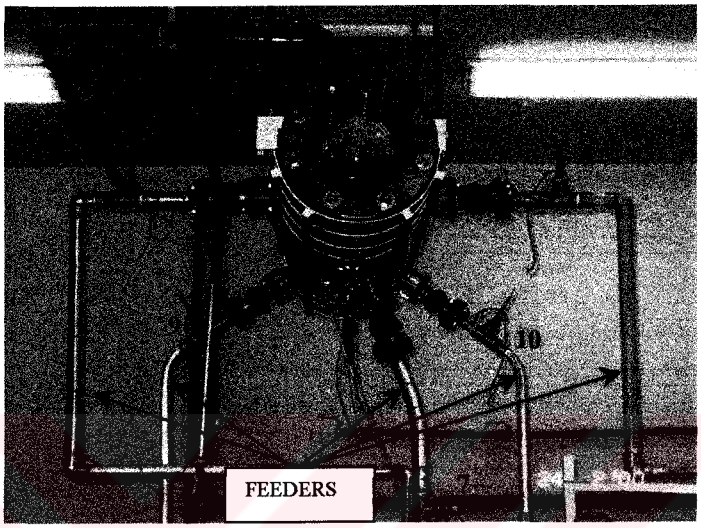

Figure 4.6: A view of 5 Feeders.

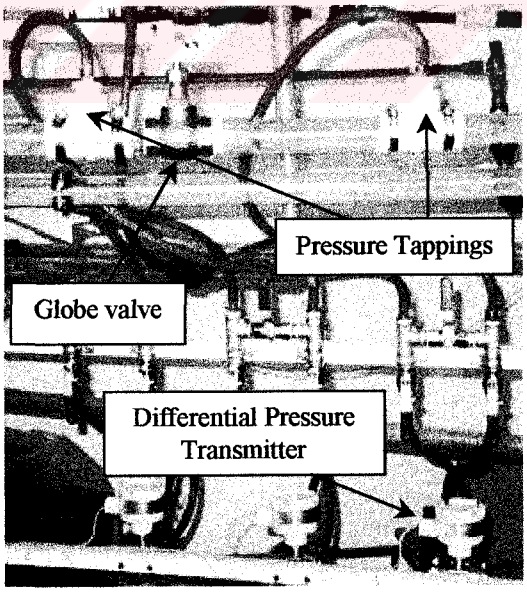

Figure 4.7: A view of globe valve with differential pressure transmitter connections.

4.1.6 Data Acquisition System

All the analog voltage outputs of the impedance probes, differential pressure transmitters, turbine type flowmeter, pressure transmitters, are conditioned and connected to PCLD 812 PG A/D Converter Card [A10] with two PCLD 789D Amplifier and Multiplexer Card [A11] via the analog signal conditioner circuits. Advantech GENIE software was used to read, to display and to log the data. It provides an object oriented graphical use interface that simplifies control strategy and run under Windows 98 enviroment in Celeron 433 processor.

4.2 DESCRIPTION OF IMPEDANCE PROBE

The existing probes on the Header and Feeders are specified with a short single-ended configuration [34, 35].

Short single-ended probes are intended to be used for applications where it is necessary to make a real time measurement distinction between water and air (Figure 4.8) [34, 35].

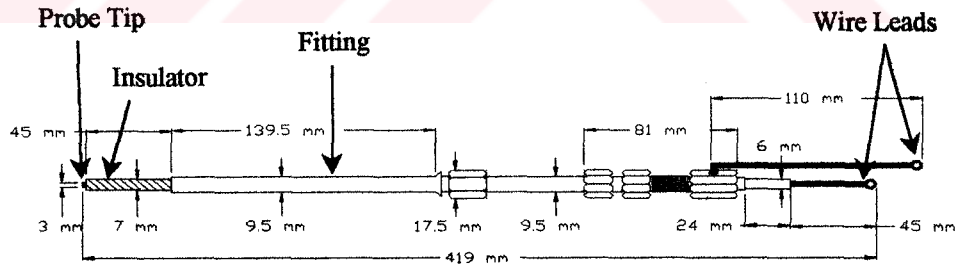

Figure 4.8: Schematic view of single-ended probe on the Header

The probe consists of a stainless steel rod sheated by a Rulon insulator. Rulon material has a low friction coefficient and it is capable of performing under severe temperature (-240 to +278.8 °C) conditions. It has a high chemical

resistance, low moisture absorption and a dielectric constant of about 2.5.

The probe is inserted through the pipe wall by means of a Conax fitting. Wire leads are attached to the protruding end of the rod and to the fitting. These leads are connected to the measuring circuit (Figure 4.9).

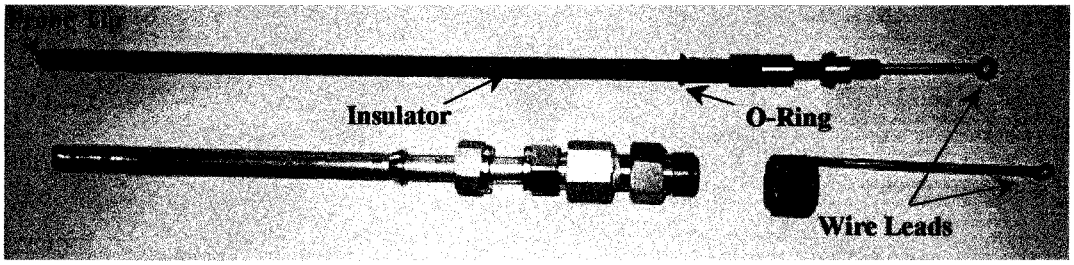

Figure 4.9:Disassembled view of the probe on the Header.

4.2.1 Impedance Probes on the Header

On the scaled model of Inlet Header, five impedance probes with ring electrodes surrounding the inner surface of the header with thickness of 25.5 mm (Figure 4.10) were located at three different locations (Figure 4.11).

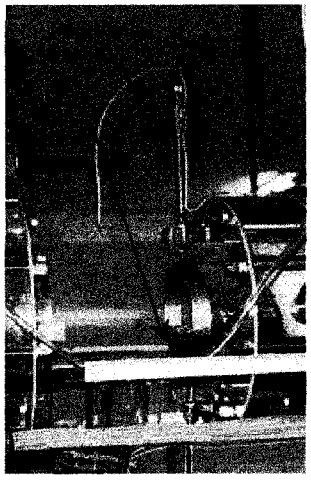

Figure 4.10: A view of impedance probe on the Header with ring electrode.

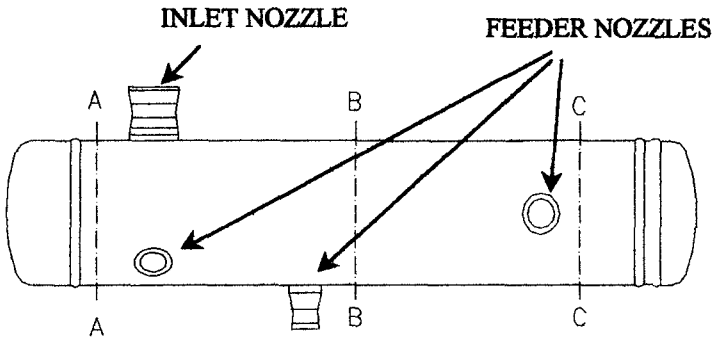

Figure 4.11: Schematic view of the probe locations on the Header.

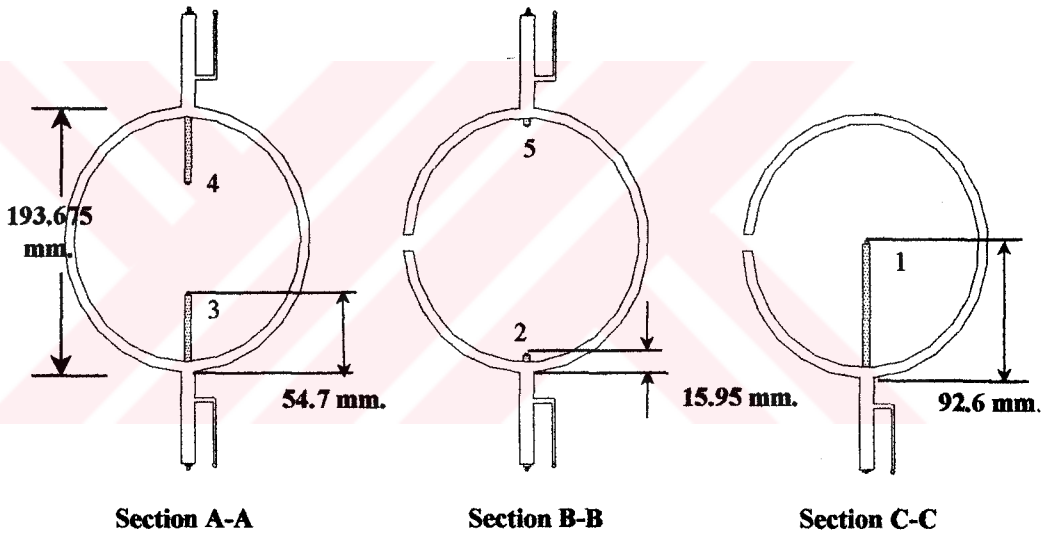

Figure 4.12: Schematic view of the probes on the Header

Distance of the probe tip with insulator part surrounding it that goes inside the header is different in each section (Figure 4.12 and Figure 4.13).

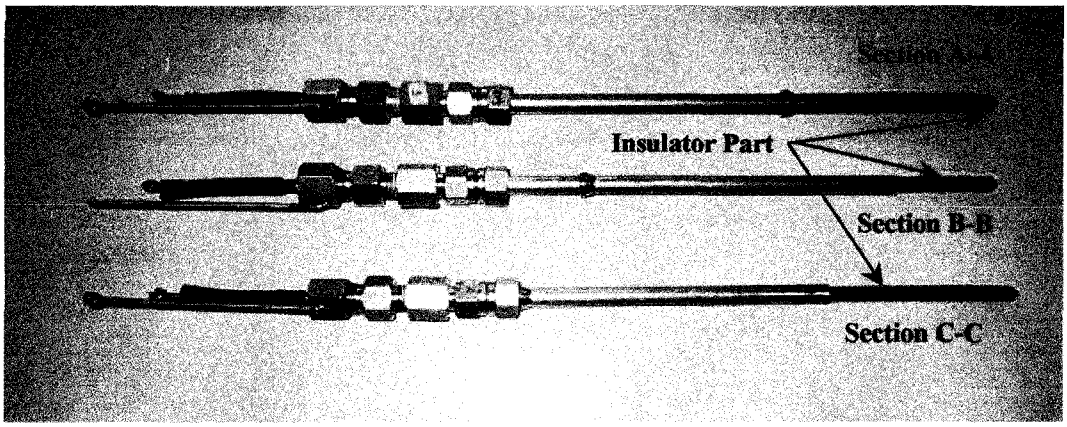

Figure 4.13: Assembled view of impedance probes on the Header

4.2.2 Impedance Probes on the Feeders

Probe configurations on the Feeders are shown in figure 4.14 and figure 4.15. Probe tip is inserted inside the probe body with the distance of the half of the diameter. Probe body is made of stainless steel .

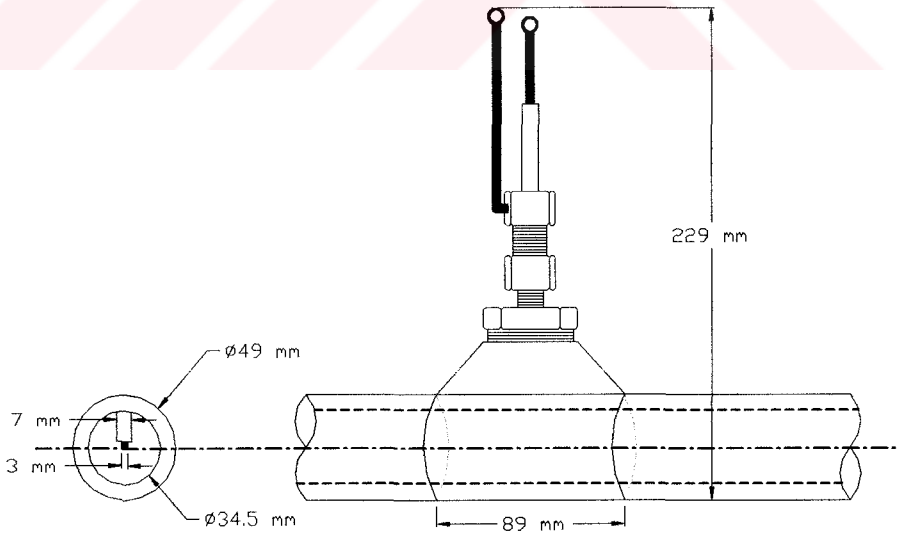

Figure 4.14: Schematic view of impedance probe on the Feeders.

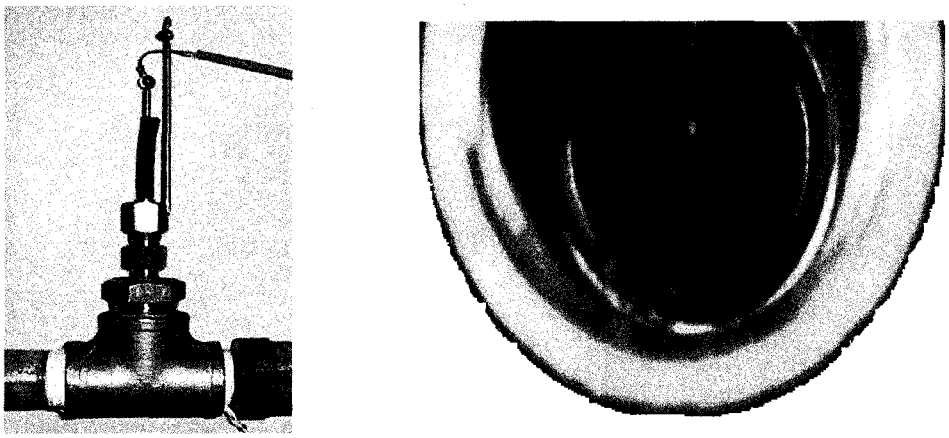

(a) (b)

Figure 4.15: Assembled view of impedance probe from outside the Feeder (a), from inside the Feeder (b)

The impedance probes were placed at each Feeder at different inclination due to the position of the Feeder. They are shown by numbers 6, 7, 8, 9, 10 in Figure 4.6.

CHAPTER 5

ANALOG SIGNAL CONDITIONER CIRCUIT

Design of an analog signal conditioner circuit of an impedance probe differs due to the probe's geometry and hardware configuration which is related to the system sensitivity.

Generally, an analog signal conditioner circuit consists of the following components:

-Signal generator (DC or AC with variable frequency).

-Resistive divider in which the probe is placed in series with the signal generator and with the pre-resistance. The voltage drop across the probe or the pre-resistance can be used in void fraction measurements.

-Instead of resistive divider, a bridge circuit (resistive or capacitive) can be used where the probe occupies one branch of the bridge configuration and voltage drop across the arms can be related to the void fraction.

-Output voltage is amplified and filtered.

-Since the output signal is proportional to the conductivity of the single phase liquid, signal conditioner circuits may include some subcircuits which are

used as a reference for comparison of changes in conductivity of the liquid due to variations in its temperature and in the concentration of impurities .

-Rectifier subcircuit and analog digital converter with signal processing units are also necessary for data processing and logging in PC based data acquisition systems.

At the beginning of this thesis work, a simple sample circuit was proposed by AECL staff for the signal conditioning (Figure 5.1).

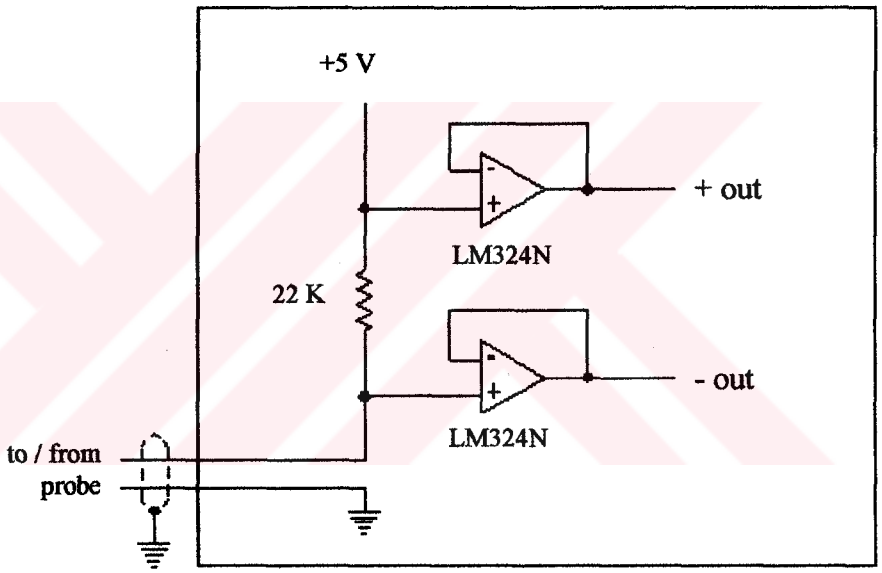

Figure 5.1: Schematic view of analog signal conditioner circuit proposed by AECL staff.

This circuit is excitated by 5V DC voltage source and the voltage drop across the 22 kΩ resistor is related to the void fraction. According to the probe's resistance in all water and in all air media, the value of the resistance can be increased to obtain higher voltage span. A lot of tests were performed with this circuit to see its response and sensitivity to the void fraction. Unfortunately, it

didn't detect the bubbles around the probe tip and gives unreliable results in stagnant water. Moreover the water base voltage shifts due to the electrolysis of water and also there is no signal filtering provision.

Later on, it was decided to get technical asistance from ODESA LTD. ŞTİ. to improve the signal conditioner circuit.

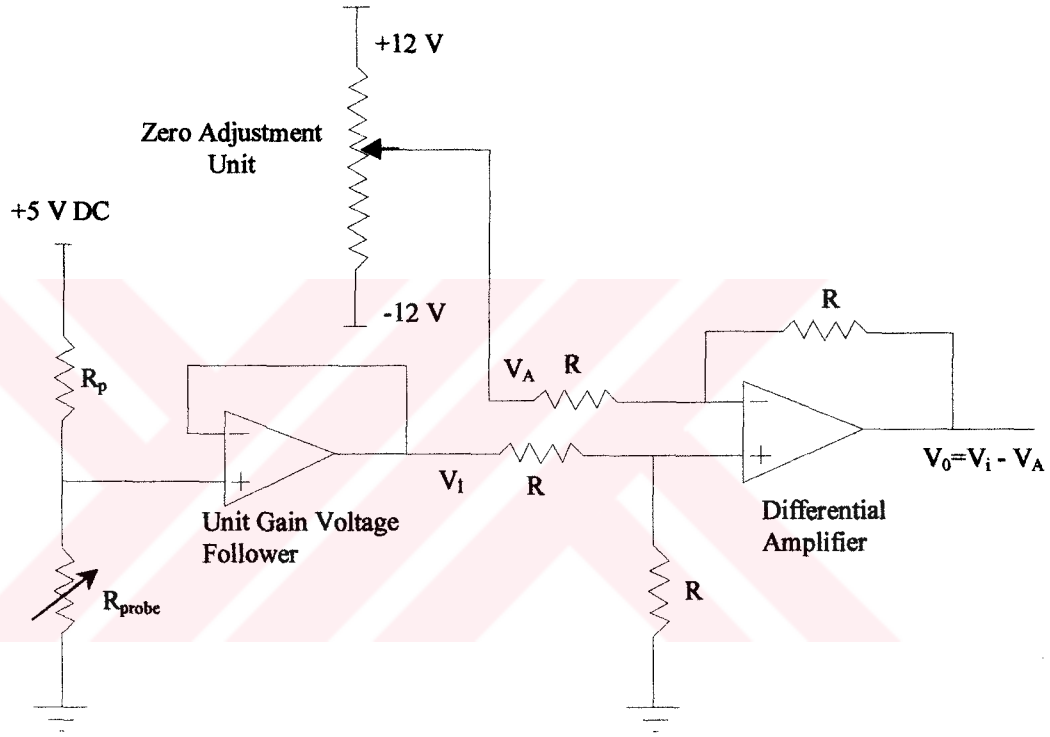

Figure 5.2: Schematic view of analog signal conditioner circuit proposed by ODESA LTD. ŞTİ. staff.

The circuit proposed by ODESA staff which contains a differential amplifier stage (Figure 5.2) is also based on DC excitation and it is an upgrade for the circuit proposed by AECL staff. In this circuit voltage drop across the probe is related to the void fraction. The value of R_p differs for each probe according to the resistance value of the probe both in all water and in all air. The probe voltage

output in all water medium can be adjusted to zero by means of a voltage divider. When it is adjusted to zero, a considerable increase in voltage level proportional to the increase of void fraction is expected in this circuit.

Same as in the circuit proposed by AECL staff, in this signal conditioner circuit, there are also no filtering subcircuits (low-pass filters) which block the interferences due to the powerlines and radio frequency radiation.

In the differential amplifier circuits, the amplifier must have high stability. The printed board design and ground loop elimination techniques are very important for stability and for the reliability in the design stage. Unfortunately, during the tests conducted, the voltage at the output terminals of the differential amplifier was not stable (oscillatory). On the other hand, zero-adjustment unit was a simple voltage divider directly connected to the power supply which may be considered as a wrong design for this type of application.

The response of this circuit to different void fraction values is not satisfactory. An increase in average voltage level could not be observed for small void fractions. Moreover the probe voltage output in all water medium shifts due to the electrolysis of water.

After gaining a considerable experience about disadvantages of previous two circuits it was decided to eliminate the uncertanties due to the DC excitation and to determine the response of the probe in capacitive and resistive conditions. It was also emphasized that the electronic components of the analog signal conditioner circuit should be available in local markets and should not be very expensive. To achieve this goal, an AC excitation voltage source with variable frequency set is used in the circuit. Depending on the differences in resistance and capacitance of each probe in all water and in all air media, a variable resistor is used to increase the probe sensitivity. It is also possible to change the voltage amplitude and the wave characteristics where necessary.

A circuit development work was undertaken with the technical advice of Mr. Okan Demirel of TDK Ltd. Şti.. Some prototypes were designed, constructed and tested until a satisfactory final version of the circuit was obtained.

The final version of the analog signal conditioner circuit consists of 5 main parts (Figure B.1). These are;

1. Power Supply
2. Signal Generator Block
3. Resistive Divider and Non-inverting Amplifier Block
4. RMS to DC Converter Block
5. Bias Shift and Gain Block

5.1 POWER SUPPLY

2×15 V 10 Watt power supply for each signal conditioner circuit is used. They have isolation between each other for eliminating the ground loops for data acquisition system (Figure B2).

5.2 SIGNAL GENERATOR

A common monolitic signal generator with variable frequency set based on 8038 IC was used. Frequency can be adjusted between DC and 20 kHz. by four-way dip switch and a variable potentiometer (P7)(Figure B3) and it is measured with frequency counter [A12] from the test point 6 (Figure B4). Output of this generator is buffer-amplified by LF 411. R18, R12 and P4 are used for the gain adjustment. The signal amplitude can be adjusted by P4 (Figure B4).

5.3 RESISTIVE DIVIDER AND NON-INVERTING AMPLIFIER

5.3.1 Resistive Divider

R11 and P1 are used to increase the pre-resistance up to a value which gives the maximum difference in voltage level, V_Z, due to the impedance change of the probe between 0 and 1 void fraction values which correspond to all water and all air media respectively. P1 is used for tuning the resistive divider for the characteristic impedance of the different probes. The total pre-resistance value can be measured with a multimeter [A13] from the test point 6 and probe(+) terminal (Figure B4). R11 is a precision metal film resistor which has low temperature drift and also P1 is selected as a low noise and low drift type (Figure 5.3).

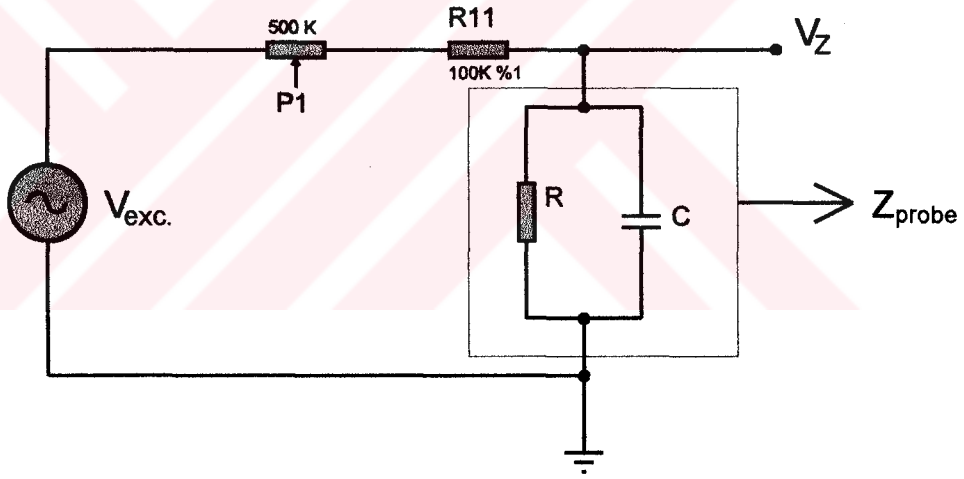

Figure 5.3 : Resistive divider part of analog signal conditioner circuit.

V_Z is the voltage drop across the probe and output of the resistive divider which is defined as;

$$V_Z = V_{exc} \frac{Z_{probe}}{Z_{probe} + R11 + P1}$$

It is obvious that there is a difference in the amplitudes of $V_{exc.}$ and V_Z . This difference can be interpreted as void fraction.

5.3.2 Non-Inverting Amplifier

V_Z point voltage is amplified by a non-inverting amplifier block. This is the most important block of the measuring circuit (Figure 5.4);

i is the total current (i_{probe} + i_{sense}) flowing in the circuit when the non-inverting amplifier block is connected to it.

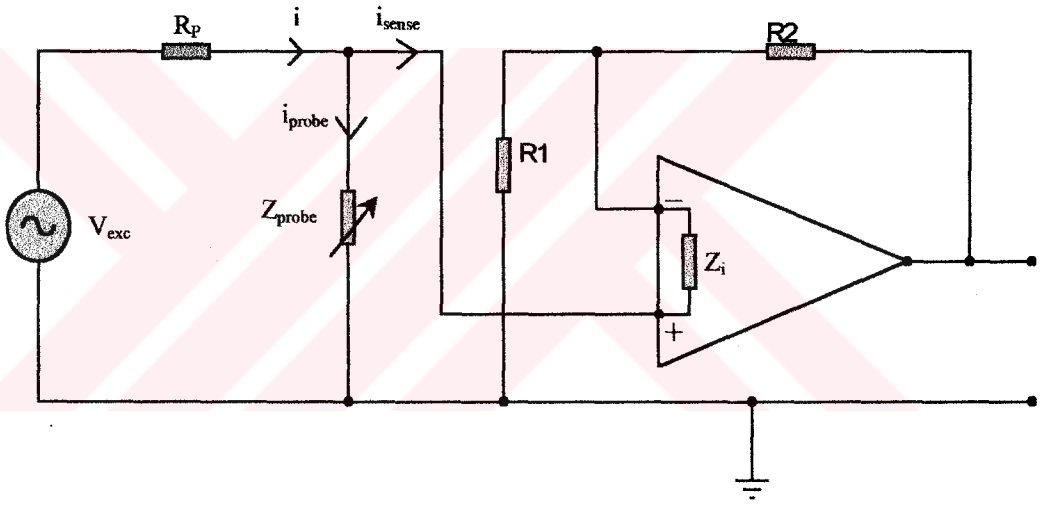

Figure 5.4: Loading effects error due to the changes of probe's impedance.

Z_i is the input impedance of the non-inverting amplifier block (LF411). The perfect amplifier should have infinite input resistance so that any signal could be supplied to it without loading problems. It is thus obvious that as Z_i gets larger compared to the equivalent impedance circuit ($Z_i >> Z_{eq}$),

where, $|Z_{eq}| = \frac{1}{|Z_{probe}|} + \frac{1}{R_p}$

then i_{sense} will be close to zero.

For decreasing i_{sense}, an operational amplifier with non-inverting configuration, LF 411, is used. Although there are more advanced operational amplifiers in the market, they are quite expensive. LF 411 has 50 pA input offset current value when connected as non-inverting mode at room temperature. The gain is fixed and approximately 1.97. Precision metal film resistors (R1, R2) are used for maximising the gain accuracy and for minimising the temperature drift. LF 411 supply bias is by-passed by tantal capacitors for voltage stability (C1, C2). The output is coupled to precision rectifier block with C3 and R3 (low-pass filter) (Figure B4).

5.4 RMS TO DC CONVERTER BLOCK

This block operates as a full wave precision rectifier and averager for pure sinusiodal signals and operates as RMS to DC converter block. This block is well known and often used in industry (Figure B5).

5.5 BIAS SHIFT AND GAIN BLOCK

This block has two sub-parts. LF 411 is used as bias shift unit. The gain is set as unity by R16 and R17 precision metal film resistors. The bias point is adjusted by P2. C16 is used as by-passing the contact noise of the potentiometer. This block is connected to inverting amplifier. Inverting part is set by R15, R14 and P3. P3 is used for gain adjustment (Figure B6).

OVERALL

Various test points are used for signal amplitude, frequency, pre-resistance, bias shift and gain adjustments. IC1, R1 and R2 are metal screened for eliminating capacitive noise couplings (Figure B4). The whole system is metal enclosured and grounded at a single point.

CHAPTER 6

PHYSICAL EFFECTS ON PROBE SENSITIVITY

6.1 EFFECT OF PRE-RESISTANCE VALUE

It should be noted that probe sensitivity can be increased by changing the value of pre-resistance which gives the maximum voltage level (V_Z) between all water and all air media.

The following numerical example will clarify this fact;

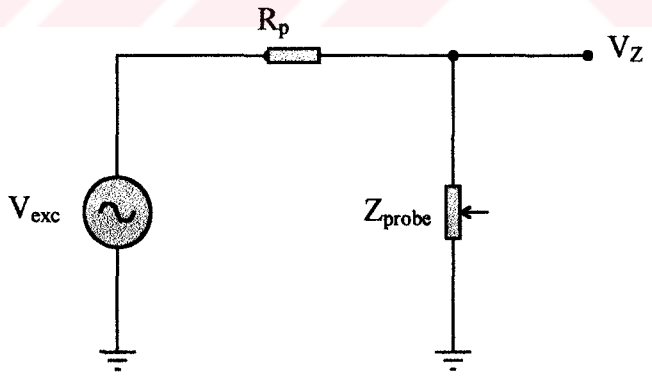

Figure 6.1: Schematic view of resistive divider part of analog signal conditioner circuit.

Shown in figure 6.1, the total current flowing in the resistive divider part of the analog signal conditioner circuit;

$$I = \frac{V_{exc}}{R_p + Z_{probe}}$$

The voltage drop across the probe is;

$$V_Z = I \times Z_{probe} = \frac{V_{exc} \times Z_{probe}}{R_p + Z_{probe}} \qquad (6.1)$$

For V_{exc}=3.18 V and f=500 Hz, the measured values of R_p, the voltage drop across the impedance probe when it is in all water, V_{OW}, and in all air, V_{OA}, are shown in Table 6.1. From equation 6.1, the impedance of the probe in all water (Z_W) and in all air (Z_A) can be calculated.

Table 6.1: Effect of pre-resistance on voltage span when probe 6 is in all air and in all water media.

R_p(kΩ)	V_{OA}(V)	V_{OW}(V)	$\Delta V = V_{OA} - V_{OW}$ (V)	Z_A(kΩ)	Z_W(kΩ)
10	3.17	3.08	0.09	2668.5	312.2
100	3.07	2.41	0.66	2668.5	312.2
400	2.77	1.40	1.37	2668.5	312.2
1500	2.26	0.61	1.65	2668.5	312.2
3000	1.50	0.30	1.20	2668.5	312.2
10000	0.67	0.10	0.57	2668.5	312.2

It is clear that 1500 kΩ pre-resistance gives a larger voltage span (ΔV) than those of the others. It should be also noted that its value is between the value of impedance when the probe is in all water (Z_W) and in all air (Z_A).

A non-dimensional probe ouput voltage may be defined;

$$\overline{V} = \frac{V_m - V_{OW}}{V_{OA} - V_{OW}} \tag{6.2}$$

where V_m is the average of 300 instantaneous voltage outputs taken in 30 seconds. An experiment with two different pre-resistances was conducted at probe 6 (Table C1, Table C2). The following graph in dimensionless form is obtained (Figure 6.2).

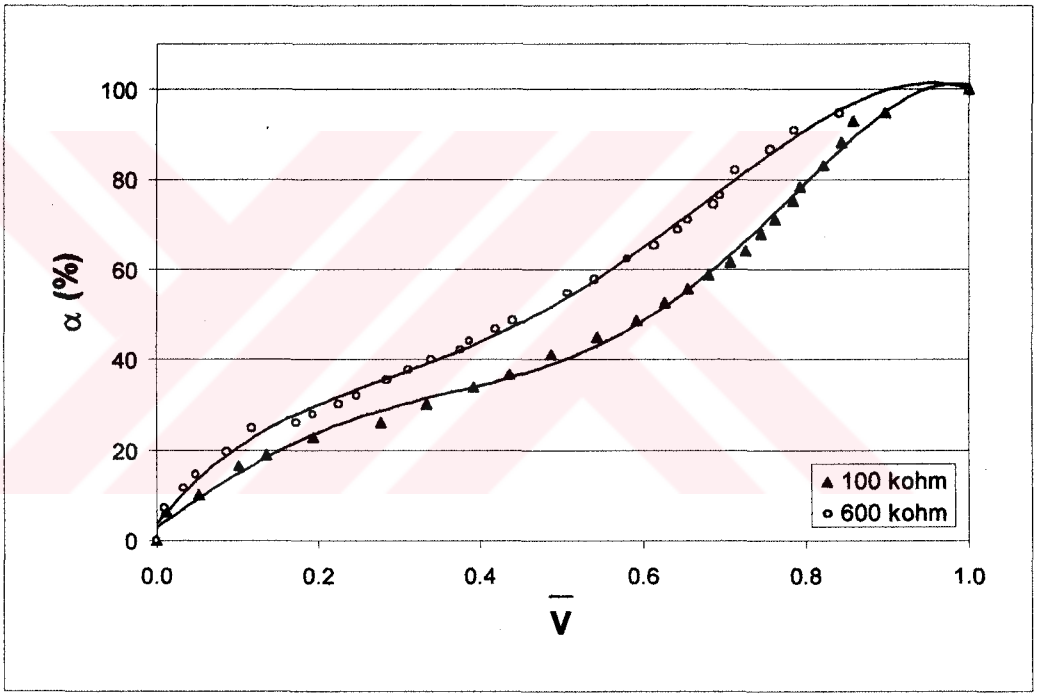

Figure 6.2 : Pre-resistance effect on non-dimensional voltage output of probe 6.

It is obvious that; between definite void fraction values, for instance, between %20 and %40 void fraction values; the circuit with 100 kΩ pre-resistance gives larger change in signal amplitude ($\Delta\overline{V}_{100k\Omega} > \Delta\overline{V}_{600k\Omega}$), on the contrary,

between %80 and %100 void fraction values 600 kΩ pre-resistance value gives larger voltage amplitude ($\Delta\overline{V}_{600k\Omega} > \Delta\overline{V}_{100k\Omega}$).

Since in the typical test matrix of the Joint Research Project, the maximum void fraction expected to be seen in each Feeder will be at most 30%, it should be better to find the appropriate pre-resistance according to the impedance change of probe between all water and air-water mixture of 30% void fraction.

The impedance of air-water mixture of 30% void fraction can be found from equation 6.1 then the appropriate pre-resistance value can be calculated by the computer code written in Fortran 77 [Appendix E1].

The algorythm of the code is as follows: The impedance of the probe in all water and two-phase mixture of 30% void fraction are calculated by the help of equation 6.1 respectively. Then it begins to calculate the voltage drop differences across the probe with a pre-resistance value equal to the probe impedance in all water and it repeats the same calculations by increasing the pre-resistance value by 1 kΩ in each step up to the value of impedance in air-water mixture of 30% void fraction. It compares the voltage drop differences to determine the appropriate pre-resistance value which gives the largest range in voltage difference.

6.2 EFFECT OF EXCITATION FREQUENCY

6.2.1 Polarisation

Excitation frequency of the circuit determines the probe characteristics, whether it is capacitive or resistive.

As it is defined in Chapter 2, the impedance of probe is analytically stated as;

$$|Z| = \frac{R}{\sqrt{(1+R^2.w^2.C^2)}} = \frac{R}{\sqrt{(1+(4.R^2.\pi^2.f^2.C^2))}} \qquad (6.3)$$

In an AC excited circuit, there is a slight amount of voltage drift in all water medium. Dimensionless probe voltage output versus water volume flow rate for 500 Hz frequency is shown in Figure 6.3.

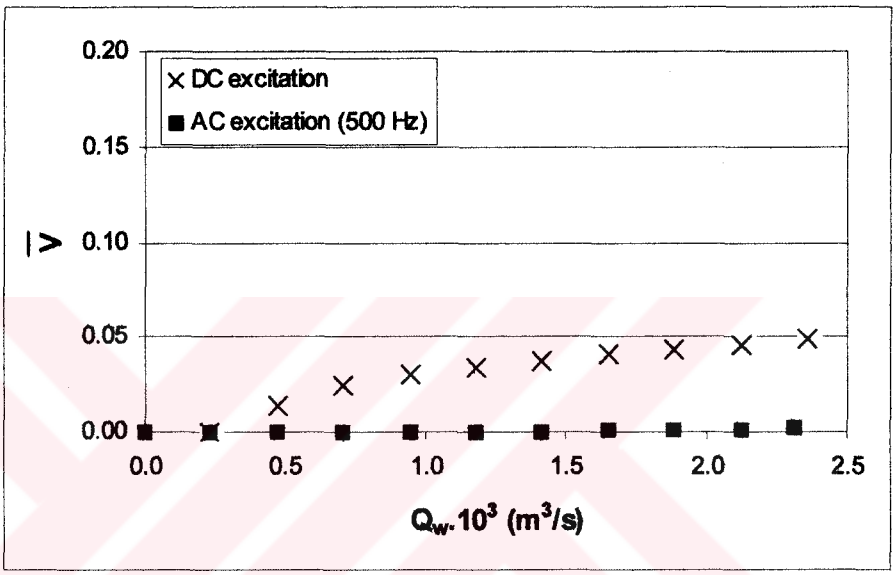

Figure 6.3: Non-dimensional probe voltage output versus water volume flow rate in DC and AC (500 Hz) excitation.

Direct voltage excitation is the easiest and the least expensive technique to use but also it has some disadvantages such as polarisation effect and electrochemical attack.

If the excitation is assured by a direct voltage source then the impedance term becomes purely resistive. Capacitance term will be eliminated since the frequency is equal to zero (Equation 6.3). On the other hand, direct excitation causes a remarkable drift in the probe voltage output in all water medium at different liquid velocities and especially in stagnant water due to the polarisation effect (Figure 6.3, Figure 6.4).

To see the effects of DC excitation voltage; voltage drop across the probe 6 was measured by using a 5V DC voltage source and 100 kΩ pre-resistance value as shown in Figure 6.1. The results are plotted in figure 6.3 and figure 6.4.

As the volume flow rate of water decreases from 2.36×10^{-3} m^3/s (5 ft^3/min) to 0.26×10^{-3} m^3/s (0.5 ft^3/min), the corresponding decrease in the probe voltage output is 5% of the total voltage span when the probe is in all water and in all air media (Figure 6.3).

Electrolysis effect of DC excitation in stagnant water is shown in figure 6.4.

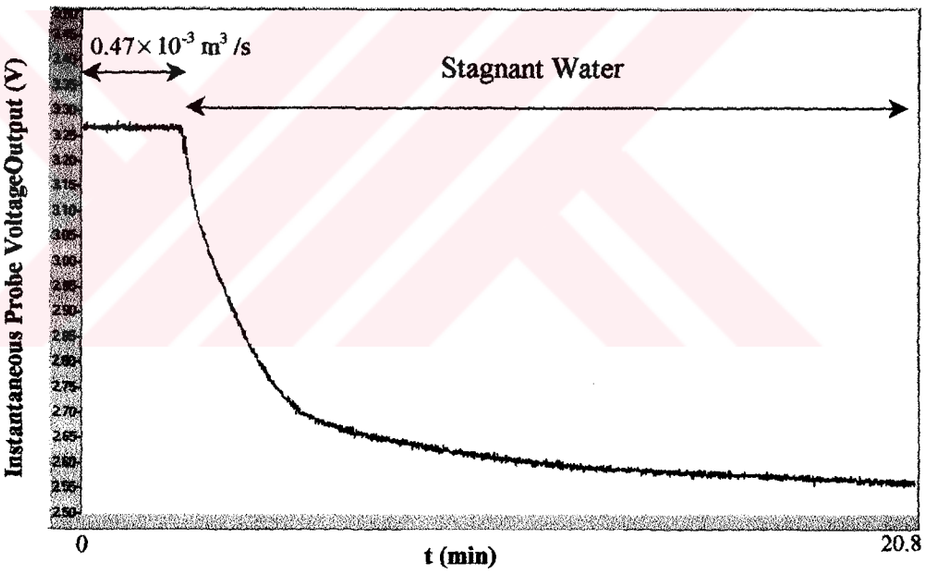

Figure 6.4: Electrolysis effect of DC excitation in stagnant water.

Since the probe voltage output in all air medium is 4.81 V, voltage drop (from 3.27 V to 2.55 V) across the probe is approximately equal to the 46% of the total voltage span when the probe is in all water and in all air media.

These results show that DC excitation gives unreliable voltage outputs in stagnant water and water must flow even with a low velocity to reduce the electrolysis effect of DC excitation.

6.2.2 Voltage Span

Increasing the excitation frequency causes to decrease the impedance range of the probe which corresponds to decrease the voltage span when it is in all water and in all air media.

The calibration test (explained in chapter 7) of probe 10 was conducted with 4 different excitation frequencies (Figure 6.5)[Table C3, C4, C5, C6].

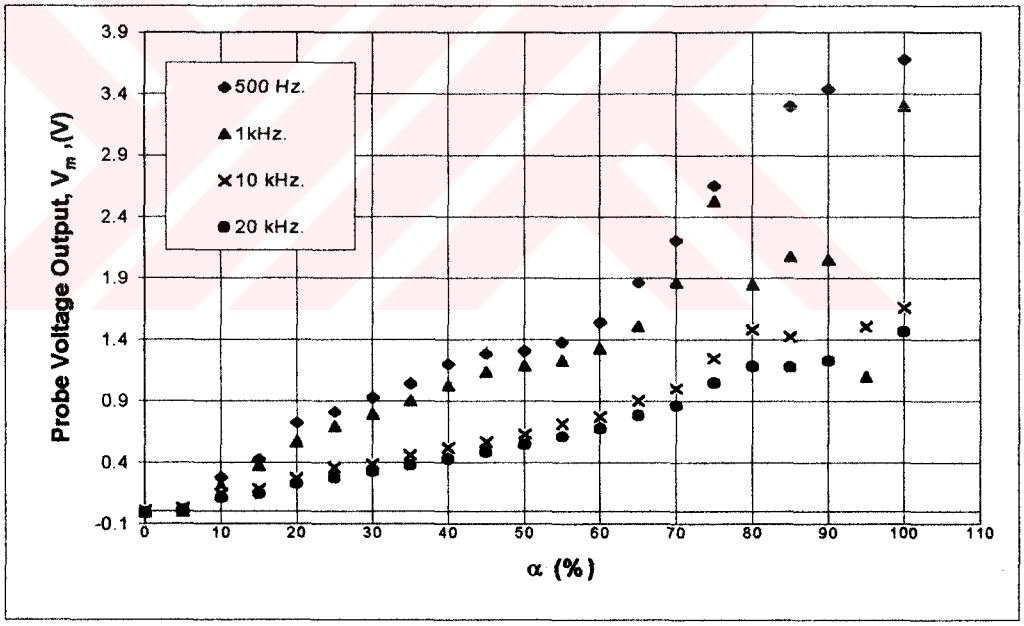

Figure 6.5: Calibration data of probe 10 in 4 different frequencies.

All the probe voltage outputs in all water medium are shifted to 0 to see the voltage span easily. It is clearly seen that 500 Hz frequency gives larger voltage span than those of the higher ones.

6.2.3 Voltage Stability

A statistical parameter, standard deviation (S), is used which is a function of voltage amplitude and gives information about how widely voltage signal values are dispersed from the average voltage value (the mean, V_m). In other words it gives information about the voltage signal fluctuations. The output of this function is a single value representing the average magnitude of voltage signal fluctuation and is given by;

$$S = \sqrt{\frac{\sum (V_i - V_m)^2}{n}}$$

where n is the the number of items in the sample and V_i is the instantaneous voltage value of a sample.

This parameter can be converted to a non-dimensional form by dividing it by the total voltage range between the probe in all water and in all air respectively and calculated with 4 different frequencies (500 Hz, 1kHz, 10 kHz, 20 kHz) in the calibration test of probe 10.

$$\bar{S}(\%) = \frac{S}{V_{OA} - V_{OW}} .100$$

For a constant void fraction value; volume flow rate of water and air and instantaneous probe output voltages were logged at 10 samples per second for 30 seconds. At the end, all 300 instantaneous probe output voltage data were analysed for the voltage fluctuations (Figure 6.6)(Table C3, C4, C5, C6).

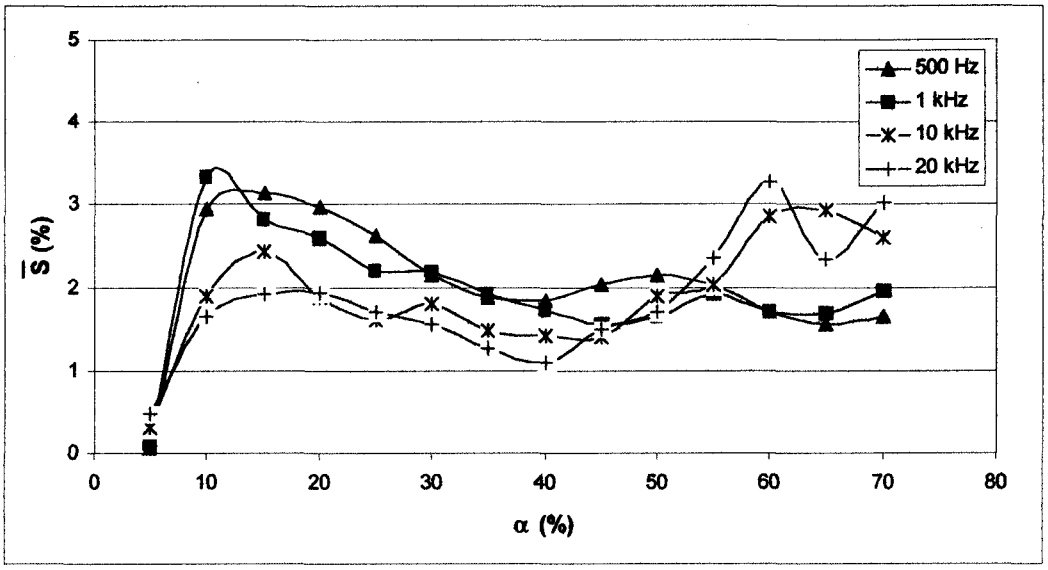

Figure 6.6: Non-dimensional standart deviation, $\bar{S}$ (%), versus void fraction for three different frequencies.

As it is shown in figure 6.6; generally under 50% of void fraction values, high excitation frequencies (10 kHz and 20 kHz) give more stable voltage outputs than those of low excitation frequencies (500 Hz and 1 kHz). On the contrary, after 50% void fraction values, low excitation frequencies give more stable voltage outputs. The same experiment was done with probe 6 in a horizontal Feeder. It was found that $\bar{S}$ increases with the void fraction (Figure 6.10). From figure 6.6, it can be concluded that there are uncertainties in bubble distribution within the flow in inclined Feeders. The probe tip may be exposed to air slugs continuously.

6.3 EFFECT OF FLOW REGIME

The main mechanism involved in forming the different flow regimes are transient effects, geometry effects, hydrodynamic effects and combinations of these effects.

Transients occur as a result of changes in system boundary conditions, for instance, opening and closing the valves cause transient conditions. Geometry effects occur as a result of changes in pipe-line geometry or inclination. In the absence of transient and geometry effects, flow regime is entirely determined by flow rates, fluid properties and pipe diameter.

In the present experimental facility; each Feeder is connected to the lower half of the Header at different inclination and they have two different inner diameters as explained in chapter 4. This causes occurrence of different flow regimes in each Feeder even if the void fraction is the same. An other factor which causes to occur different flow regimes in each Feeder is the change in volume flow rate of air and water. Flow regimes can be observed by recording the flow with a video camera since the Header and Feeders are transparent acrylic.

Depending on the probe's geometry, the distribution of electric field is not uniform in the cross-section of the pipe especially near the electrodes then the probe voltage output is dependent on the radial location of the gas phase and axial distance from the probe tip even if the void fraction is the same as shown in figure 6.7.

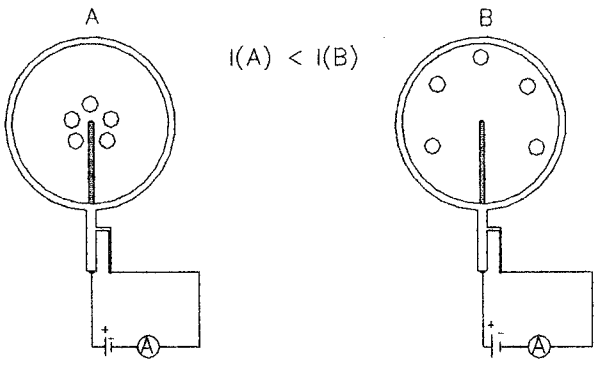

Figure 6.7: Radial location of gas phase in probe cross section

The detected void fraction in case of A is higher than that of B.

The same void fraction value can be obtained by mixing water and air with different volume flow rates. Calibration tests with 3 different initial water volume flow rates were performed (Figure 6.8) by using probe 6 with 500 Hz excitation frequency and 409 kΩ pre-resistance.

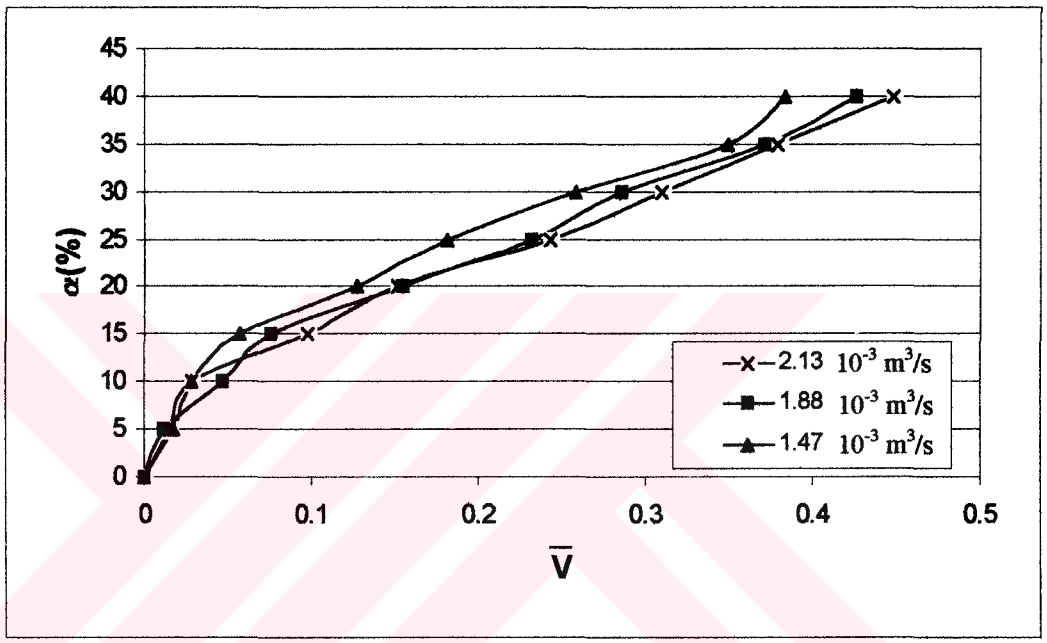

Figure 6.8: Calibration data of probe 6 with different initial water volume flow rate.

A non-dimensional increase in initial water volume flow rate may be defined for this case:

$$\Delta\bar{Q}_w(\%) = \frac{(2.13-1.47)\times10^{-3}}{1.47\times10^{-3}}.100 = 45\%$$

For a constant non-dimensional probe voltage output, the difference in void fraction percent obtained from Figure 6.8 is maximum 4% in most cases upto 40% void fraction.

This difference can be attributed to the different flow regimes occurence after the mixing.

There is a poor accuracy in void fraction data obtained in especially stratified and annular flow regimes where the probe tip can be exposed to all air medium.

The calibration data in stratified flow are obtained at probe 6 with different excitation frequencies to see also the effect of frequency. Calibration procedure will be explained in chapter 7. Probe voltage output is converted to non-dimensional form for comparison .(Figure 6.9)[Table C7].

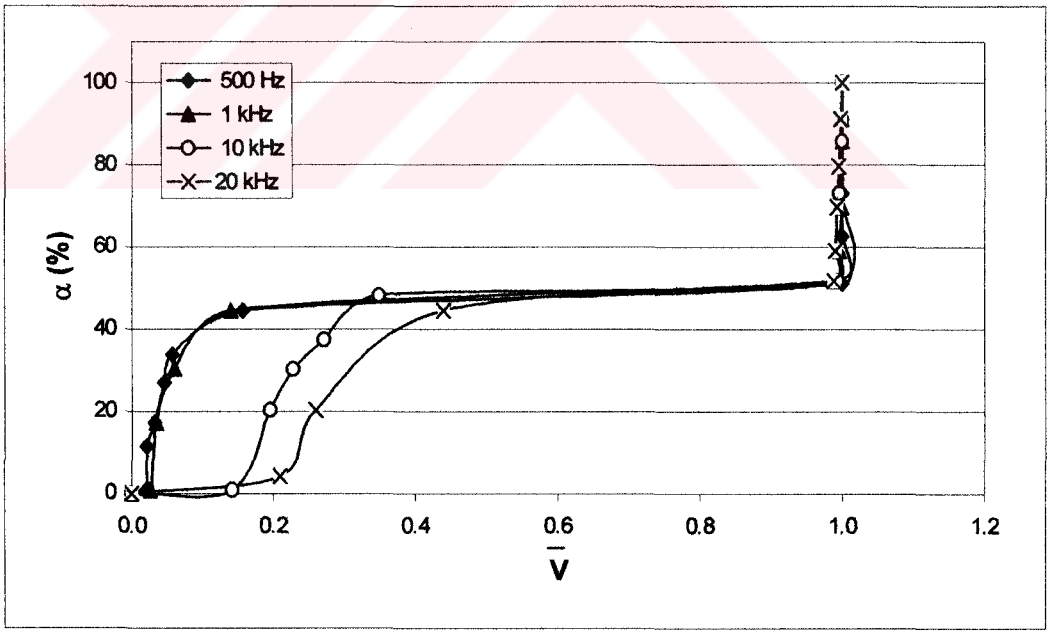

Figure 6.9: Calibration data of probe 6 obtained in stratified flow regime.

It is apparent that after 50 % void fraction values (α=0.5) when the probe tip is exposed to all air medium, the non-dimensional probe voltage output approachs to voltage output in all air medium.

During the calibration tests, different flow regimes are observed and recorded with camera (Appendix D). Depending on the configuration of the calibration mixer and the position of the probe, as the void fraction increases, the tip of probe 6 can be exposed to the all water and all air media. The oscillatory voltage outputs are shown in figure 6.10.

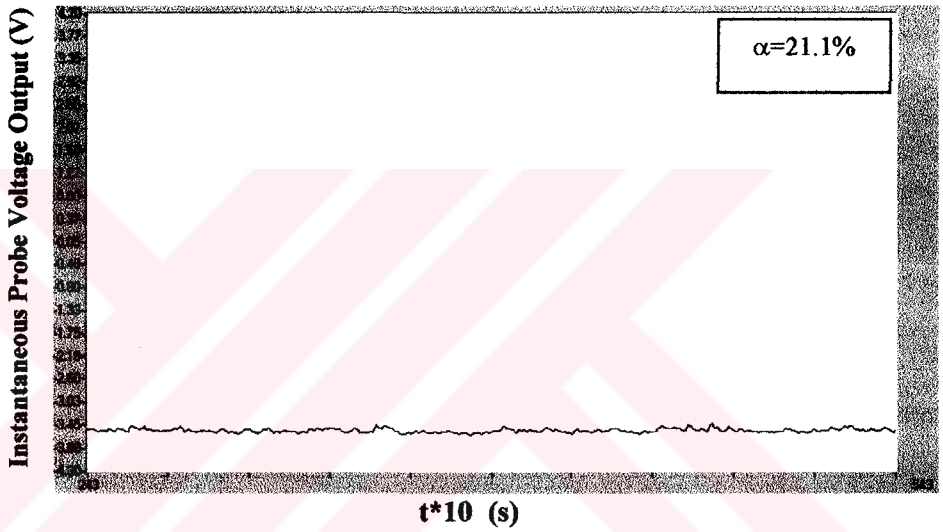

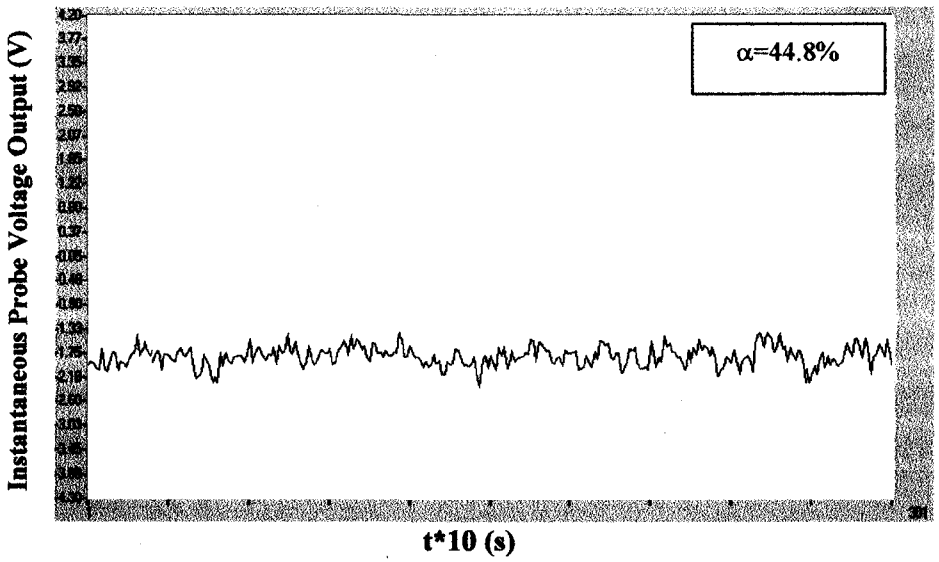

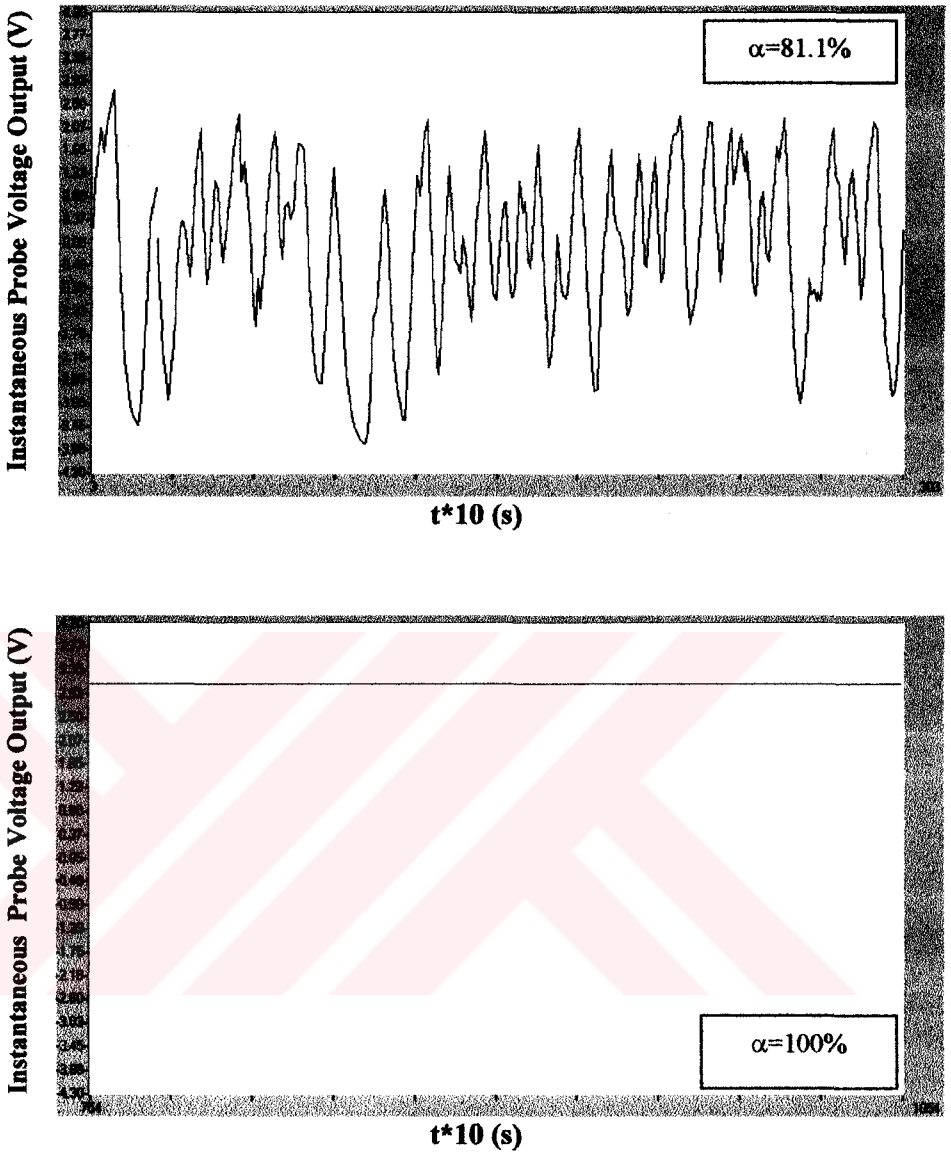

Figure 6.10: Screenshots of data acquisition program in different void fraction values.

6.4 EFFECT OF WATER TEMPERATURE

Conductivity of water is related to the nature and concentration of ionized substances present in the solution and to the temperature of the water itself.

Pure water consists almost entirely of H_2O molecules and is a poor conductor of electricity because it does not ionize to any great extent [36].

Ionization of water results in the production of H^+ and OH^- ions. At room temperature, one in a billion water molecules can ionize even in the absence of electric current;

$$H_2O \rightleftharpoons H^+ + OH^-$$

The conductivity of water is the sum of the conductivities of the individual species of positive and negative ions. The mobility of the ions depends on the temperature so the conductivity of water depends on its temperature (Figure 6.11).

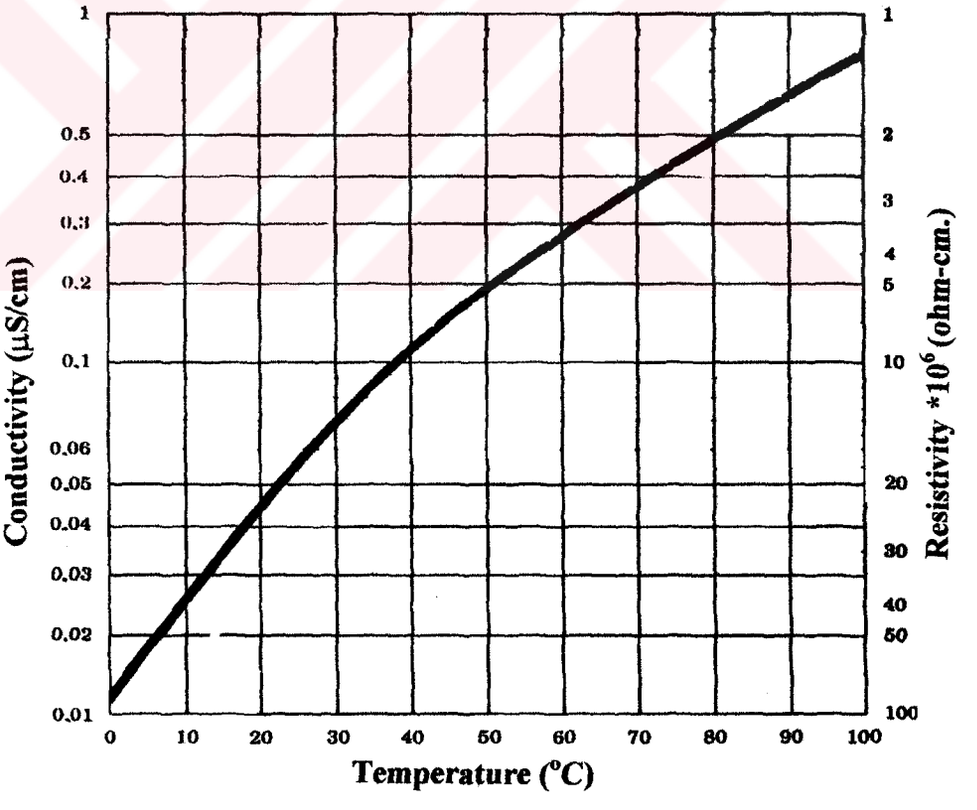

Figure 6.11: Conductivity of pure water versus temperature[36]

To determine the water temperature effect on probe impedance, the following test was done with the impedance probe 6;

- Temperature of water was measured at the exit of Feeder by means of a digital thermometer [A14].

- 10 kW electrical heater was immersed in the water storage tank and its power was adjusted by a rheostat for controlling the temperature of water circulating in the system.

Tests were performed with 3 different excitation frequencies (500 Hz, 1 kHz, 10 kHz) with 409 kΩ pre-resistance and for a temperature range from 16.9 °C to 26.3 °C [Table C8]. Impedance change of probe versus water temperature is shown in figure 6.12.

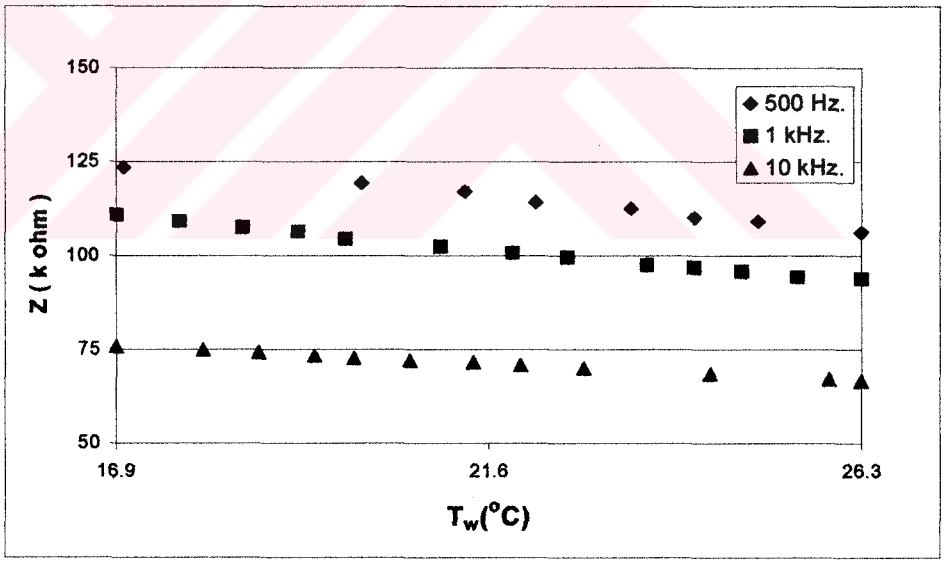

Figure 6.12: Impedance change of probe 6 versus water temperature.

A non-dimensional impedance, $\bar{Z}$, can be defined;

$$\bar{Z} = \left(\frac{Z_{16.9\,^{\circ}C} - Z_{T\,^{\circ}C}}{Z_A - Z_{16.9\,^{\circ}C}} \right)$$

Variation of non-dimensional impedance with the water temperature is shown in figure 6.13.

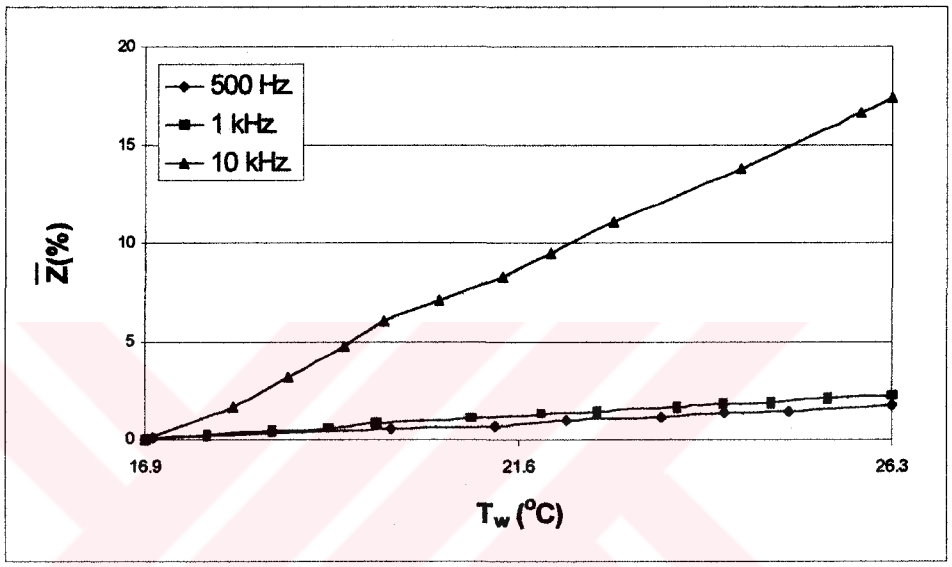

Figure 6.13: Non-dimensional impedance versus water temperature.

Similar tests were also conducted with probe 7 in stagnant water to make it possible to obtain lower water temperatures. Probe resistance and capacitance variations due to water temperature variations between 10.9 °C and 23.2 °C were measured with HP 4262A LCR Meter [A15] for 3 excitation frequencies (120 Hz, 1 kHz, 10 kHz)[Table C9]. Impedance, Z, was calculated analytically according to the equation 6.1 and it is shown in figure 14.

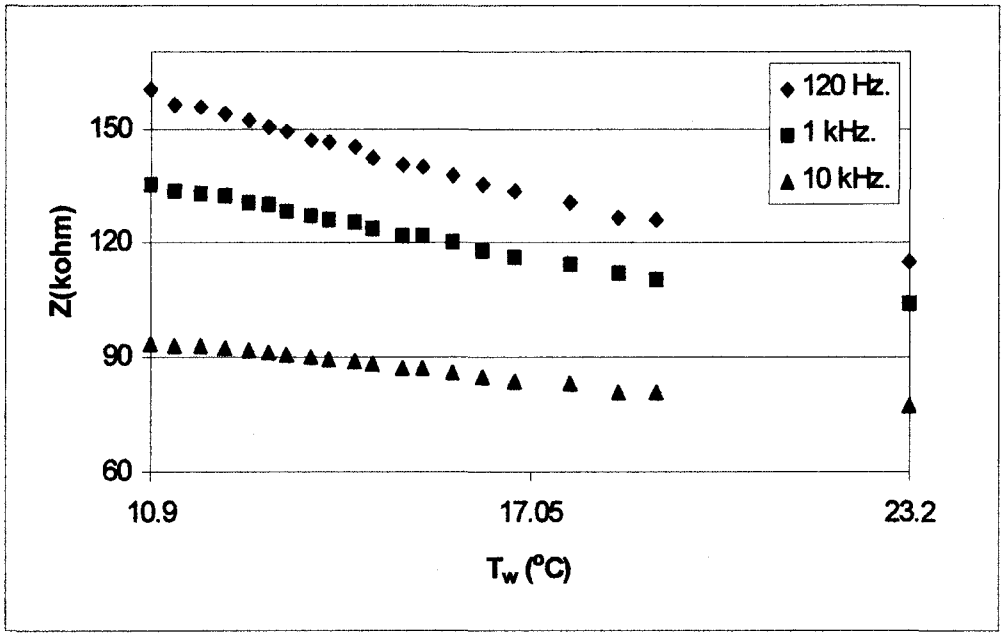

Figure 6.14: Impedance change of probe 7 versus water temperature in stagnant water.

A non-dimensional probe impedance, $\overline{Z}$, may be defined for stagnant water case as follows:

$$\overline{Z} = \left(\frac{Z_{10..9\,^\circ C} - Z_{T\,^\circ C}}{Z_A - Z_{10..9\,^\circ C}} \right)$$

Variation of non-dimensional impedance with the water temperature is shown in figure 6.15.

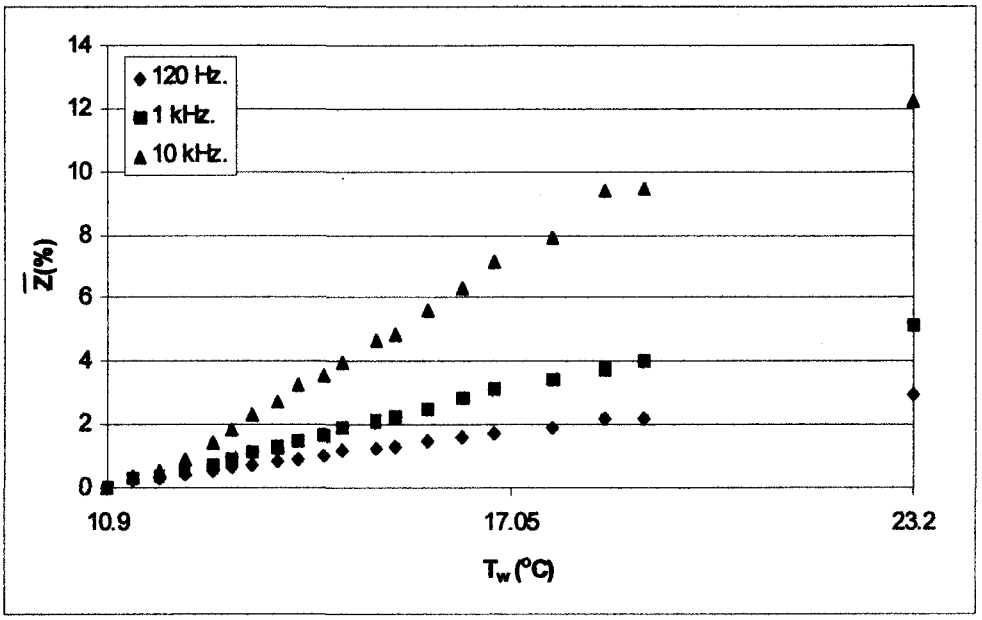

Figure 6.15: Non-dimensional impedance versus water temperature.

It is seen from figure 6.13 and figure 6.15 that at lower excitation frequencies, water temperature effect on the probe voltage output is less than those of the higher ones.

Probe impedance change due to the water temperature causes a shift in the probe voltage output in all water medium.

A typical calibration test results for 3 different water temperature values are shown in figure 6.16. Probe voltage output in all water medium at T_w = 17.6 °C is gained and shifted to – 4 V and probe voltage output in all air medium is around 4 V. Detailed explanation about the calibration procedure is given in chapter 7. Calibration data of probe 6 for three different water temperatures were logged and are shown in table C10, table C11 and table C12.

It is apparent that; for a constant probe voltage output, the void fraction found from the calibration curve is quite different for different water temperatures (Figure 6.16).

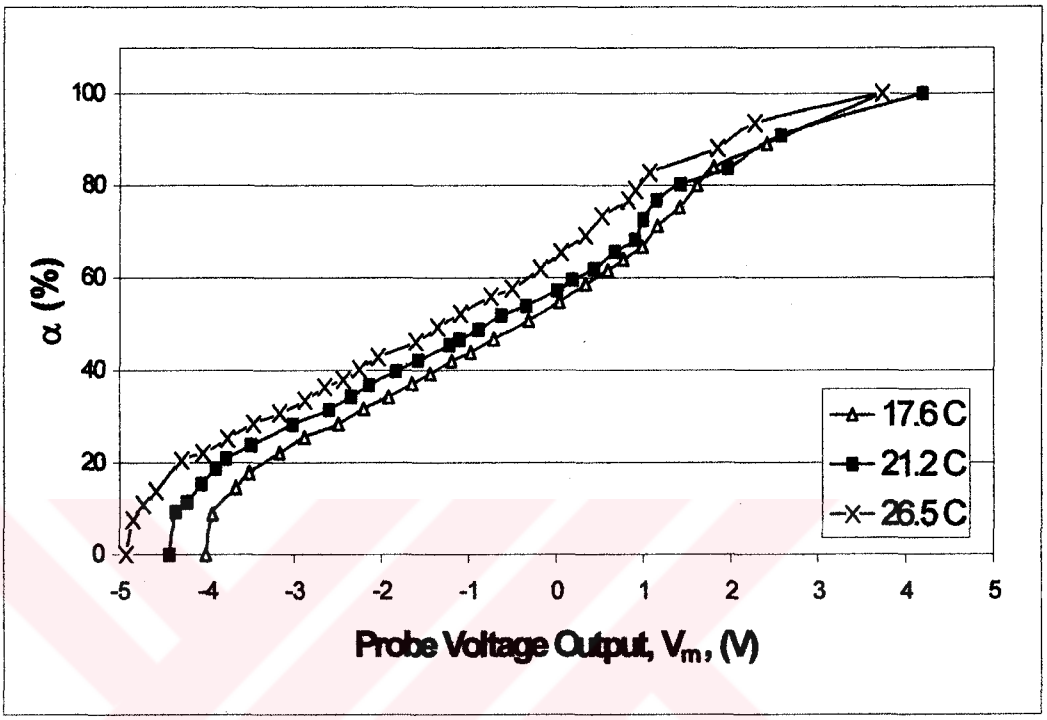

Figure 6.16: Calibration data of probe 6 at 3 different water temperatures.

To eliminate the voltage shift due to the changes in water temperature, a non-dimensional probe output voltage may be defined;

$$\overline{V} = \frac{V_m - V_{OW}}{V_{OA} - V_{OW}}$$

The probe voltage output data of figure 6.16 are converted to the non-dimensional form and shown in figure 6.17.

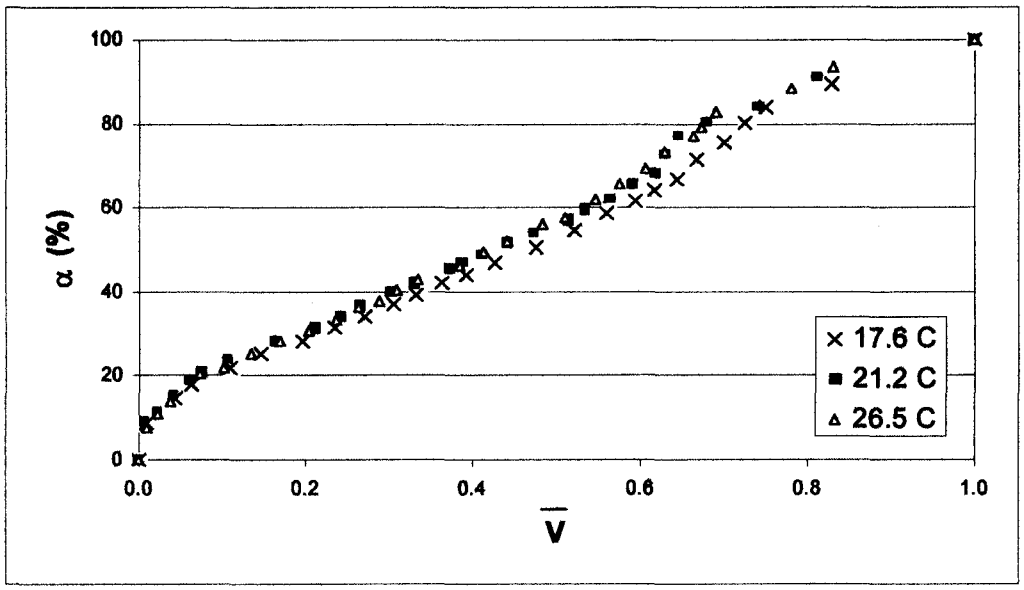

Figure 6.17: Calibration data of probe 6 in non-dimensional form at 3 different water temperatures.

As a result; during the calibration test of the impedance probes, it is necessary to convert all the probe voltage outputs to non-dimensional form in order to minimize the effect of water temperature.

6.5 EFFECT OF MOISTURE

At high void fractions, when the agitated slug and annular flow regimes occur, the probe can be exposed completely to all air medium instantaneously. Therefore, probe voltage output in all air medium, V_{OA}, should be measured instantaneously when the probe is completely removed from water medium. Otherwise, by the time, probe voltage output in all air medium, V_{OA}, continues to increase.

A typical test was conducted with probe 7 at 500 Hz excitation frequency. The instantaneous probe voltage output in all air medium versus time is shown in figure 6.18.

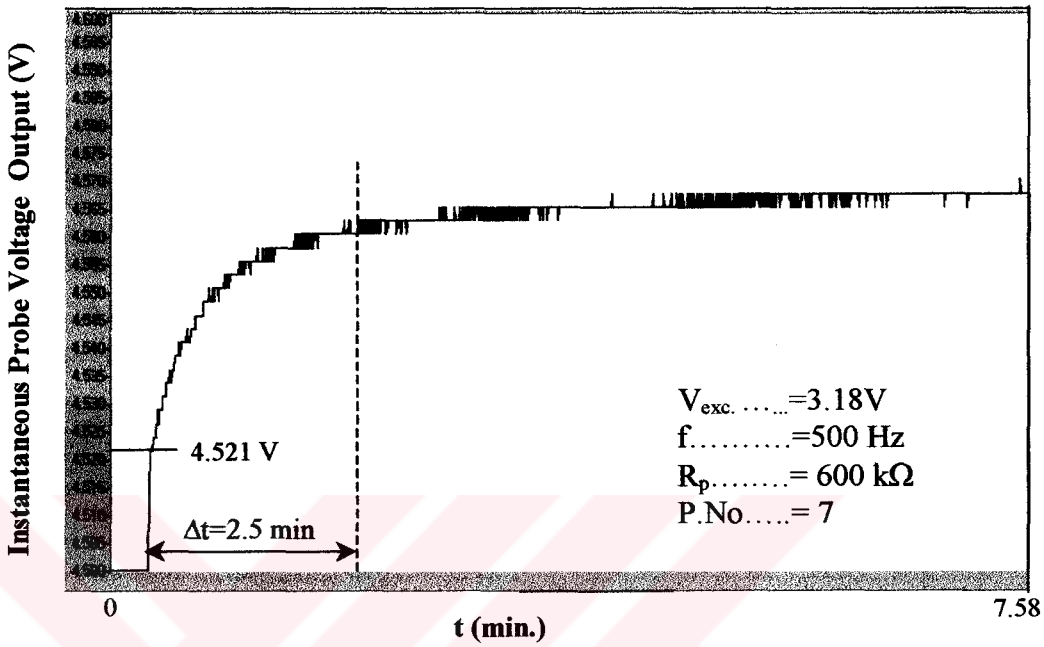

Figure 6.18: Effect of moisture on probe voltage output in air medium.

When the probe is removed from a liquid enviroment, the instantaneous probe voltage output is 4.521 V. By the time, in 2.5 minutes, it increases up to 4.562 V. The voltage difference between 4.521 V and 4.562 V, 0.04 V, introduces no significiant effect in non-dimensional probe voltage output where the probe voltage output in all water medium, V_{OW}, is 0.808V :

$$\overline{V} = \frac{4.562 - 4.521}{4.521 - 0.808} = \frac{0.04}{3.713} = 0.011 = 1.1\%$$

Moisture coating the insulator between the electrodes may be the cause.

6.6 CONCLUSION

Excitation frequency was selected as 500 Hz in order to get away from the uncertainty of DC excitation, to minimize the water temperature effect on probe impedance, to increase the voltage span of the probe voltage output when it is all water and in all air media, to minimize the effects of capacitance variations of the impedance probes and also to obtain more stable output of signal generator.

Depending on the readings from the HP 4262A LCR Meter (Table C9), it is clear that for 500 Hz excitation frequency, the probe impedance is almost resistive according to the equation 6.1.

CHAPTER 7

CALIBRATION OF IMPEDANCE PROBES

7.1 CALIBRATION TEST FACILITY

Two-phase flow test facility except its mixer and Header (Figure 7.1) were used for the calibration of the probes on the Feeders.

7.1.1 Calibration Mixer

A new mixer was made of copper and manufactured in cylindrical shape with 35 mm axial length. There is a flange at the downstream of the mixer that is coupled to the Feeder.

A gate valve to control the air flow rate and a check valve to prevent water to enter into the air side were inserted in the air line before the air inlet part of the mixer (Figure 7.1).

To fix the air line to the mixer, a hole (ID 12 mm) was drilled and a 90° elbow which has a threaded pipe joint at one end was welded at that point. A pipe (ID 10 mm) which was made of copper and open at one end was screwed to the 90° elbow joint. This pipe was centered along the mixer body.

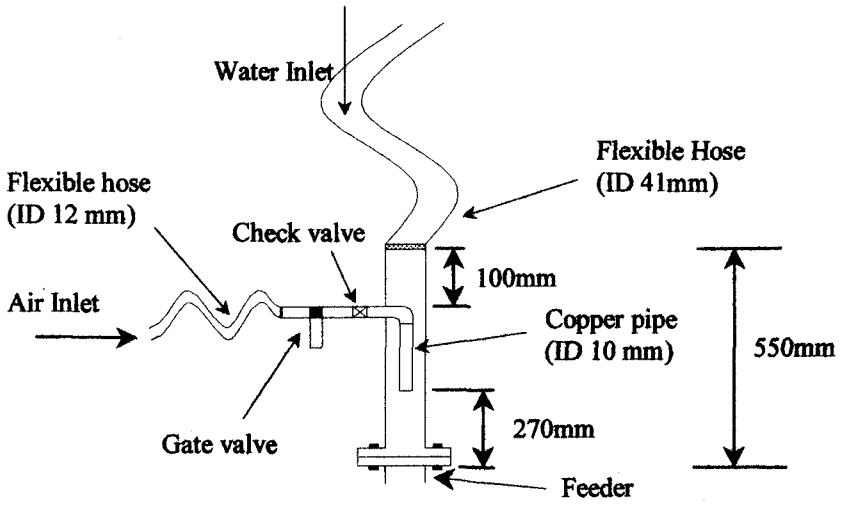

Figure 7.1: Schematic view of the calibration mixer.

7.1.2 Water Supply Line

Water supply line was connected to the inlet of the mixer (Figure 7.2) after turbine type flow meter with a flexible hose (ID 41 mm).

7.1.3 Air Supply Line

Air supply line was connected to the air inlet of the mixer with flexible hose (ID 10 mm) after the pressure transducer (Figure 7.2).

7.1.4 Data Acquisition System

The analog voltage outputs of differential pressure transmitter connected to the up and downstream of the orifice, of the turbine type flow meter and of the impedance probes are conditioned and connected to PCLD 812 PG A/D Converter Card [A10] with two PCLD 789D Amplifier and Multiplexer Card [A11] via the analog signal conditioner circuits.

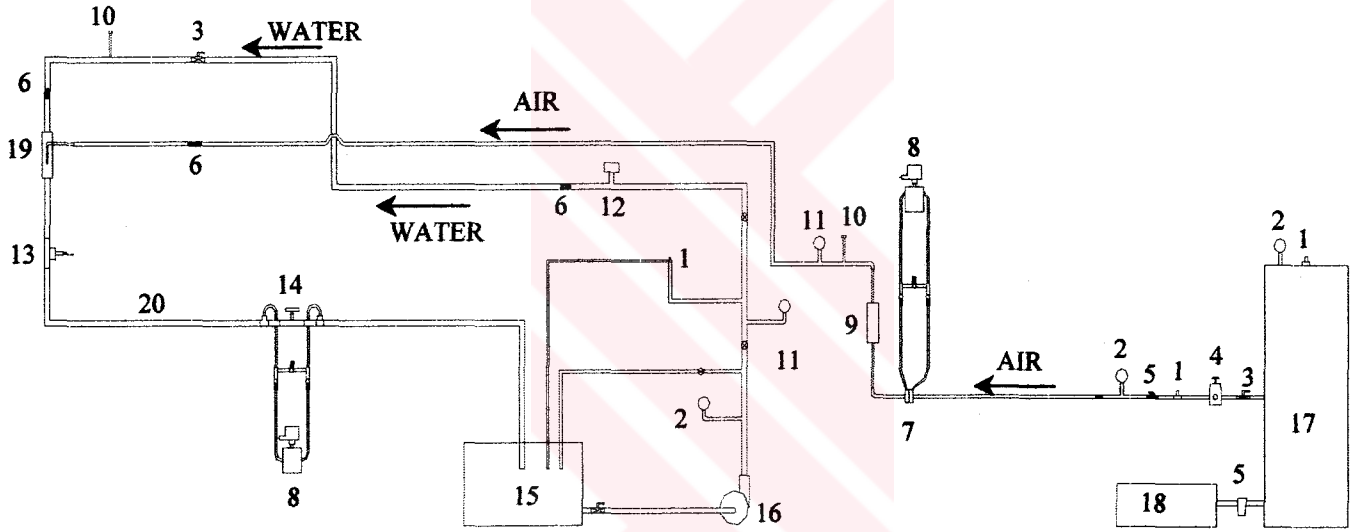

1-RELIEF VALVE
2-PRESSURE GAGE
3-GATE VALVE
4-AIR REGULATOR VALVE
5-AIR FILTER
6-CHECK VALVE
7-ORIFICE METER
8-DP TRANSMITTER
9-ROTAMETER
10-PRESSURE TRANSDUCER
11-TEMPERATURE GAGE
12-TURBINE FLOWMETER
13-IMPEDANCE PROBE
14-GLOBE VALVE
15-WATER TANK
16-WATER PUMP
17-AIR TANK
18-AIR COMPRESSOR
19-MIXER
20-FEEDER

Figure 7.2: Schematic view of calibration test facility.

7.2 CALIBRATION PROCEDURE

Calibration procedure of the probes on the Feeders and on the Header will be explained separately.

7.2.1 Calibration of the probes on the Feeders

The calibration tests basically consists of 4 stages that will be described in this section.

7.2.1.1 Preparation

Probe on each Feeder is calibrated at its own position and the Feeder is detached from the Header and it is kept at its original position by some wood supports. The calibration mixer is connected to the Feeder.

Air is compressed in three storage tanks by means of the air compressor. Once the air storage tanks reach the required pressure level (approximately 4 bar) the compressor is turned off.

After adjusting the proper pre-resistance value for each impedance probe and the excitation frequency in the analog conditioner circuit (500 Hz)(Chapter 6), in order to use the dynamic range most efficiently, the probe voltage output is adjusted to around –4 V and to +4 V when the probe is in all water and in all air media respectively by the bias and shift part of the analog signal conditioner circuit (Chapter 5).

The water temperature and concentrations of impurities can vary in daily labaratory conditions. To avoid the shift in probe voltage output when it is in all water medium, output voltages are converted to a non-dimensional form (explained in chapter 6). Therefore, the output voltages of the probe when it is in all water and in all air media are determined and logged.

Voltage outputs of turbine flow meter and of differential pressure transmitter connected to the orifice are converted to volumetric flow rate units by using equations of calibration fits [33], in a user program of data acquisition software.

7.2.1.2 Start of a Calibrational Run

The water circulating pump is turned on and water is allowed to flow in the system. To avoid severe oscillations which may take place in the calibration test facility due to the high volume flow rates of water and air, volume flow rate of water flowing in the system is adjusted to approximately 1.75×10^{-3} m^3/s by means of the by-pass valve placed after the water circulating pump.

Volume flow rate of air is varied with the regulator valve placed after the air storage tanks and increased step by step to obtain different void fraction values between 0 and 1 but the oscillations in the system does not allow to do this. To obtain high void fraction values; after a certain void fraction value (approximately 40 %), water flow rate is decreased by means of the by-pass valve and the flow control valve placed after the water circulating pump while the air flow rate remains almost constant.

7.2.1.3 Data Logging

Actually there are two types of "averaging method" available in Genie software program which is used in data acquisition system. These are "moving average" and "whole average". If the "moving average" method is selected then the input is averaged over a number of samples. In the calibration circuit, this will tend to smooth out instantaneous voltage fluctuations of turbine flow meter and of DP transmitter connected to the orifice. "Whole average" method is used to take an average of all samples. For a constant void fraction value, when the system reachs steady state, the data logging on the computer starts. All the moving average voltage outputs of turbine type flowmeter and of differential pressure

transmitter connected to the orifice are monitored with 10 samples per second for about 30 seconds and logged in a file where necessary. Whole average of probe output voltages is entered as an input in a user program to make the probe output voltage non-dimensional and monitored in experimental conditions (Figure 7.4).

For a constant void fraction value, a single whole average (mean) of non-dimensional probe voltage output is obtained. A graph of void fraction (%) versus non-dimensional probe output is plotted for each probe.

Finally, a curve fit is applied to the data relating the void fraction and non-dimensional probe voltage output (Figure 7.3).

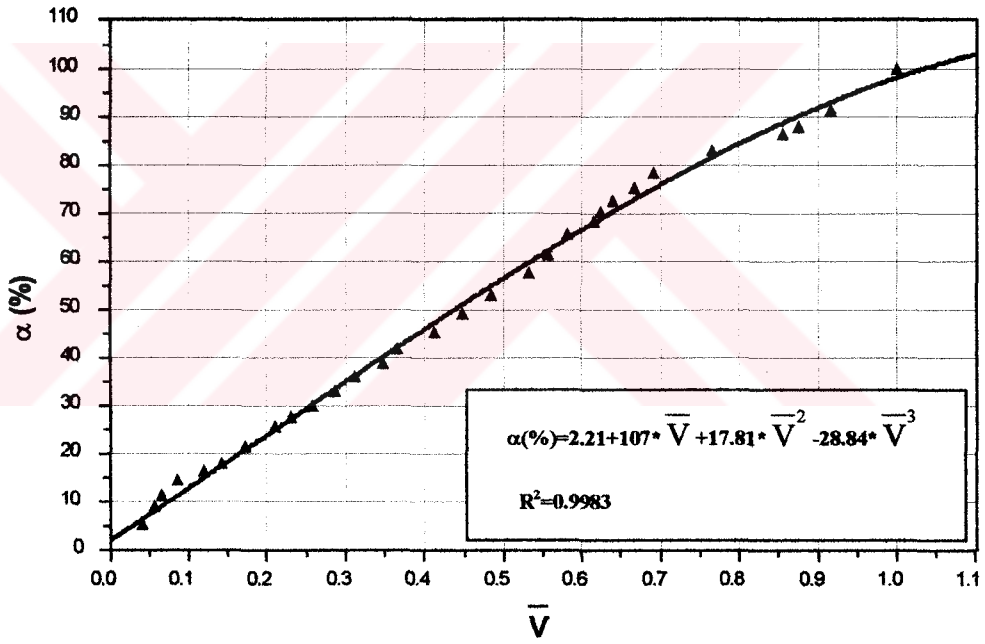

Figure 7.3: Calibration data and curve fit of probe 8.

A value of correlation coefficient, R^2=1.0 means that curve data fit equation passes through every data point. Detailed explanation about the correlation coefficient, R^2, is given in Appendix C.

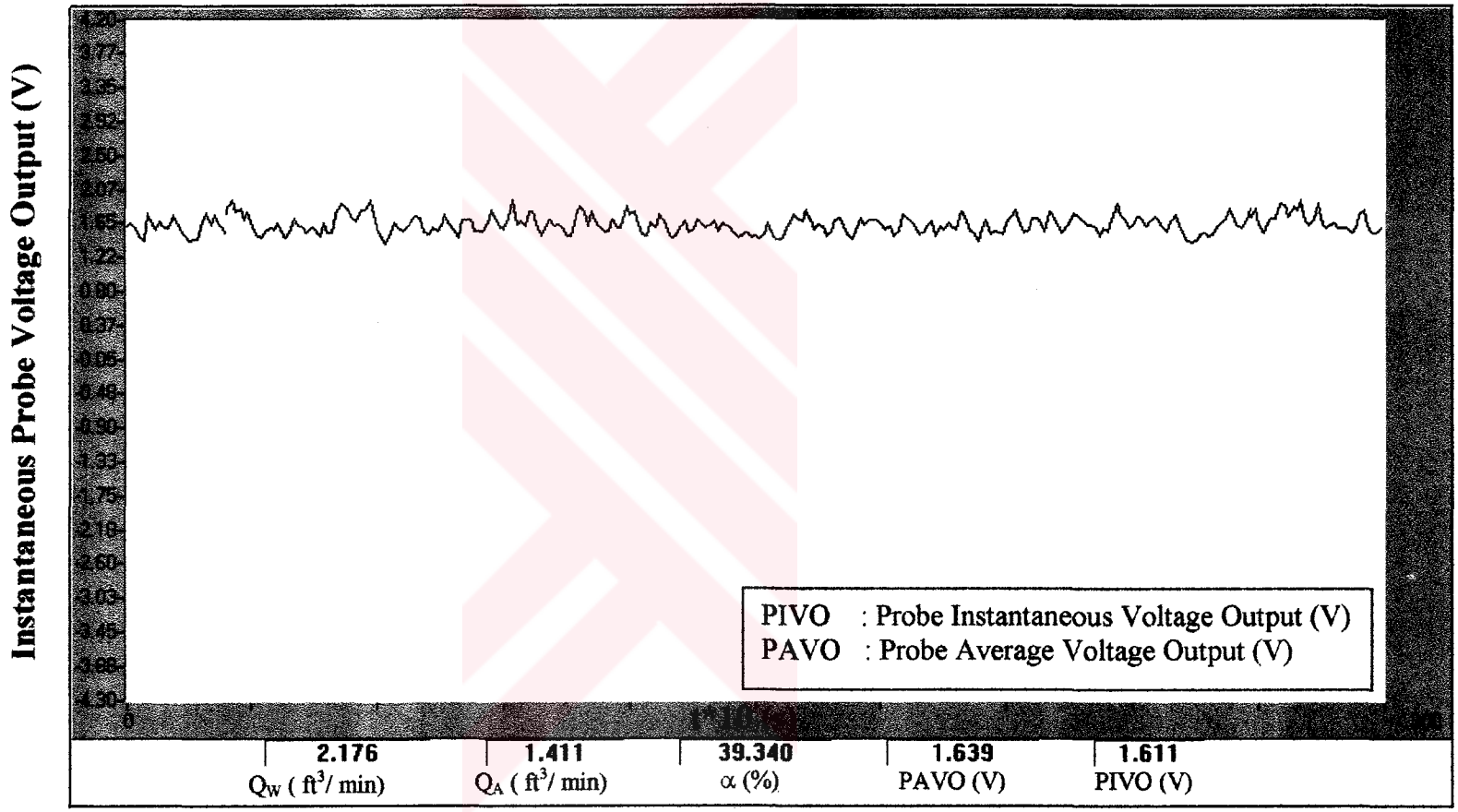

Figure 7.4: A screenshot of data acquisition software program used in calibration tests.

Results of calibration data and calibration curves of all impedance probes are given in Appendix C.

7.2.1.4 System Shutdown

The system shutdown starts with turning off the water circulating pump. Afterwards air regulator valve is closed. Ultimately, software program is stopped and all the system components including the laboratory equipment are finally checked for the following calibration tests.

7.2.1.5 Working range of system parameters

Table 7.1: Working range of system parameters.

Volume flow rate of water $\times 10^3$ .....(m^3/s)	0 - 1.830
Volume flow rate of air $\times 10^3$ .....(m^3/s)	0 - 1.850
Water temperature .....(^oC)	21.2 – 25.6
Air temperature .....(^oC)	21.5 - 26
Water gage pressure at the exit of water pump. (Pa)	0 – 2.15
Air gage pressure at the exit of the orifice .....(Pa)	0 - 1.35

It should be noted that pressure gage in the water supply line is located after the water circulating pump before the by-pass line. Since by-pass valve is not fully closed during the calibration tests, water pressure will not be the same at the water line before mixing.

7.2.1.6 Repeatability of Calibration Test

The repeatability tests were conducted with probe 6 at a horizontal Feeder. During the calibration tests, water temperature was kept constant between 21.7

and 22.4 °C. Four different runs were performed with the same experimental conditions (Figure 7.5).

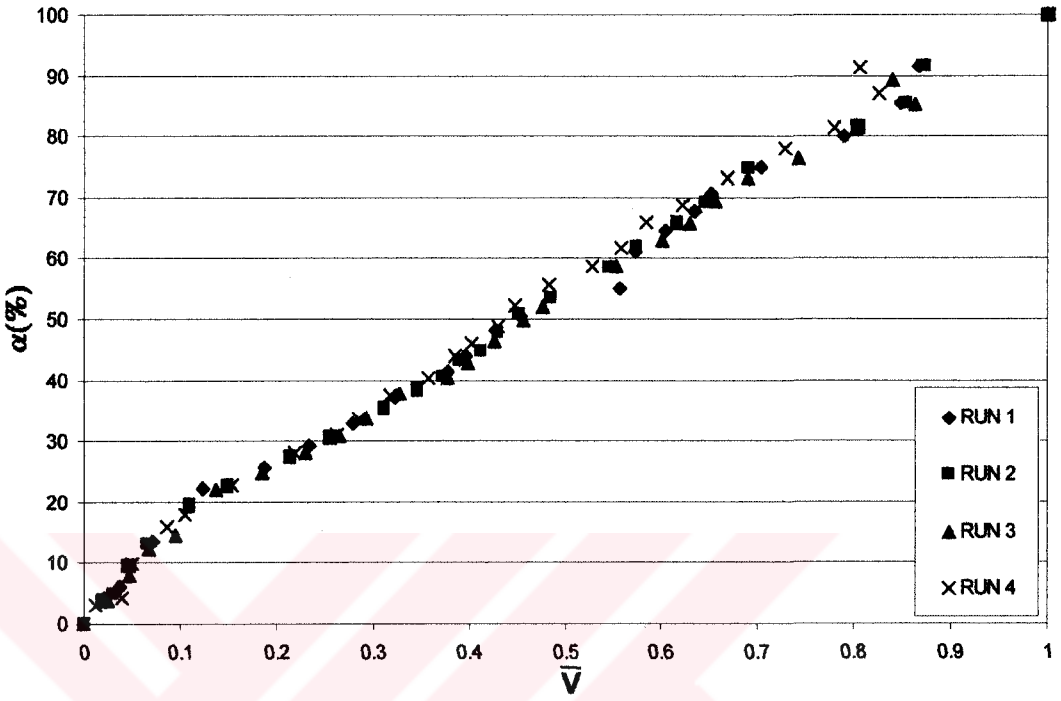

Figure 7.5: Calibration data of probe 6 in 4 different runs in the same experimental conditions.

The repeatability of the calibration test is almost satisfactory up to 50% void fraction in which the data are within 2% error band at most. Between 50% and 70% void fraction values, the data are within almost 4% error band and after 70% void fraction, the data are within 8% error band since the flow becomes highly agitated and the probe probably is exposed to the all air and to all water media haphazardly (Figure 7.6).

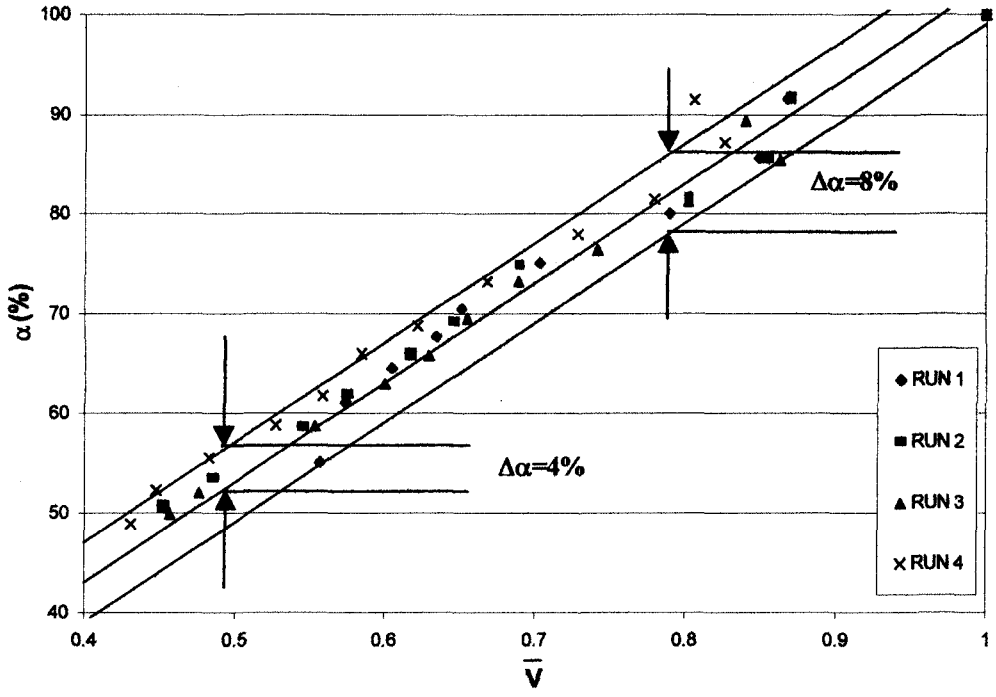

Figure 7.6 : Repeatability of calibration test of probe 6 in a horizontal Feeder.

7.2.2 Calibration of probes on the Header

Generally, the probes on the Header are used as a water/air level indicator. Because of the Header geometry and probe locations, there is no chance to observe the probes' behaviour in all flow patterns like those of the probes on the Feeders .

In actual conditions, mostly, stratified flow regime is expected to occur except the inlet part of the Header where bubbly mixing takes place because of the water falling from the inlet nozzle when especially the Header is not completely full of water. Therefore calibration process is only possible for the stratified flow regime condition.

7.2.2.1 Preparation

A calibration method applied for the stratified flow regime in the Header was as follows:

A millimetric paper was placed at one circular face of the cylinder as shown in figure 7.7.

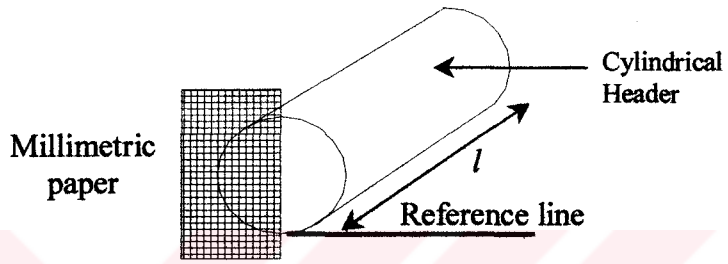

Figure 7.7: Apparatus for the level indication on the header

Reference line can be determined by means of the probe extensions inside the Header (Figure 7.8). Once the Header is completely full of water, the globe valve of the Feeder which is connected to the bottom of the Header is slightly opened and the water level inside the Header begins to drop slowly. At the same time; voltage output of probe 4 is monitored. When the tip of probe 4 is in contact with the air medium, a sudden increase in the probe voltage output is observed. Immediately the globe valve is closed and then water level seen on the milimetric paper is marked. Since height of the probe tip from the reference line is known, the reference line can be determined easily. To confirm the reference line location the same procedure is repeated for the probe 5 and the results of two tests are compared.

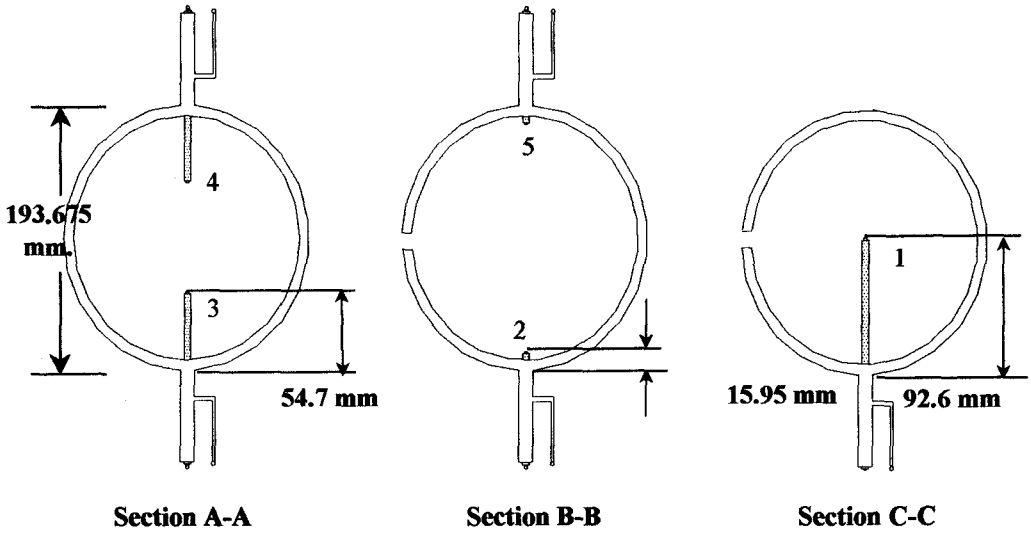

Figure 7.8: Schematic view of the probes with extensions inside the Header.

The relation between the water level from the reference line and the void fraction can be found by using a computer code written in Fortran 77 [Appendix E2].

The computer code basically calculates the area occupied by air by subtracting the area occupied by water from the total circular crosssectional area of the Header as it is shown in figure 7.9;

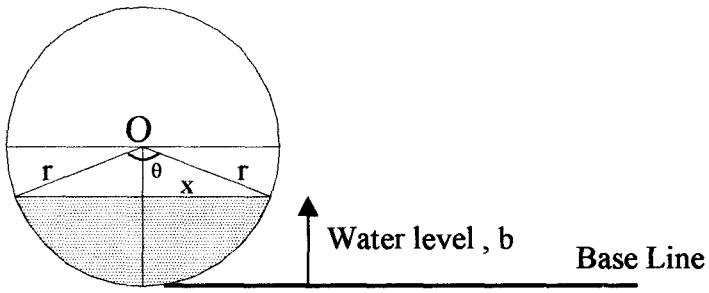

Figure 7.9: Schematic representation of stratified flow in the Header

Since the water level from the reference line, b, is read from the milimetric paper and the crossectional radius, r is known, area occupied by water can be calculated:

$$\text{Area of water} = \frac{2.\theta}{360}.\pi.r^2 - 2.x\frac{(r - b)}{2}$$

where θ = Arcsin (x / r) and $x = \sqrt{r^2 - (r - b)^2}$

The void fraction can be determined from:

$$\alpha = \frac{\text{Area occupied by air}}{\text{Total crossectional area of Header}}$$

For this calibration test, Two-phase Flow Test Facility is used.

7.2.2.2 Start of a Calibrational Run

In analog conditioner circuit; the value of excitation voltage and pre-resistance value are adjusted to 3.18 V and 100 kΩ respectively. Probe voltage outputs are determined in 3 different excitation frequencies (500 Hz, 5 kHz, 20 kHz).

All the globe valves in Feeders are closed and water circulating pump is turned on. Once the Header is full of water (α=0), the circulating pump is turned off and all the probe voltage outputs are logged, then the globe valve at the Feeder which is connected to the bottom of the Header is slightly opened and the water level inside the Header is allowed to decrease slowly. At certain water levels (different void fraction values), the globe valve is closed and the probe voltage outputs are logged. Finally, water in the Header is completely discharged and probe voltage outputs in all air medium are logged.

7.2.2.3 Data Logging

The mean of instantaneous probe voltage outputs are monitored with 10 samples per second for 10 seconds.

Finally, for a pre-determined void fraction value; the mean probe voltage output is obtained. A graph of void fraction (%) versus non-dimensional probe voltage output is plotted for each probe [Appendix C]. As an example calibration data of probe 1 is shown in figure 7.10.

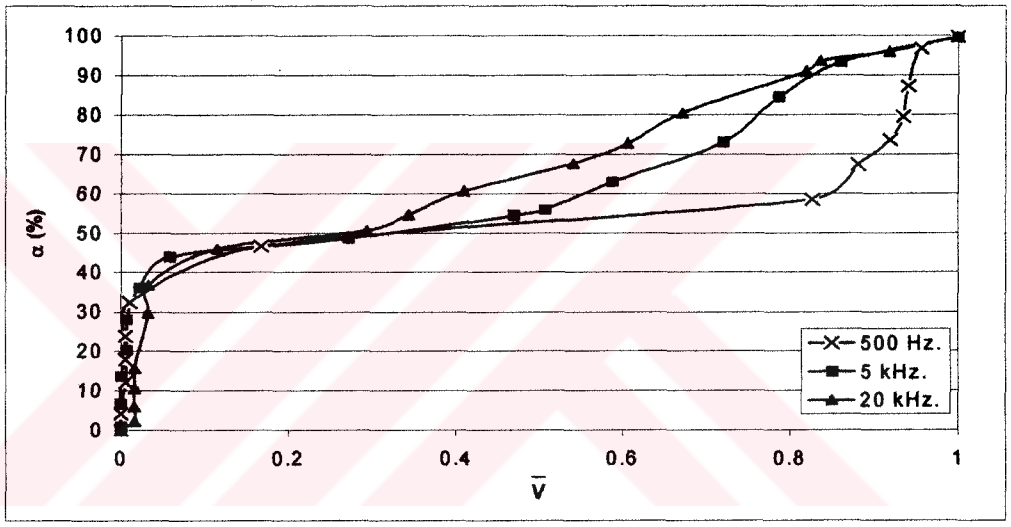

Figure 7.10: Calibration data of probe 1.

It is seen that, upto the approximately 50% void fraction when the probe tip is water medium, the non-dimensional probe voltage outputs are close to the probe voltage output in all water medium and could not sense the void fraction. On the contrary, after 50% void fraction the probe still could sense the void fraction.

Since the existing probes on the Header do not give reliable voltage outputs, a ring type probe configuration is also tried as a level indicator inside the Header. The ring electrodes of probe 1 and probe 2 that surround inside the Header surface are used as a ring type electrode . The leads of two ring electrodes are connected to the probe terminals in the analog conditioner circuit. The value of the excitation voltage and pre-resistance are 3.18V and 100 kΩ respectively. The calibration tests for the ring type probe were performed with 4 different excitation frequencies (500 Hz, 5 kHz, 10 kHz, 20 kHz).

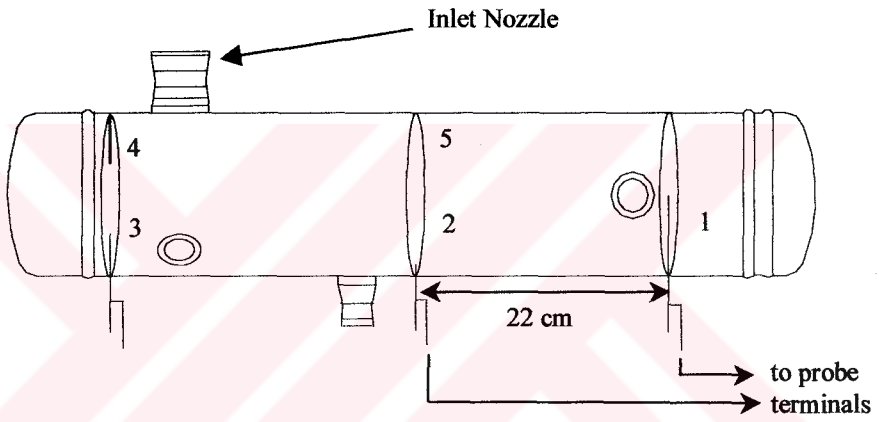

Figure 7.11: Schematic view of ring electrode configuration.

A graph of non-dimensional probe output versus void fraction value is plotted in figure 12.

The results are more satisfactory in comparison to those of impedance probes on the Header.

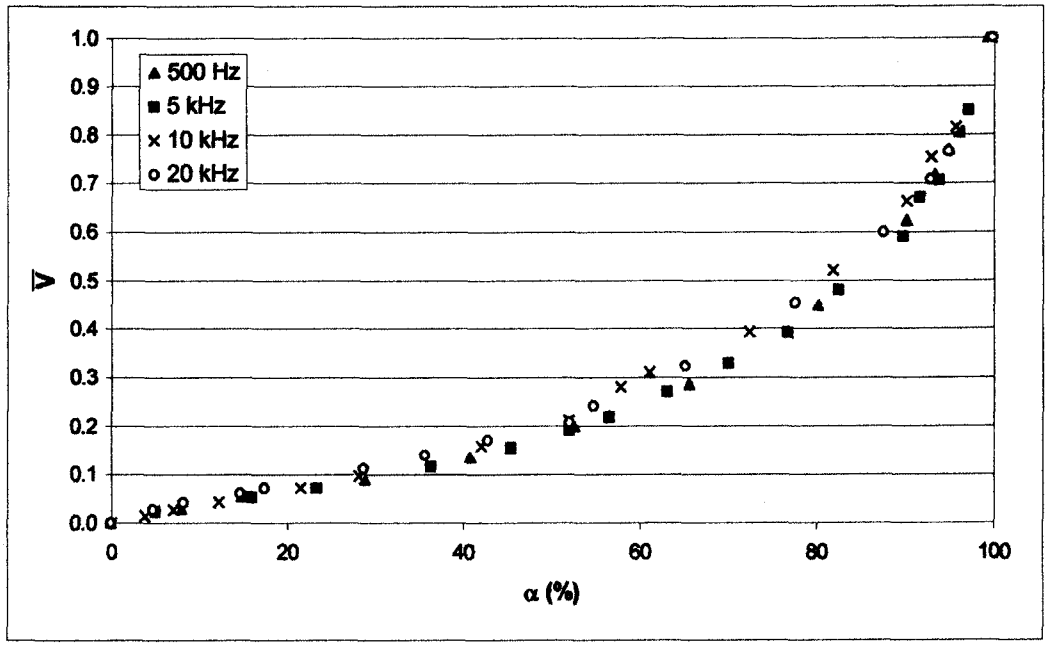

Figure 7.12: Calibration data of ring electrode.

7.2.2.4 System Shutdown

Software program is stopped and all the system components including the laboratory equipments are checked for the following tests.

CHAPTER 8

RESULTS AND RECOMMENDATIONS

In the literature generally, calibration tests of the probes are done by means of the other void fraction measurement techniques especially by using quick closing valves or radiation technique. Considering the shielding problems of the radiation technique and the restrictions in the experimental test facility for using the quick closing valve technique, these two methods could not be used in the present study. In the calibration tests of the impedance probes on the Feeders, homogenous two-phase flow model is used in which the average velocities of water and air phases are assumed to be equal to each other (s=1) and therefore volume flow ratio, β, is equal to the void fraction, α, as explained in chapter 2. In fact, this is not valid for all two-phase flow regimes. Detailed explanation about the agreement of void fraction with the volume flow ratio is given in Appendix H.

In addition to the error analysis of given in appendix G, while considering the total uncertainty of void fraction estimation, all the physical parameter effects, namely water temperature, flow regime, repeatability, which were explained in chapter 6 and chapter 7, should be taken into the consideration.

The probe voltage output measurements must be insensitive, as far as possible, to the void distribution within the flow. To provide this, the probe geometry should be designed to distribute the electric field evenly between the electrodes. The uncertainty due to the effects of void distributions with this type of probe geometry can not be eliminated completely. Especially in stratified flow conditions, the probe voltage outputs are unreliable.

The value of the pre-resistance is of considerable importance in sensitivity of analog signal conditioner circuit depending on the probe characteristics. The value of the pre-resistance may be changed according to the expected void fraction values in each Feeder. This will result in larger voltage span in the non-dimensional probe voltage output during the experiments (Chapter 6.1).

Temperature is found to have a strong effect on the measured impedance which causes a considerable shift in probe voltage output in all water medium. Therefore the probe voltage outputs must be converted to the non-dimensional form by the probe voltage outputs in all water, V_{OW}, and in all air, V_{OA}, media measured at the beginning of each experimental run (Chapter 6.4).

Excitation frequency is another important parameter which determines the probe characteristics whether it is resistive or capacitive. Since DC excitation gives unreliable voltage outputs in stagnant water due to the electrolysis effect, it is preferred to use AC excitation with variable frequency set. In low excitation frequencies (500 Hz, 1 kHz), non-dimensional probe voltage outputs are less influenced from the water temperature variations than those in high excitation frequencies (10kHz, 20kHz) and also give larger voltage span when the impedance probe is in all water and in all air media respectively (Chapter 6.2).

In the calibration tests, the probe voltage output in all air medium, V_{OA}, should be measured instantaneously when the probe is removed from the water medium completely. Otherwise, by the time, the probe voltage output in all air medium, V_{OA}, continues to increase due to the moisture effect (Chapter 6.5).

Although all the impedance probes on the Feeders have the same geometrical shape, the calibration curves are quite different. This may be attributed to the different position and different inner diameter of each probe body which may result in different void distribution within the flow.

Since the output signal is proportional to the conductivity of the single phase liquid, signal conditioner circuit may include some sub-circuits which are used as a reference for comparison of changes in conductivity of the liquid phase due to variations in its temperature and in the concentration of impurities.

In the calibration procedure, sampling frequency was selected as 10 Hz. In fact; during the calibration tests, the analysed data are unsteady, a higher sampling frequency (i.e 1 kHz) should be selected in order to obtain more reliable average values and to minimise the effect of flow regime. Data acquisition system is based on Windows operating system which has several drawbacks. Input/Output access times are relatively low which is order of 15 to 30 milliseconds. A computer code should be written which is based on direct memory access (DMA) for fast data acquisition and Input/Output port access.

The system pressure effect on void fraction calculations was not investigated since the system pressures in tests of the Joint Project are not far from the atmospheric pressures and also water pump capacity is not sufficient to obtain high pressures. The pressure effect should be considered with different pump type (i.e positive displacement pump).

REFERENCES

1. O.C. JONES, JF. and N. ZUBER, Multiphase Flow , pp.540-545, 1975.

2. Abdullah Abbas KENDOUSH, "A comparative study of various nuclear radiations used for void fraction measurements", Nuclear Engineering and Design, pp. 249-257, 1992.

3. N.H.AFGAN, Transient Phenomena in Multiphase Flow, pp. 894-896, 1998.

4. E.ABRO, G.A.JOHANSEN, "Improved void fraction determination by means of multi-beam γ-ray attenuation measurements", vol. 10, pp. 99-108, 1999.

5. Rousseau J.C., Czerny J. and Riegel B., "Void fraction measurement during blowdown by neutron absorption of scattering methods", Europan Two-Phase Flow Meeting, Erlangen, pp. 55, 1976.

6. A.S.MORRIS, Principles of Measurement and Instrumentation, pp. 300-305, 1993.

7. J.S.CHANG and E.Ç.MORALA, "Determination of two-phase interfacial areas by an ultrasonic technique", Nuclear Engineering and Design, vol 122., pp. 143-156, 1990.

8. L.MATIKAINEN and G.A.IRONS, "Ultrasonic system for the detection of transient liquid/gas interfaces using the pulse-echo technique.", Rev. Sci.Instrum., pp. 1661-1666, 1986.

9. O.C.JONES and Jean Marc DELHAYE, "Transient and statistical measurement techniques for two-phase flows: A critical review", Int.J.Multiphase Flow, vol. 3, pp. 89-116, 1975.

10. Denis MORRIS, Alberto TEYSSEDOU, Jean LAPIERRE and Altan TAPUCU, "Optical fiber probe to measure local void fraction profiles", Applied Optics, vol.26, pp. 4660-4664, 1987.

11. N.H.AFGAN, Transient Phenomena in Multiphase Flow, pp. 873-888, 1988.

12. H.TORAL, "A study of the hot-wire anemometer for measuring void fraction in two-phase flow", J.Phys. E:Sci.Instrum., vol.14, pp.822-827, 1981.

13. G.F.HEWITT, Measurement of Two-Phase Flow Parameters, pp. 61-61, 1978.

14. H.V.KOK, W.C.HEERENS, T.H.J.J.VAN DER HAGEN, H.VAN DAM, "A new principle for designing optimal capacitive void fraction sensors applied to a rod bundle geometry", Measurement Sci. Technology, pp. 119-131, 1995.

15. Chul.Hwa.SONG, Moon Ki.CHUNG, Hee Cheon NO, "Measurement of void fraction by an improved multi-channel conductance void meter", Nuclear Eng.Design, pp.269-285, 1998.

16. A.TEYSSEDOU and A.TAPUCU, "Impedance probe to measure local void fraction profiles", Rev.Sci.Instrum., pp.631-638, 1987.

17. One Dimensional Two-phase Flow, Graham B. WALLIS, 1969.

18. Two-phase Flow in Pipelines and Heat Exchangers, D. CHISHOLM, 1983.

19. Convective Boiling and Condensation, James W. NILSSON, 1993.

20. Electric Circuits, James W. NILSSON, 1993.

21. V.I.SUBBOTIN, Yu.E.POKHVALOV, L.E.MIKHAILOV, I.V. KRONIN, V.A.LEONOV, "Calculating the gas contents of a mixture with bubble flow according to the measurement results of resistance and capacitance methods", Thermal Engineering, pp.70-75, 1975.

22. MERILLO M., DECHENE R. L., and W.M.CICHOWLAS, "Void fraction measurement with a rotating electric field conductance gauge", Trans. ASME J. Heat Transfer", vol 99, pp. 330-332, 1977.

23. J.E. HARDY and J.O. HYLTON, "Electrical impedance string probes for two-phase void and velocity measurements", Int. J. Multiphase Flow, vol. 10, pp. 541-556, 1984.

24. R.VAN DER WELLE, "Void fraction, bubble velocity and bubble size in two phase flow", Int. J. Multiphase Flow, vol 11, pp. 317-345, 1985.

25. A.TOURNAIRE, "Dependence of the instantaneous response of impedance probes on the local distribution of the void fraction in a pipe", Int.J. Multiphase Flow, vol 12, pp. 1019-1024, 1986.

26. A.TEYSSEDOU, A.TAPUCU, "Impedance probe to measure local void fraction profiles", Rev.Sci.Instrum., pp. 631-638, 1988.

27. P.ANDREUSSI, A. DI DONFRANCESCO and M.MESSIA, "An impedance method for the measurement of liquid hold-up in two phase flow", Int.J. Multiphase Flow, pp. 777-785, 1988.

28. G. DELTIN and A. NEGRINI, "Development of the electrical impedance probes for void fraction measurements in air-water flow", Multiphase Transport, T. Nejat VEZİROĞLU, vol 5, pp. 2709-2731.

29. R.K. DAS and S. PATTANAYAK, "Electrical impedance method for flow regime identification in vertical upward gas-liquid two-phase flow", Measurement Sci. Technology, pp. 1457-1463, 1993.

30. R.K. DAS and S.PATTANAYAK, "Measurement of void fraction in different flow regimes of a vertical gas-liquid flow through narrow tubes", Measurement Sci.Technology, pp. 1538-1545, 1994.

31. Chul Hwa SONG, Moon Ki CHUNG, Hee Cheon NO, "Measurement of void fraction by an improved multi-channel conductance void meter", Nuclear Engineering and Design, pp. 269-285, 1998.

32. E. KREPPER, A.K. KRUSSENBERG, H.M. PRASSER, A. SCHAFFRATH, "High resolution void fraction measurements for the validation of flow maps and CFD codes", Two-Phase Modelling and Experimentation, Pisa, pp-1371-1378, 1999.

33. KAYA M.B. "Flow rate Measurements in a Two-phase Flow System", Master thesis, Mechanical Engineering Department, Middle East Technical University, ANKARA, 2001.

34. J.E SWIDDLE, "Conductivity probe, COG WPIR-1502 instrument development", AECL and EACL Thermal-hydraulics Branch THB-93-178 memo note, May 31 1993.

35. W.HANER, "Conductivity probe COG WPIR-1502 instrument development", AECL and EACL Safety Thermal-hydraulics Branch STHB-95-293 memo note, October 12 1995.

36. Methods for Physical & Chemical Analysis of Fresh Waters, H.L GOLTERMAN, R.S. CLYMO, M. A. M. OHNSTAD, Second edition, pp.49-51, pp.182-184, 1978.

APPENDIX A

SPECIFICATIONS OF INSTRUMENTATION AND DATA ACQUISITION SYSTEM

A.1 Water-Circulating Pump

Manufacturer.....: WILO

Type.....: Multi-stage normal suction, horizontal ,high pressure centrifugal pump.

Supply Voltage.....: 1~200 V (± 10%) / 50 Hz

Fluid Temperature.....: -15 °C to 110 °C with gaskets- EPDM, -15 °C to 80 °C version with gaskets- VITON

Max. Permissible Working Pres..: 10 Bar

Max. Permissible Inlet Pres.....: 6 Bar

Max. ambient temperature.....: 40 °C

A.2 Air Compressor

Manufacturer.....: KOMSAN KOMPRESÖR

Type.....: T-175 KDT-15

Number of Cylinder.....: 1

Tank Volume .....: 100 liter

Stroke Volume.....: 216 lt/min

Motor Power.....: 1.5 kW

Revolution.....: 700 rpm

Operating Pressure.....: 15 kgf/ cm^2

Piston Displacement.....: 13 m^3/h

Max. Pressure.....: 10 kg/cm^2

Weight.....: 110 kg

A.3 Water-Distiller

Manufacturer.....: ŞİMŞEK LTD. ŞTİ.

Type.....: SS-200 Model

Supply Voltage.....: 220/380 V AC 50 Hz

A.4 Pressure Gage

Manufacturer.....: PAKKENS LTD. ŞTİ.

Pressure Element.....: CuSnb Bourden Tube over 60 Bar stainless Steel

Measuring Range.....: 0-6 Bar

Operating Range.....: 3/4 of f.s deflection for static loads, 2/3 of f.s deflection for fluctuating loads.

Accuracy.....: 1.0 % f.s

Temperature Range.....: -25 to +60 °C

Working Medium.....: Fluid - Gas

A.5 Temperature Gage

Manufacturer.....: PAKKENS LTD. ŞTİ.

Measuring Range.....: 0-120 °C

Operating Range.....: 3/4 of f.s, short time peaks up to the full scale

Accuracy.....: 2.0 % f.s

Working Medium.....: Fluid – Gas

A.6 Turbine Type Flow Meter

Manufacturer.....: CHEMLINE PLASTIC
Model.....: 2110 TM & 110 TM
Supply Voltage.....: 12-24 V dc
Output.....: 4 to 20 mA, load resistance < 500 ohm
Velocity Range.....: 0.15 to 10 m/s
Electrical Connection.....: 4 pole, DIN 43650,NEMA 4X
Accuracy.....: ± 1% over calibrated flow rate range
Repeatability.....: ± 0.5% over calibrated flow rate range
Linearity.....: ± 1% over calibrated flow rate range
Viscosity Range.....: 0.5 to 20 cST (outside this range transmitter needs recalibration)
Working Medium.....: Liquids only

A.7 Pressure Transducer

Manufacturer.....: OMEGA
Model.....: PX 605-100 GI
Supply Voltage.....: 24 V dc (10-30 V dc)
Output.....: 4-20 mA (2 wire)
Max. Loop Resistance.....: 50 × (supply voltage-10) Ω
Accuracy.....: ± 0.4% at full scale
Storage Temperature.....: -65° to 250°F (-53° to 121°C)
Operating Temperature.....: -20° to 180°F (-28° to 82°C)
Compensated Temperature.....: -20° to 160°F (-28° to 71° C)
Thermal Effect.....: (zero) ± 0.04% full scale/ F
(span) ± 0.04% full scale/F
Proof Pressure.....: 15-2000 psi = 200 % full scale

3000-5000 psi=150% full scale

7500-20000 psi=120% full scale

Burst Pressure.....: 15-2000 psi=800% full scale

3000-5000 psi=300% full scale

7500-20000 psi=150% full scale

Response Time.....: 1 ms

Working Medium.....: Liquid/gas/steam

A.8 Differential Pressure Transmitter

Manufacturer.....: OMEGA

Model.....: PX 711-100WDI

Output.....: 4-20 mA dc output corresponding 1-5 V dc through 250 ohm load resistor

Max. Pressure Range.....: 0-100 in. H_2O

Min. Pressure Range.....: 0-17 in. H_2O

Supply Voltage.....: 24 V dc nominal

12.5 V dc min. at transmitter

15.25 V dc min. with digital meter option

36 V dc max. at transmitter

42 V dc with external load specified

Reverse polarity protection provided

Accuracy.....: (Includes independent linearity, hysteresis and repetability)

$\pm$ 0.15 % of calibrated span

Working Pressure.....: 2000 psi

Working Medium.....: Liquid/gas/steam

A.9 Differential Pressure Transmitter

Manufacturer.....: OMEGA

Model.....: PX 771-100DI

Output.....: 4-20 mA dc output corresponding 1-5 V dc through 250 ohm load resistor

Max. Pressure Range.....: 0-100 psi

Min. Pressure Range.....: 0-17 psi

Supply Voltage.....: 24 V dc nominal
12.5 V dc min. at transmitter
15.25 V dc min. with digital meter option
36 V dc max. at transmitter
42 V dc with external load specified
Reverse polarity protection provided.

Accuracy.....: (Includes independent linearity, hysteresis and repetability)
± 0.15 % of calibrated span

Working Pressure.....: 2000 psi

Working Medium.....: Liquid/gas/steam

A.10 MultiLab Analog and Digital I/O Card

Manufacturer.....: ADVANTECH

Type.....: PCL-812 PG

Analog Input Channels.....: 16 single-ended.

A/D Converter.....: 12-bit, 25 μs conversion time

Analog Input Range.....: ± (10,5,2.5,1.25,0.625,0.3125)

Analog Trigger Mode.....: Software, pacer or external trigger

Data Transfer.....: Program controlled, interrupt 2~7,9~12,14, 15 or DMA(Channel 1 or 3) for

Accuracy.....: 0.01% of reading ± 1 bit

Input Impedance.....: >100 MΩ

Overvoltage.....: Continuous ± 30 V dc max

Analog Output Channels.....: Two doubled buffered 12-bit channels

D/A range (in V).....: 0~5, 0~10 w/internal reference; ± 10 V max.

with external AC or DC reference (accuracy for output above ±9V may vary depending on power supply used)

Settling Time.....: 30 μs

Output Current.....: ±5 mA max.

Linearity.....: ±1/2 bit

Digital Input Channels.....: 16, TTL level

Digital Output Channels.....: 16, TTL compatible

Counter.....: One 16-bit counter with a 20 MHz time base

Power Consumption.....: +5V@500 mA typical,1.0 A max.
+12 V@ 50 mA typical ,100 mA max.
-12 V@ 14 mA typical, 20 mA max.

Operating Temperature.....: 0~50°C (32~122°F)

I/O Ports.....: 16 consecutive bytes

Connectors.....: Two 20-pin flat-cable connectors

Dimensions.....: 185× 100 mm

A.11 Amplifier and Multiplexer Board

Manufacturer.....: ADVANTECH

Type.....: PCLD-789D

Input Channels.....: 16 differential

Input Range.....: ±10 V max., depending on selected gain

Output Range.....: ±10 V max.

Overvoltage Protection.....: ±30 V continuous

Cold-junction Compensation..: +24.4 mV/°C, 0 V at 0°C

Power Consumption.....: +5 V @ 10 mA maximum
+12 V @ 80 mA maximum

Connectors For D/A buses.....: One DB-37 connector , two 20-pin flat cable connectors for daisy chaining

Dimensions.....: 205 mm × 114 mm

A.12 Frequency Counter

Manufacturer.....: Thurlby & Thandar

Type.....: TF830 Universal Counter

Frequency Range.....: 5 Hz to 25 MHz, 20 MHz – 1.3 GHz

L.S.D Displayed.....: With 8 significant digits irrespective of actual input frequencies .

Operating Range.....: +5 °C to +40 °C

Enviromental Storage Range.....: -20 °C to +70 °C

Crystal Oscillator Frequency.....: 10 M Hz

Input Impedance(A).....: 1 MΩ // 25 pF

Sensitivity (A).....: Sinewave 15 mV rms 10 Hz to 20 MHz
Pulse 40 mV p-p 0 Hz to 14 MHz

Trigger Level.....: Continuously adjustable by front panel Control.

Max. Permissible Input Voltage.: 200 V dc; 250 V rms 50/60 Hz

Low Pass Filter.....: Switchable 50 kHz low pass noice filter.

Input Impedance (B).....: 50 Ω nominal

Sensitivity (B).....: 10 mV rms 20 MHz to 700 MHz

Power Consumption.....: 8 VA max.

A.13 Digital Multimeter

Type.....: OGSM MY64 Digital Multimeter

DC Voltage/ Basic Accuracy.....: 200m/2/20/200/1000 V ± 0.05%

Input Imp/Max. AC Voltage.....: 10M / / 2/20/200/700 V

Basic Accuracy/Input Impedance: ± 0.8 % / 2M

Frequency Range.....: 40-1000 Hz

Basic Accuracy.....: ± 0.8 %

Resistance.....: 200/2 k/20 k/200 k/ 2M/ 20M

Basic Accuracy.....: ± 0.15%

Temperature/ Basic Accuracy....: -50 °C /1000 °C / ± 0.75%

A.14 Digital thermometer

Manufacturer.....: OMEGA ENGINEERING

Type.....: CL23A

L.C.D Displayed.....: 5 digit

Accuracy.....: ± 0.5 °F from –50 to 1250 °F

0.04% over 1250 °F

± 1.0 under –50 °F

Ambient Temperature.....: 0 to 50 °C (32 to 122 °F)

Power.....: 9 V dc battery.

Reading Rate.....: 1 per second.

A.15 Digital LCR Meter

Manufacturer.....: Hewlett Packard

Type.....: Model 4262A

Test Frequency.....: 120 Hz, 1 kHz, 10 kHz ± 3%

Display.....: 3-1/2 digits max. display 1999

Basic Accuracy.....: 0.2 %

Equivalent Circuit Modes.....: Auto, parallel , series

Parameters used.....: L-D .Q, C-D Q, R(ESR), Δ LCR

Test Signal Level.....: 1 V , 50 mV (C_p mode only)

DC Bias.....: Internal : 1.5V, 2.2V, 6V ± 5 %, selectable

External : 0 to 40 V

Measuring Terminal.....: 5-terminal configuration

APPENDIX B

SCHEMATIC DIAGRAMS OF ANALOG CONDITIONER CIRCUIT

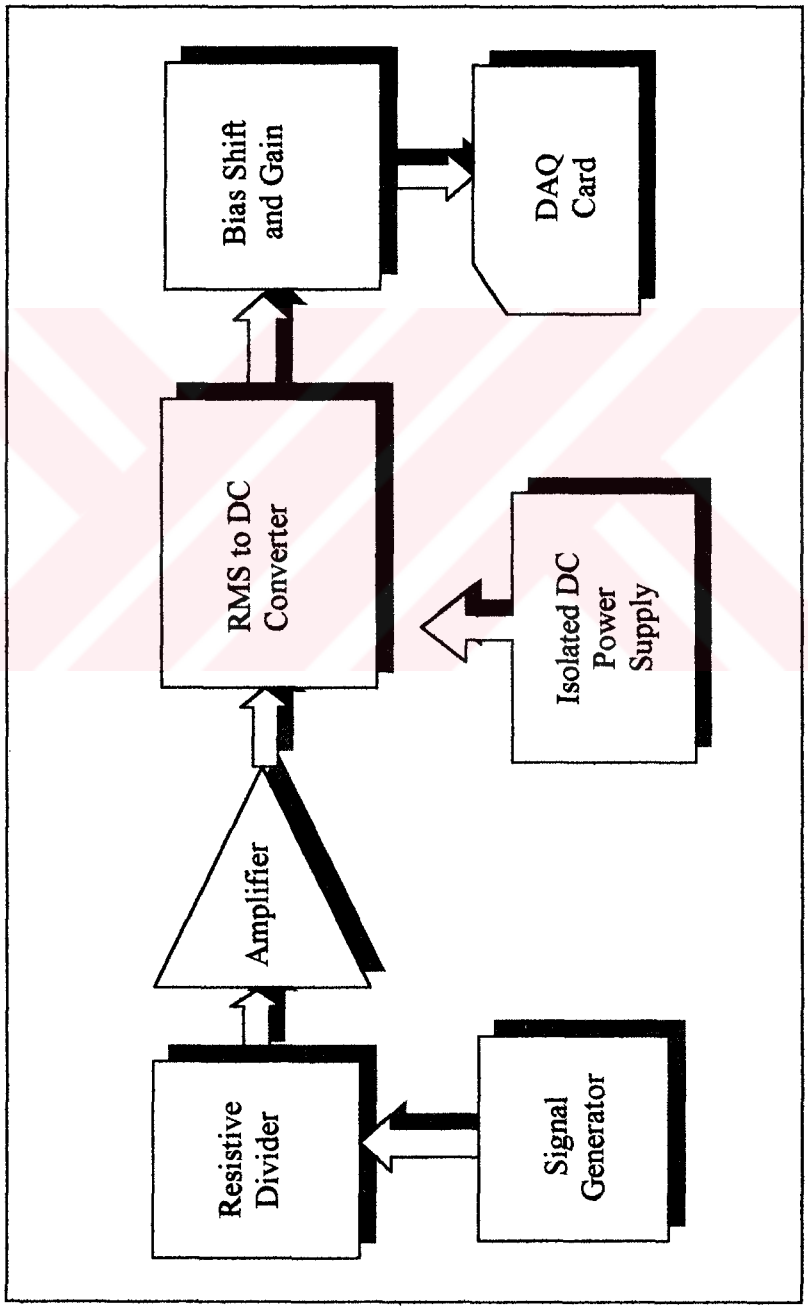

Figure B.1 : Analog signal conditioner unit signal flow diagram

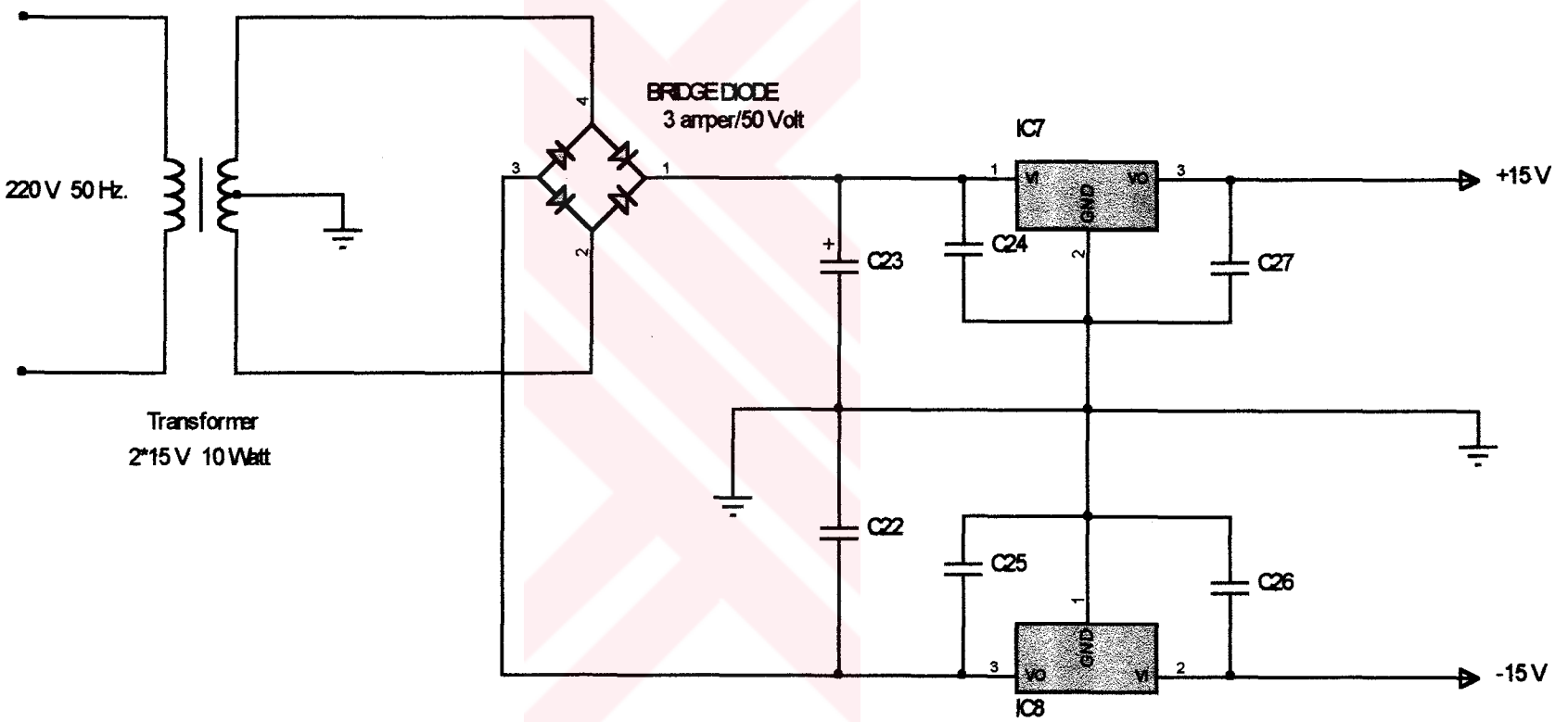

Figure B.2 : 2×15 V 10 Watt power supply.

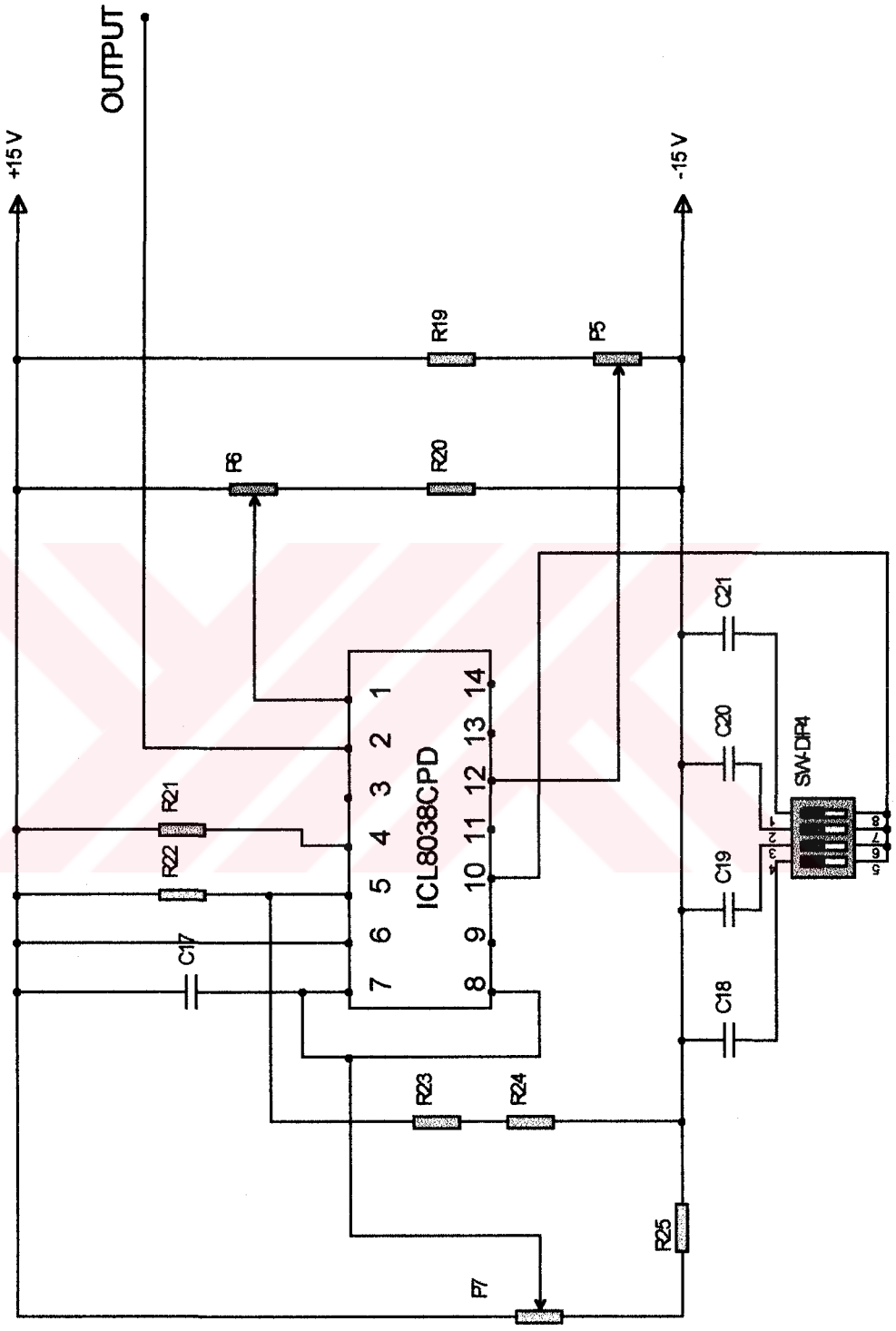

Figure B.3 : AC Signal generator with variable frequency set.

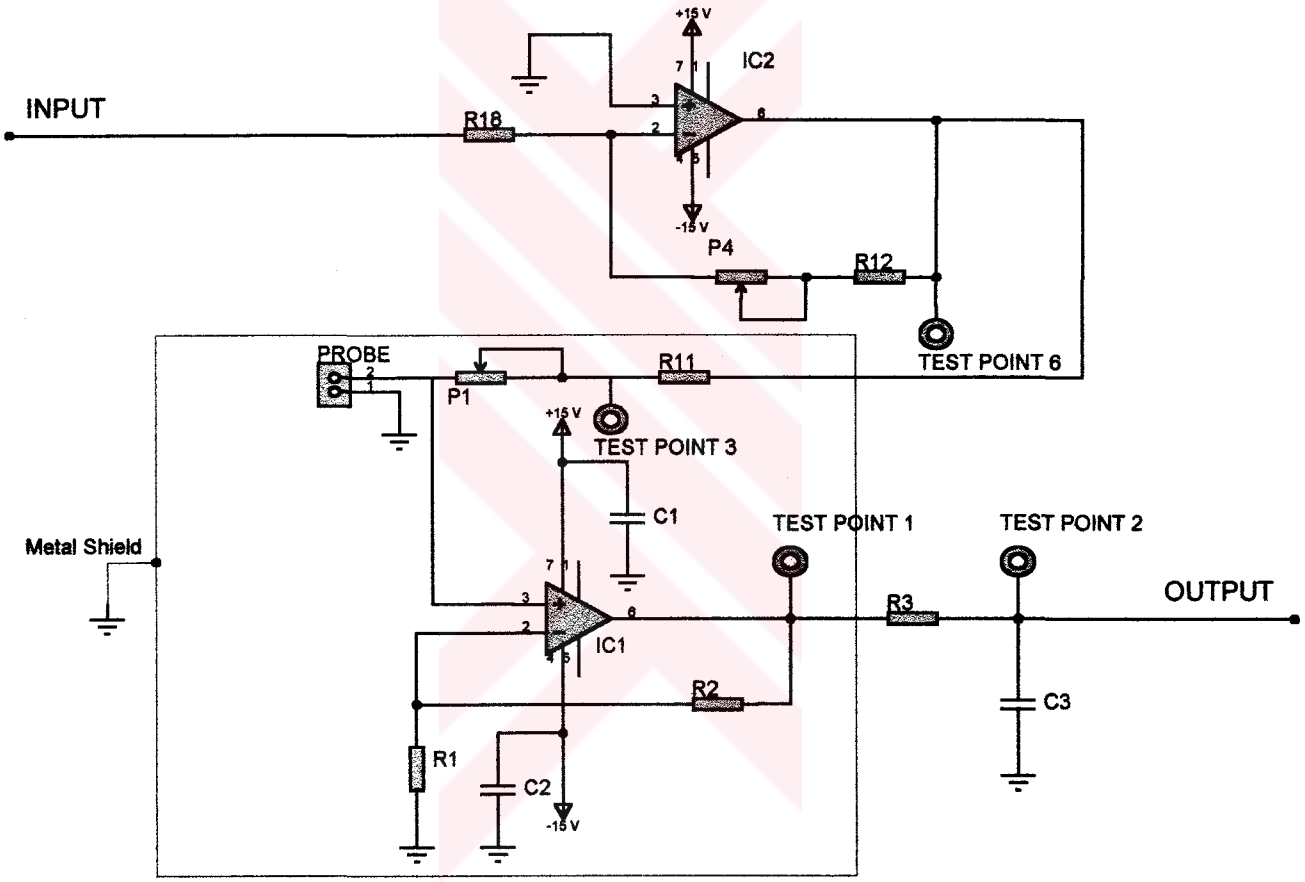

Figure B.4 : Resistive divider and non-inverting amplifier.

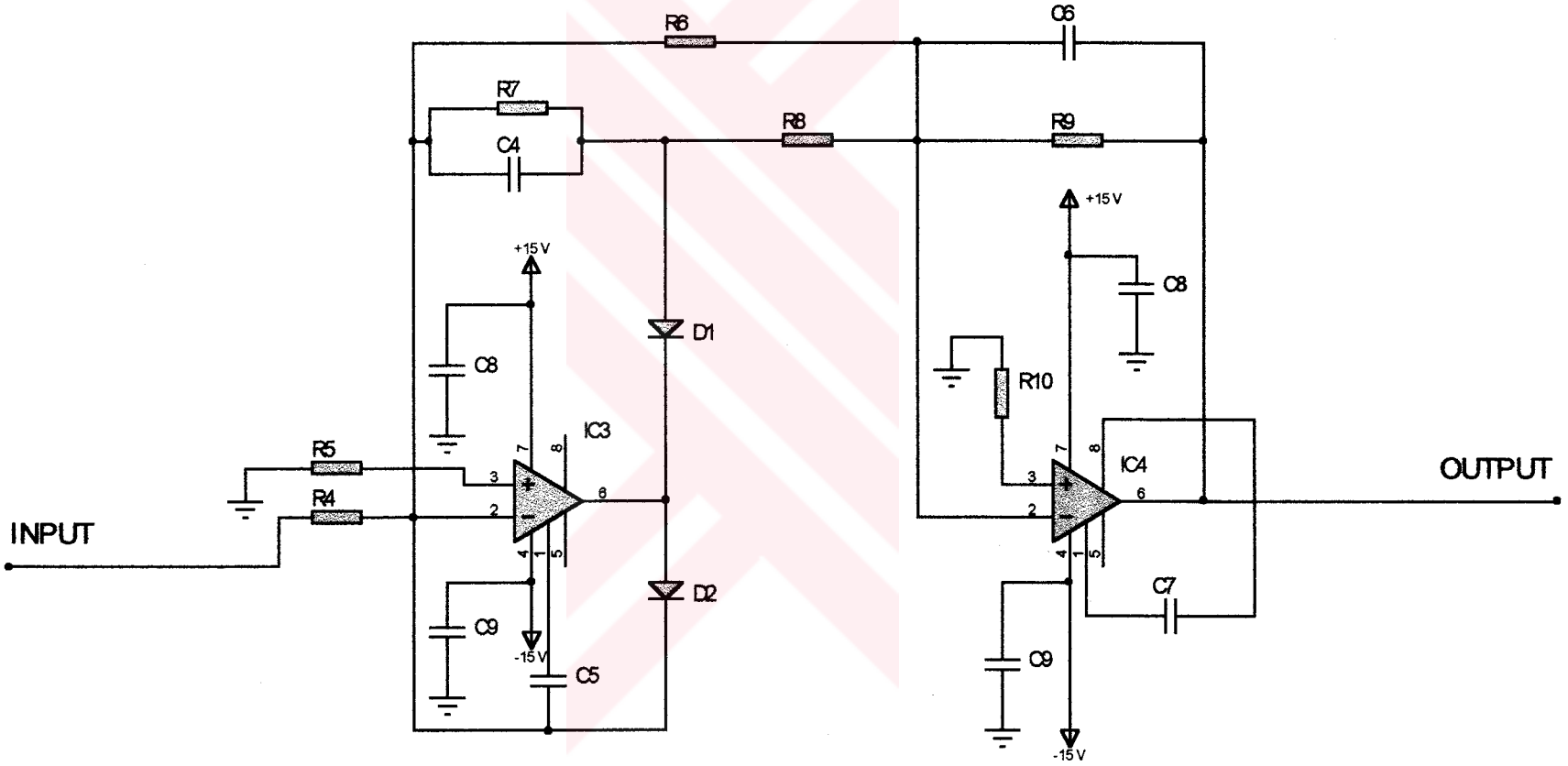

Figure B.5 : RMS to DC converter.

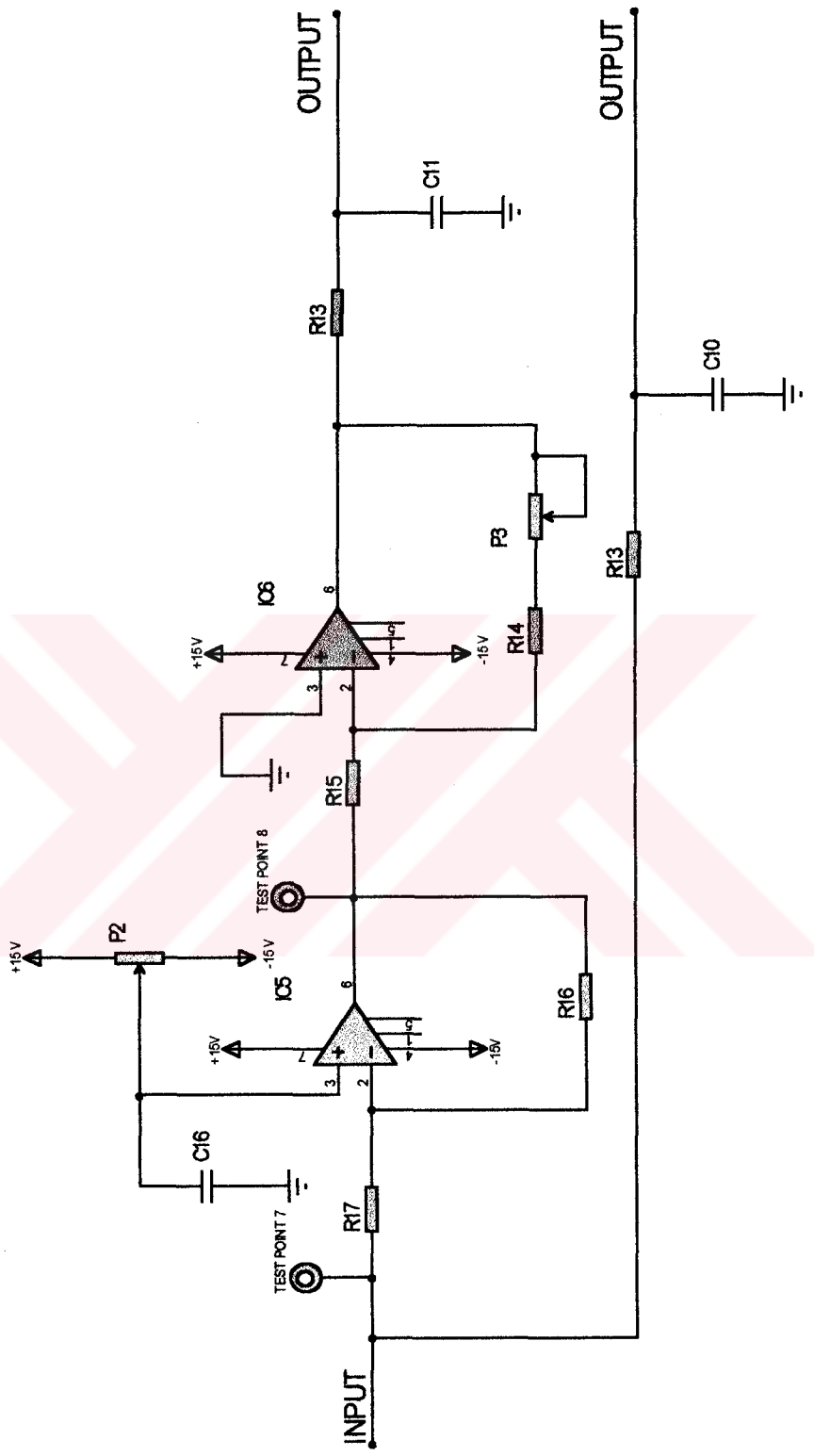

Figure B.6 : Bias shift and gain block.

Table B1: Part list of the analog signal conditioner circuit.

REF	VALUE	#1	#2
R1	100K	%0.1	
R2	100K	%0.1	
R3	3.3 K	%5	
R4	20K	%1	
R5	15K	%1	
R6	20K	%1	
R7	20K	%1	
R8	10K	%1	
R9	22.2K	%1	
R10	6.2K	%1	
R11	100K	%1	
R12	68K	%5	
R13	3.3K	%1	
R14	47K	%1	
R15	47K	%1	
R16	47K	%1	
R17	47K	%1	
R18	47K	%1	
R19	10K	%5	
R20	10K	%5	
R21	2.2K	%1	
R22	2.2K	%1	
R23	10M	%1	
R24	4.7M	%1	
R25	22K	%1	
R26	1.5K	%5	
R27	1.5K	%5	
R28	3.3K	%1	
C1	1μF	25V	Tantal
C2	1μF	25V	Tantal
C3	470μF	25V	Electrolitic
C4	10Pf	63V	Polysteren
C5	150pF	63V	Polysteren
C6	10μF	25V	Electrolitic
C7	30pF	63V	Polysteren
C8	1μF	25V	Tantal
C9	1μF	25V	Tantal

C10	100pF	63V	Polysteren
C11	100pF	63V	Polysteren
C12	1µF	25V	Tantal
C13	100nF	25V	Polysteren
C14	1µF	25V	Tantal
C15	100nF	25V	Polysteren
C16	100pF	63V	Polysteren
C17	1µF	25V	Polyster
C18	220nF	63V	Polyster
C19	22nF	63V	Polyster
C20	2.2nF	63V	Polysteren
C21	220pF	63V	Polysteren
C22	470µF	25 V	Electrolitic
C23	470µF	25 V	Electrolitic
C24	470nF	25V	Polysteren
C25	470nF	25V	Polysteren
C26	1µF	25V	Tantal
C27	1µF	25V	Tantal
P1	500K	Linear	Multi-turn Trimpot
P2	100K	Linear	Multi-turn Trimpot
P3	100K	Linear	Multi-turn Trimpot
P4	47K	Linear	Multi-turn Trimpot
P5	100K	Linear	Single-turn Trimpot
P6	100K	Linear	Single-turn Trimpot
P7	10K	Linear	Multi-turn Trimpot
IC1	LF 411 A	IC	
IC2	LF 411 A	IC	
IC3	LM 101/301 A	IC	
IC4	LM 101/301 A	IC	
IC5	LF 411 A	IC	
IC6	LF 411 A	IC	
IC7	ICL8038 CCPD	IC	Plastic DIP
D1	1N914/AA118		
D2	1N914/AA118		
D3	Red Led	5 mm	
D4	Red Led	5 mm	
DP1	4 way dip-switch		

APPENDIX C

EXPERIMENTAL AND CALIBRATION DATA

Glossary of names/ symbols used in table and figures:

P.No	Probe number
Q_W	Volume flow rate of water (m^3/s)
Q_A	Volume flow rate of air (m^3/s)
V_{exc}	Excitation voltage (V)
f	Excitation frequency (Hz)
R_p	Pre-resistance in the resistive divider part of the analog signal conditioner circuit (Ω)
$\alpha(\%)$	Void fraction percent
V_m	The average of probe voltage output which can be measured from the output of the Bias shift and gain block of the analog signal conditioner circuit.
$\overline{V}$	Non-dimensional probe voltage output of analog signal conditioner circuit

T_W	Water temperature (^oC)
T_A	Air temperature (^oC)
WL	Water level from the reference line (mm)
R^2	Correlation coefficient
S	Standard deviation
$\bar{S}$ (%)	Non dimensional standard deviation percent

- Probe numbers are shown in figure 4.6 and figure 4.12.

- During the calibration tests, volume flow rate of water and air values (Q_W, Q_A) are taken as moving averages of the instantaneous values taken 10 samples per second in 30 seconds interval to see the fluctuations in volume flow rate of two-phase mixture.

- Excitation voltage (V_{exc}) can be measured from test point 6 and ground point [Figure B4] by means of a digital multimeter [A13]. The measured voltage is the rms value which is equal to 1.11 of the average value for pure sinusoidal voltage. All the measured voltages are converted to average voltages by the 1.11 conversion factor.

- Excitation frequency (f) can be measured from the test point 6 and ground point [Figure B4] by means of a frequency counter [A12].

- V_m is averaged over 300 instantaneous probe voltage output taken in 30 seconds for the calibration test of the probes on the Feeders.

seconds for the calibration test of the probes on the Header.

- Temperature of water is measured by means of a digital thermometer [A14] at the exit of each Feeder and temperature of air is measured by means of a temperature gage [A5] on the air supply line (Figure 4.5)

- Correlation coefficient (R^2) measures the proportion of variation in the data points which is explained by the regression model. A value of $R^2 = 1.0$ means that the curve (data fit equation) passes through every data point. A value of $R^2 = 0.0$ means that the regression model does not describe the data any better than a horizontal line passing through the average of the data points. To explain the meaning of these measures, the standard deviation which quantifies the spread of the data around the mean must be defined.

$$S_t = \sum_{i=1}^{n_{points}} (\bar{y} - y_i)^2$$

where the average of the data points ($\bar{y}$) is simply given by

$$\bar{y} = \frac{1}{n_{points}} \sum_{i=1}^{n_{points}} y_i$$

and y denotes the value calculated from the regression model, y_i denotes the data points.

The quantity S_t considers the spread around a constant line (the mean) as opposed to the spread around the regression model. This is the uncertainty of the dependent variable prior to regression. We also define the deviation from the fitting curve as;

$$S_r = \sum_{i=1}^{n_{points}} (y_i - f(x_i))^2$$

Thus, the improvement (or error reduction) due to describing the data in terms of a regression model can be quantified by subtracting the two quantities. Because the magnitude of the quantity is dependent on the scale of the data, this difference is normalized to yield

$$R^2 \equiv \sqrt{\frac{S_t - S_r}{S_t}}$$

- Standard deviation, S, is defined in chapter 6 as;

$$S = \sqrt{\frac{\sum (V_i - V_m)^2}{n}}$$

- Non dimensional standard deviation, $\bar{S}$ is defined in chapter 6 as;

$$\bar{S}(\%) = \frac{S}{V_{OA} - V_{OW}} .100$$

where V_{OA} and V_{OW} are the probe voltage output of analog signal conditioner circuit where the probe is in all air and in all water media respectively.

Table C1: Calibration data of probe 6 with 100 kohm pre-resistance.

$V_{exc.}$= 3.18 V f= 500 Hz R_p= 100 kohm

P. No	$Q_W.10^3$ (m^3/s)	$Q_A.10^3$ (m^3/s)	α(%)	V_m(V)	$\overline{V}$	T_W (°C)	T_A (°C)
6	1.79	0.00	0.0	-0.018	0.000	20.8	20
	1.76	0.12	6.5	0.008	0.012		
	1.74	0.20	10.4	0.096	0.052		
	1.74	0.35	16.8	0.202	0.101		
	1.71	0.41	19.4	0.278	0.136		
	1.70	0.52	23.4	0.405	0.194		
	1.70	0.62	26.6	0.586	0.277		
	1.68	0.74	30.7	0.712	0.334		
	1.64	0.87	34.6	0.840	0.393		
	1.63	0.98	37.4	0.936	0.437		
	1.61	1.16	41.7	1.047	0.488		
	1.61	1.36	45.7	1.172	0.545		
	1.57	1.52	49.3	1.275	0.592		
	1.39	1.57	53.1	1.351	0.627		
	1.26	1.61	56.1	1.412	0.655		
	1.14	1.64	59.1	1.468	0.680		
	1.04	1.67	61.7	1.528	0.708		
	0.95	1.70	64.1	1.569	0.727		
	0.83	1.72	67.5	1.609	0.746		
	0.73	1.75	70.6	1.646	0.762		
	0.61	1.77	74.5	1.697	0.785		
	0.53	1.79	77.3	1.713	0.793		
	0.41	1.80	81.4	1.778	0.822		
	0.29	1.81	86.1	1.825	0.844		
	0.19	1.81	90.3	1.892	0.858		
	0.13	1.80	93.2	1.941	0.897		
	0.00	1.80	100.0	2.166	1.000		

Table C2: Calibration data of probe 6 with 600 kohm pre-resistance.

$V_{exc.}$= 3.18 V f= 500 Hz R_p=600 kohm

P. No	$Q_W.10^3$ (m^3/s)	$Q_A.10^3$ (m^3/s)	α(%)	V_m(V)	$\overline{V}$	T_W(°C)	T_A(°C)
6	1.79	0.00	0.0	0.015	0.000	21.4	20
	1.79	0.14	7.5	0.043	0.010		
	1.79	0.24	11.9	0.112	0.033		
	1.79	0.32	15.0	0.157	0.049		
	1.75	0.45	20.3	0.264	0.086		
	1.74	0.59	25.4	0.359	0.118		
	1.76	0.64	26.6	0.518	0.173		
	1.74	0.69	28.5	0.579	0.194		
	1.74	0.77	30.8	0.669	0.225		
	1.74	0.85	32.8	0.735	0.248		
	1.71	0.97	36.2	0.843	0.285		
	1.70	1.06	38.5	0.922	0.312		
	1.70	1.17	40.8	1.003	0.340		
	1.70	1.27	42.8	1.106	0.375		
	1.70	1.38	44.8	1.142	0.388		
	1.66	1.50	47.5	1.231	0.418		
	1.57	1.53	49.4	1.295	0.440		
	1.30	1.60	55.0	1.488	0.507		
	1.17	1.63	58.1	1.590	0.542		
	1.01	1.66	62.2	1.705	0.581		
	0.91	1.70	65.2	1.798	0.613		
	0.80	1.73	68.4	1.887	0.644		
	0.73	1.74	70.5	1.921	0.655		
	0.62	1.75	73.8	2.009	0.686		
	0.57	1.75	75.5	2.035	0.695		
	0.42	1.75	80.5	2.090	0.714		
	0.31	1.74	84.7	2.215	0.757		
	0.23	1.72	88.3	2.301	0.786		
	0.16	1.76	91.7	2.463	0.842		
	0.00	1.74	100.0	2.923	1.000		

Table C3: Calibration data of probe 10 with 500 Hz excitation frequency

$V_{exc.}$= 3.18 V f = 500 Hz R_p= 597 kohm

P.No	$Q_W.10^3$ (m^3/s)	$Q_A.10^3$ (m^3/s)	α(%)	V_m(V)	S	$\bar{S}$(%)	T_W (°C)	T_A (°C)
10	1.84	0.09	4.8	0.011	0.002	0.05	24.5	25
	1.82	0.21	10.5	0.279	0.109	2.95		
	1.80	0.31	14.7	0.422	0.115	3.14		
	1.78	0.47	20.8	0.724	0.109	2.96		
	1.75	0.58	25.0	0.812	0.096	2.62		
	1.74	0.74	29.8	0.929	0.079	2.15		
	1.70	0.90	34.6	1.041	0.069	1.87		
	1.66	1.12	40.3	1.200	0.067	1.83		
	1.52	1.23	44.8	1.283	0.075	2.04		
	1.36	1.34	49.5	1.308	0.079	2.14		
	1.17	1.45	55.5	1.380	0.075	2.03		
	1.01	1.52	60.1	1.542	0.063	1.71		
	0.85	1.58	65.0	1.864	0.058	1.56		
	0.66	1.56	70.1	2.208	0.061	1.65		
	0.52	1.50	74.1	2.655	0.091	2.48		
	0.19	1.01	84.1	3.301	0.179	4.88		
	0.15	1.11	88.4	3.442	0.213	5.79		

Table C4: Calibration data of probe 10 with 1kHz excitation frequency

$V_{exc.}$ = 3.18 V f = 1 kHz R_p = 492 kohm

P.No	$Q_W.10^3$ (m^3/s)	$Q_A.10^3$ (m^3/s)	α(%)	V_m(V)	S	$\bar{S}$(%)	T_W (°C)	T_A (°C)
10	1.80	0.10	5.2	0.001	0.004	0.11	24.7	25
	1.82	0.20	9.8	0.209	0.112	3.33		
	1.80	0.33	15.5	0.372	0.094	2.81		
	1.77	0.46	20.4	0.567	0.087	2.61		
	1.73	0.58	25.1	0.696	0.074	2.21		
	1.70	0.74	30.2	0.793	0.073	2.19		
	1.69	0.91	34.9	0.900	0.064	1.91		
	1.66	1.09	39.7	1.024	0.058	1.72		
	1.62	1.31	44.6	1.136	0.059	1.55		
	1.42	1.44	50.3	1.187	0.055	1.64		
	1.24	1.53	55.3	1.229	0.064	1.92		
	1.08	1.61	59.9	1.327	0.057	1.70		
	0.90	1.64	64.6	1.506	0.057	1.69		
	0.71	1.65	69.9	1.865	0.065	1.95		
	0.47	1.46	75.6	2.526	0.123	3.67		
	0.35	1.29	78.9	1.847	0.062	1.84		
	0.19	1.14	85.5	2.077	0.085	2.54		
	0.10	0.95	90.7	2.050	0.075	2.24		
	0.05	0.87	94.5	1.998	0.073	2.17		

Table C5: Calibration data of probe 10 with 10 kHz excitation frequency

$V_{exc.}$ = 3.18 V f = 10 kHz R_p = 156 kohm

P.No	$Q_W.10^3$ (m^3/s)	$Q_A.10^3$ (m^3/s)	α(%)	V_m(V)	S	$\bar{S}$(%)	T_W (°C)	T_A (°C)
10	1.84	0.09	4.7	0.031	0.005	0.31	24.9	25
	1.82	0.21	10.3	0.145	0.032	1.90		
	1.80	0.33	15.4	0.183	0.040	2.44		
	1.76	0.44	20.0	0.270	0.031	1.87		
	1.74	0.60	25.7	0.358	0.026	1.60		
	1.70	0.72	29.6	0.386	0.030	1.80		
	1.66	0.89	35.0	0.459	0.024	1.48		
	1.66	1.09	39.8	0.519	0.023	1.42		
	1.61	1.30	44.8	0.565	0.023	1.39		
	1.42	1.44	50.4	0.631	0.031	1.89		
	1.23	1.56	55.8	0.715	0.034	2.03		
	1.09	1.62	59.9	0.774	0.047	2.86		
	0.90	1.71	65.5	0.904	0.048	2.93		
	0.76	1.75	69.8	1.004	0.043	2.61		
	0.57	1.76	75.5	1.246	0.044	2.65		
	0.43	1.68	79.6	1.480	0.033	1.99		
	0.29	1.16	85.0	1.426	0.035	2.13		
	0.10	1.55	94.1	1.506	0.034	2.06		

Table C6: Calibration data of probe 10 with 20 kHz excitation frequency

$V_{exc.}$ = 3.18 V f = 20 kHz R_p = 100 kohm

P.No	$Q_W.10^3$ (m^3/s)	$Q_A.10^3$ (m^3/s)	α(%)	V_m(V)	S	$\bar{S}$(%)	T_W (°C)	T_A (°C)
10	1.84	0.09	4.5	0.010	0.007	0.47	25.1	25
	1.84	0.21	10.4	0.111	0.024	1.64		
	1.80	0.33	15.7	0.145	0.028	1.91		
	1.76	0.44	20.0	0.226	0.029	1.93		
	1.75	0.57	24.5	0.276	0.025	1.70		
	1.70	0.73	30.0	0.325	0.023	1.56		
	1.70	0.91	34.9	0.376	0.019	1.27		
	1.66	1.09	39.8	0.424	0.016	1.09		
	1.52	1.22	44.6	0.483	0.022	1.49		
	1.33	1.37	50.7	0.547	0.025	1.70		
	1.18	1.46	55.2	0.609	0.035	2.35		
	1.04	1.53	59.5	0.675	0.048	3.27		
	0.85	1.62	65.5	0.782	0.035	2.34		
	0.72	1.68	70.2	0.859	0.045	3.03		
	0.57	1.73	75.3	1.049	0.037	2.52		
	0.43	1.76	80.3	1.184	0.039	2.67		
	0.29	1.74	85.8	1.179	0.024	1.65		
	0.19	1.72	89.9	1.226	0.036	2.41		

Table C7: Calibration data of probe 6 in smooth stratified flow condition with 4 different excitation frequencies.

$V_{exc.}$ = 3.18 V R_p = 100 kohm T_W=24.6 °C

f	WL (mm)	α (%)	V_m (V)	V
500 Hz	35.4	0.0	3.01	0.00
	34	0.3	3.07	0.02
	29	9.1	3.07	0.02
	27	14.8	3.10	0.03
	24	25.8	3.14	0.05
	22	32.7	3.17	0.06
	19	43.6	3.44	0.16
	17	50.9	5.73	1.00
	14	61.9	5.73	1.00
	10	76.0	5.73	1.00
	5	91.1	5.73	1.00
	0	100.0	5.73	1.00
1 kHz	35.4	0.0	3.09	0.00
	34	0.3	3.15	0.03
	27	14.8	3.17	0.03
	23	29.2	3.24	0.06
	19	43.6	3.44	0.14
	17	50.9	5.58	0.99
	15	58.3	5.59	1.00
	12	69.1	5.60	1.00
	7	85.5	5.60	1.00
	5	91.1	5.60	1.00
	0	100.0	5.60	1.00
10 kHz	35.4	0.0	3.46	0.00
	34	0.3	3.65	0.14
	26	19.2	3.73	0.19
	23	29.2	3.77	0.23
	21	36.3	3.83	0.27
	18	47.2	3.93	0.35
	17	50.9	4.81	0.99
	11	72.6	4.82	1.00
	7	85.5	4.82	1.00
	5	91.1	4.82	1.00
	0	100.0	4.82	1.00
20 kHz	35.4	0.0	3.35	0.00
	32	3.2	3.56	0.21
	26	19.2	3.61	0.26
	19	43.6	3.80	0.44
	17	50.9	4.37	0.99
	15	58.3	4.37	0.99
	12	69.1	4.37	0.99
	9	79.2	4.38	1.00
	5	91.1	4.38	1.00
	0	100.0	4.38	1.00

Table C8: Water temperature effect on probe impedance with 3 different excitation frequencies.

$V_{exc.}$ = 3.18 V R_p=409 kohm

P.No	f	T (°C)	V_m (V)	$\bar{V}$(%)	Z (kohm)	$\bar{Z}$(%)
6	500 Hz	16.90	1.632	0.00	124.53	0.00
		17.00	1.622	0.29	123.49	0.10
		20.00	1.578	1.50	119.22	0.49
		21.30	1.555	2.14	116.99	0.70
		22.20	1.526	2.95	114.20	0.96
		23.40	1.508	3.45	112.48	1.12
		24.20	1.482	4.17	110.02	1.34
		25.00	1.472	4.45	109.07	1.43
		26.30	1.440	5.35	106.09	1.71
		All air medium	5.220		1205.21	
	1 kHz	16.90	1.490	0.00	110.77	0.00
		17.70	1.471	0.57	108.98	0.23
		18.50	1.454	1.08	107.39	0.43
		19.20	1.443	1.42	106.37	0.56
		19.80	1.421	2.08	104.33	0.81
		21.00	1.400	2.71	102.40	1.06
		21.90	1.381	3.28	100.68	1.28
		22.60	1.368	3.67	99.50	1.42
		23.60	1.345	4.37	97.43	1.69
		24.20	1.337	4.61	96.71	1.78
		24.80	1.326	4.94	95.73	1.90
		25.50	1.310	5.42	94.30	2.08
		26.30	1.304	5.60	93.77	2.15
		All air medium	4.810		901.86	
	10 kHz	16.90	1.093	0.00	75.75	0.00
		18.00	1.082	0.95	74.89	1.63
		18.70	1.072	1.86	74.07	3.19
		19.40	1.062	2.77	73.26	4.73
		19.90	1.054	3.50	72.60	5.99
		20.60	1.047	4.13	72.03	7.07
		21.40	1.039	4.86	71.39	8.29
		22.00	1.031	5.58	70.75	9.50
		22.80	1.021	6.49	69.94	11.04
		24.40	1.003	8.13	68.50	13.78
		25.90	0.984	9.85	66.99	16.65
		26.30	0.979	10.30	66.60	17.39
		All air medium	2.194		128.354	

Table C9: Water temperature effect on probe resistance and capacitance measured with HP 4262 A DIGITAL LCR METER

P.No	T(°C)	f								
		120 Hz			1 kHz			10 kHz		
		R(k ohm)	C (pF)	Z(k ohm)	R(k ohm)	C (pF)	Z(k ohm)	R(k ohm)	C (pF)	Z(k ohm)
7	10.9	161.2	930	160.2	137.6	208	137.6	108.0	84.5	93.7
	11.3	157.2	930	156.3	135.7	208	133.6	107.3	84.5	93.2
	11.7	156.2	940	155.3	135.2	208	133.1	106.9	84.5	93.0
	12.1	154.8	940	153.9	134.3	208	132.3	106.2	84.6	92.5
	12.5	152.9	940	152.0	132.8	209	130.8	105.2	84.7	91.8
	12.8	151.3	940	150.4	131.7	209	129.8	104.4	84.8	91.2
	13.1	149.7	950	148.8	130.3	209	128.4	103.5	84.9	90.6
	13.5	147.8	950	147.0	129.1	209	127.3	102.7	85.0	90.0
	13.8	146.9	950	146.1	128.0	209	126.2	101.6	85.2	89.3
	14.2	145.6	950	144.8	126.9	209	125.2	101.0	85.2	88.8
	14.5	143.0	950	142.3	125.4	209	123.7	100.2	85.4	88.3
	15.0	141.2	960	140.5	123.8	210	122.2	99.0	85.6	87.4
	15.3	140.5	960	139.8	123.3	210	121.7	98.6	85.7	87.1
	15.8	138.2	960	137.5	121.5	211	120.0	97.3	86.0	86.1
	16.3	135.7	960	135.1	119.5	212	118.0	95.9	86.3	85.1
	16.8	133.9	960	133.3	117.5	213	116.1	94.5	86.6	84.0
	17.7	131.2	960	130.6	115.7	215	114.3	93.1	87.0	83.0
	18.5	127.2	950	126.7	113.3	217	112.0	90.4	87.5	81.0
	19.1	126.6	950	126.1	111.9	217	110.6	90.4	87.7	80.9
	23.2	115.2	960	114.8	104.9	221	103.8	85.3	88.3	77.1
	All air medium	2090	450	1704.9	960	132.2	750.6	405	57.2	229.3

Table C10:Calibration data of probe 6 at 17.6 °C water temperature

$V_{exc.}$ = 3.18 V f = 500 Hz R_p = 409 kohm

P. No	$Q_W.10^3$ (m^3/s)	$Q_A.10^3$ (m^3/s)	α(%)	V_m (V)	$\overline{V}$	T_W(°C)	T_A(°C)
6	1.79	0.00	0.0	-4.008	0.000	17.6	17
	1.74	0.17	8.8	-3.941	0.009		
	1.74	0.30	14.6	-3.670	0.044		
	1.74	0.38	17.8	-3.517	0.063		
	1.74	0.49	22.1	-3.167	0.109		
	1.71	0.58	25.4	-2.881	0.146		
	1.70	0.67	28.3	-2.495	0.195		
	1.70	0.79	31.6	-2.201	0.233		
	1.70	0.88	34.2	-1.915	0.270		
	1.66	0.98	37.1	-1.642	0.306		
	1.65	1.07	39.3	-1.435	0.332		
	1.66	1.20	42.0	-1.199	0.363		
	1.64	1.28	43.9	-0.978	0.391		
	1.61	1.42	46.8	-0.713	0.426		
	1.44	1.48	50.7	-0.315	0.477		
	1.26	1.52	54.7	0.035	0.522		
	1.11	1.57	58.6	0.338	0.561		
	1.00	1.60	61.6	0.592	0.594		
	0.91	1.62	64.1	0.774	0.618		
	0.82	1.65	66.8	0.991	0.646		
	0.68	1.68	71.3	1.161	0.668		
	0.56	1.70	75.3	1.419	0.701		
	0.42	1.72	80.2	1.615	0.726		
	0.33	1.73	84.0	1.798	0.750		
	0.21	1.75	89.2	2.408	0.829		
	0.00	1.77	100.0	3.735	1.000		

Table C11: Calibration data of probe 6 at 21.2 °C water temperature

$V_{exc.}$ = 3.18 V f = 500 Hz R_p = 409 kohm

P. No	$Q_W.10^3$ (m^3/s)	$Q_A.10^3$ (m^3/s)	α(%)	V_m (V)	$\bar{V}$	T_W(°C)	T_A(°C)
6	1.79	0.00	0.00	-4.426	0.000	21.2	18
	1.79	0.18	9.23	-4.356	0.008		
	1.77	0.23	11.34	-4.227	0.023		
	1.74	0.32	15.37	-4.067	0.042		
	1.74	0.40	18.64	-3.901	0.061		
	1.74	0.46	20.83	-3.785	0.074		
	1.71	0.53	23.73	-3.494	0.108		
	1.70	0.67	28.26	-3.017	0.164		
	1.70	0.78	31.35	-2.601	0.212		
	1.70	0.88	34.20	-2.346	0.241		
	1.68	0.97	36.68	-2.136	0.266		
	1.66	1.09	39.75	-1.830	0.301		
	1.66	1.21	42.21	-1.583	0.330		
	1.63	1.36	45.48	-1.220	0.372		
	1.61	1.41	46.72	-1.107	0.385		
	1.52	1.45	48.72	-0.890	0.410		
	1.39	1.49	51.78	-0.624	0.441		
	1.30	1.53	53.97	-0.339	0.474		
	1.17	1.57	57.25	0.006	0.514		
	1.08	1.59	59.56	0.183	0.535		
	1.00	1.62	61.89	0.432	0.564		
	0.86	1.65	65.61	0.673	0.592		
	0.77	1.67	68.27	0.906	0.619		
	0.64	1.70	72.56	1.000	0.630		
	0.51	1.71	76.92	1.149	0.647		
	0.42	1.72	80.25	1.425	0.679		
	0.34	1.73	83.74	1.955	0.741		
	0.17	1.73	90.92	2.564	0.811		
	0.00	1.74	100.00	4.190	1.000		

Table C12: Calibration data of probe 6 at 26.5 °C water temperature

$V_{exc.}$=3.18 V f = 500 Hz R_p= 409 kohm

P. No	$Q_W.10^3$ (m^3/s)	$Q_A.10^3$ (m^3/s)	α(%)	V_m (V)	$\overline{V}$	T_W(°C)	T_A(°C)
6	1.79	0.00	0.0	-4.922	0.000	26.5	18
	1.79	0.15	7.6	-4.841	0.009		
	1.79	0.22	10.8	-4.728	0.022		
	1.79	0.29	13.8	-4.582	0.039		
	1.79	0.46	20.4	-4.286	0.073		
	1.79	0.51	22.1	-4.043	0.102		
	1.77	0.59	25.2	-3.767	0.133		
	1.77	0.70	28.3	-3.465	0.168		
	1.77	0.78	30.6	-3.162	0.203		
	1.74	0.87	33.4	-2.873	0.237		
	1.74	0.99	36.3	-2.643	0.263		
	1.74	1.06	37.9	-2.431	0.288		
	1.73	1.16	40.2	-2.250	0.309		
	1.74	1.30	42.8	-2.035	0.333		
	1.74	1.49	46.1	-1.603	0.383		
	1.58	1.54	49.3	-1.356	0.412		
	1.44	1.57	52.2	-1.093	0.442		
	1.28	1.63	55.9	-0.739	0.483		
	1.21	1.65	57.6	-0.500	0.511		
	1.04	1.69	61.9	-0.179	0.548		
	0.91	1.72	65.5	0.057	0.575		
	0.78	1.75	69.2	0.333	0.607		
	0.64	1.77	73.4	0.528	0.630		
	0.54	1.79	76.9	0.830	0.664		
	0.48	1.80	79.0	0.911	0.674		
	0.38	1.82	82.8	1.067	0.692		
	0.25	1.83	88.1	1.843	0.781		
	0.13	1.85	93.5	2.266	0.830		
	0.00	1.85	100.0	3.735	1.000		

Table C13: Calibration data of probe 6

$V_{exc.}$ = 3.18 V f = 500 Hz R_p = 409 kohm

P. No	$Q_W.10^3$ (m^3/s)	$Q_A.10^3$ (m^3/s)	α(%)	V_m (V)	$\overline{V}$	T_W(°C)	T_A(°C)
6	1.79	0.00	0.0	-4.018	0.000	21.2	21.5
	1.79	0.14	7.2	-3.979	0.005		
	1.79	0.20	9.9	-3.861	0.020		
	1.79	0.29	13.8	-3.698	0.040		
	1.77	0.40	18.3	-3.423	0.075		
	1.74	0.57	24.6	-2.942	0.135		
	1.73	0.68	28.2	-2.449	0.197		
	1.74	0.84	32.5	-1.957	0.259		
	1.72	0.93	35.0	-1.686	0.293		
	1.70	1.07	38.7	-1.381	0.331		
	1.70	1.20	41.3	-1.088	0.368		
	1.68	1.35	44.6	-0.765	0.408		
	1.65	1.49	47.5	-0.470	0.445		
	1.44	1.55	51.9	-0.086	0.493		
	1.26	1.60	55.9	0.235	0.534		
	1.04	1.66	61.5	0.723	0.595		
	0.95	1.68	63.8	0.930	0.621		
	0.78	1.70	68.7	1.251	0.661		
	0.69	1.69	71.1	1.339	0.672		
	0.62	1.68	72.9	1.425	0.683		
	0.47	1.65	77.9	1.626	0.708		
	0.35	1.61	82.3	1.755	0.724		
	0.25	1.57	86.5	2.090	0.766		
	0.20	1.54	88.3	2.250	0.787		
	0.13	1.49	92.0	2.670	0.839		
	0.00	1.49	100.0	3.951	1.000		

Table C14: Calibration data of probe 7

$V_{exc.}$ = 3.18 V f = 500 Hz R_p = 371 kohm

P. No	$Q_W.10^3$ (m^3/s)	$Q_A.10^3$ (m^3/s)	α(%)	V_m (V)	$\overline{V}$	T_W(°C)	T_A(°C)
7	1.83	0.00	0.0	-4.005	0.000	23.1	23.5
	1.82	0.09	4.9	-3.969	0.005		
	1.83	0.18	9.0	-3.626	0.047		
	1.79	0.22	10.8	-3.540	0.058		
	1.79	0.30	14.2	-3.273	0.092		
	1.79	0.35	16.4	-3.144	0.108		
	1.79	0.41	18.7	-2.964	0.130		
	1.74	0.51	22.7	-2.176	0.229		
	1.73	0.60	25.7	0.335	0.543		
	1.70	0.72	29.9	0.998	0.625		
	1.70	0.81	32.3	1.203	0.651		
	1.69	0.93	35.5	1.516	0.690		
	1.66	1.04	38.5	1.685	0.711		
	1.66	1.15	40.9	1.792	0.725		
	1.65	1.28	43.6	1.936	0.743		
	1.52	1.33	46.6	2.022	0.753		
	1.35	1.39	50.8	1.970	0.747		
	1.21	1.44	54.2	1.843	0.731		
	1.13	1.46	56.5	1.926	0.741		
	1.04	1.50	59.0	2.024	0.754		
	0.95	1.53	61.6	2.155	0.770		
	0.86	1.55	64.3	2.219	0.778		
	0.77	1.58	67.1	2.289	0.787		
	0.69	1.60	70.0	2.349	0.794		
	0.60	1.62	73.1	2.485	0.811		
	0.53	1.62	75.3	2.529	0.817		
	0.45	1.64	78.4	2.557	0.820		
	0.30	1.65	84.6	2.604	0.826		
	0.25	1.65	86.8	2.654	0.832		
	0.20	1.66	89.2	2.849	0.857		
	0.00	1.23	100.0	3.995	1.000		

Table C15: Calibration data of probe 8

V_{exc} = 3.18 V f = 500 Hz R_p = 287 kohm

P. No	$Q_W.10^3$ (m^3/s)	$Q_A.10^3$ (m^3/s)	α(%)	V_m (V)	$\overline{V}$	T_W(°C)	T_A(°C)
8	1.78	0.00	0.0	-4.009	0.000	22.4	23
	1.74	0.10	5.4	-3.673	0.042		
	1.74	0.18	9.3	-3.558	0.056		
	1.71	0.22	11.6	-3.472	0.067		
	1.70	0.30	14.9	-3.322	0.086		
	1.70	0.34	16.8	-3.043	0.121		
	1.68	0.38	18.2	-2.862	0.144		
	1.67	0.47	21.8	-2.630	0.173		
	1.64	0.57	25.9	-2.331	0.210		
	1.65	0.63	27.7	-2.163	0.231		
	1.65	0.71	30.1	-1.951	0.258		
	1.63	0.81	33.2	-1.726	0.286		
	1.61	0.91	36.1	-1.525	0.311		
	1.61	1.03	39.0	-1.236	0.347		
	1.57	1.13	41.9	-1.085	0.366		
	1.55	1.29	45.5	-0.710	0.413		
	1.44	1.39	49.2	-0.419	0.449		
	1.30	1.48	53.2	-0.138	0.485		
	1.17	1.59	57.5	0.239	0.532		
	1.04	1.66	61.5	0.432	0.556		
	0.91	1.73	65.6	0.628	0.580		
	0.82	1.77	68.4	0.899	0.614		
	0.76	1.80	70.2	0.974	0.624		
	0.69	1.82	72.6	1.104	0.640		
	0.60	1.84	75.5	1.313	0.666		
	0.51	1.84	78.3	1.525	0.693		
	0.38	1.86	83.0	2.115	0.767		
	0.29	1.85	86.5	2.836	0.857		
	0.25	1.83	88.1	2.988	0.876		
	0.17	1.80	91.3	3.321	0.918		
	0.00	1.80	100.0	3.980	1.000		

Table C16: Calibration data of probe 9

$V_{exc.}$= 3.18 V f = 500 Hz R_p= 238 kohm

P. No	$Q_W.10^3$ (m^3/s)	$Q_A.10^3$ (m^3/s)	α(%)	V_m (V)	$\overline{V}$	T_W(°C)	T_A(°C)
9	1.79	0.00	0.0	-4.041	0.000	25.6	26
	1.75	0.10	5.3	-3.815	0.028		
	1.74	0.16	8.5	-3.769	0.034		
	1.74	0.20	10.4	-3.686	0.044		
	1.74	0.25	12.6	-3.580	0.057		
	1.74	0.31	15.2	-3.448	0.074		
	1.70	0.35	17.1	-3.373	0.083		
	1.70	0.40	19.0	-3.274	0.095		
	1.66	0.48	22.5	-3.188	0.106		
	1.65	0.56	25.2	-3.124	0.114		
	1.66	0.63	27.5	-3.060	0.122		
	1.63	0.70	30.1	-2.945	0.136		
	1.61	0.83	33.9	-2.766	0.159		
	1.61	0.94	36.8	-2.608	0.178		
	1.57	1.07	40.5	-2.368	0.208		
	1.57	1.15	42.4	-2.238	0.224		
	1.54	1.29	45.6	-2.065	0.246		
	1.37	1.34	49.3	-1.649	0.298		
	1.26	1.43	53.1	-1.173	0.357		
	1.17	1.48	55.8	-0.962	0.383		
	1.06	1.54	59.2	-0.620	0.426		
	0.95	1.61	62.8	-0.213	0.476		
	0.86	1.65	65.6	0.036	0.507		
	0.77	1.69	68.5	0.351	0.547		
	0.70	1.71	70.9	0.606	0.578		
	0.69	1.72	71.4	0.886	0.613		
	0.64	1.73	73.0	1.054	0.634		
	0.56	1.75	75.6	1.262	0.660		
	0.43	1.74	80.0	1.959	0.747		
	0.36	1.71	82.4	2.193	0.776		
	0.28	1.69	85.7	2.533	0.818		
	0.21	1.64	88.6	3.387	0.925		
	0.15	1.60	91.2	3.428	0.930		
	0.00	1.60	100.0	3.993	1.000		

Table C17: Calibration data of probe 10

$V_{exc.}$ = 3.18 V f = 500 Hz R_p = 238 kohm

P. No	$Q_W.10^3$ (m^3/s)	$Q_A.10^3$ (m^3/s)	α(%)	V_m (V)	$\overline{V}$	T_W(°C)	T_A(°C)
10	1.79	0.00	0.0	-4.016	0.000	24.6	25
	1.78	0.05	3.0	-4.008	0.001		
	1.76	0.16	8.4	-3.503	0.064		
	1.74	0.19	9.9	-3.387	0.078		
	1.74	0.21	10.8	-3.360	0.082		
	1.74	0.28	13.9	-3.227	0.098		
	1.74	0.33	16.0	-2.996	0.127		
	1.70	0.41	19.4	-2.656	0.169		
	1.71	0.45	21.0	-2.601	0.176		
	1.70	0.53	23.7	-2.316	0.211		
	1.69	0.58	25.6	-2.194	0.227		
	1.66	0.64	27.8	-2.036	0.246		
	1.66	0.73	30.6	-1.939	0.258		
	1.66	0.81	32.9	-1.872	0.267		
	1.61	0.91	36.2	-1.658	0.293		
	1.61	0.98	37.8	-1.503	0.313		
	1.61	1.08	40.2	-1.417	0.323		
	1.57	1.19	43.1	-1.209	0.349		
	1.57	1.26	44.6	-1.067	0.367		
	1.50	1.31	46.7	-1.055	0.368		
	1.44	1.36	48.6	-0.982	0.377		
	1.35	1.43	51.4	-0.885	0.389		
	1.26	1.49	54.1	-0.804	0.399		
	1.17	1.53	56.7	-0.902	0.387		
	1.08	1.57	59.3	-0.726	0.409		
	1.00	1.62	61.9	-0.538	0.433		
	0.92	1.65	64.2	-0.207	0.474		
	0.86	1.67	66.0	0.121	0.514		
	0.73	1.70	69.9	0.696	0.586		
	0.65	1.70	72.3	0.984	0.622		
	0.60	1.69	73.9	1.499	0.686		
	0.56	1.65	74.8	1.942	0.741		
	0.49	1.64	76.8	2.256	0.780		
	0.38	1.56	80.5	2.829	0.851		
	0.26	1.50	85.3	3.613	0.949		
	0.00	1.50	100.0	4.025	1.000		

Table C18: Calibration data of ring electrode.

$V_{exc.}$ = 3.18 V R_p = 100 kohm.

		WL(mm)	α(%)	V_m (V)	$\bar{V}$	T_w (°C)
f	500 Hz	193.7	0.0	1.20	0.000	23.8-24.2
		168.0	7.9	1.34	0.029	
		154.0	14.7	1.46	0.054	
		130.0	28.6	1.63	0.090	
		111.0	40.7	1.85	0.135	
		104.0	45.3	1.94	0.154	
		93.0	52.5	2.16	0.200	
		87.0	56.5	2.25	0.219	
		73.0	65.5	2.57	0.285	
		49.0	80.1	3.35	0.448	
		30.0	90.2	4.19	0.623	
		23.0	93.3	4.64	0.717	
		19.0	94.9	4.89	0.769	
		5.0	99.3	6.00	1.000	
	5 kHz	193.7	0.0	1.15	0.000	
		175.0	4.9	1.25	0.022	
		152.0	15.8	1.39	0.053	
		139.0	23.2	1.48	0.072	
		118.0	36.2	1.68	0.116	
		104.0	45.3	1.86	0.156	
		94.0	51.9	2.02	0.191	
		87.0	56.5	2.15	0.219	
		77.0	63.0	2.38	0.270	
		66.0	69.9	2.65	0.329	
		55.0	76.6	2.94	0.393	
		45.0	82.4	3.34	0.480	
		31.0	89.7	3.84	0.590	
		27.0	91.5	4.21	0.671	
		22.0	93.7	4.37	0.706	
		16.0	96.1	4.82	0.805	
		13.0	97.1	5.03	0.851	
		3.0	99.7	5.71	1.000	

Table C18 (continued)

$V_{exc.}$ = 3.18 V R_p = 100 kohm.

		WL(mm)	α(%)	V_m (V)	$\bar{V}$	T_W (°C)
f	10 kHz	193.7	0.0	1.13	0.000	23.5-24.1
		178.0	3.8	1.18	0.013	
		170.0	7.0	1.23	0.027	
		159.0	12.2	1.29	0.043	
		142.0	21.4	1.4	0.072	
		131.0	28.0	1.49	0.096	
		109.0	42.0	1.72	0.158	
		94.0	51.9	1.92	0.211	
		85.0	57.8	2.18	0.281	
		80.0	61.0	2.29	0.310	
		62.0	72.4	2.6	0.393	
		46.0	81.8	3.08	0.521	
		30.0	90.2	3.61	0.663	
		24.0	92.9	3.95	0.754	
		17.0	95.7	4.18	0.816	
		3.0	99.7	4.87	1.000	
	20 kHz	193.7	0.0	0.95	0.000	
		174.0	4.7	1.03	0.027	
		166.0	8.1	1.07	0.041	
		153.0	14.6	1.13	0.061	
		148.0	17.3	1.16	0.071	
		129.0	28.6	1.28	0.112	
		118.0	35.5	1.36	0.139	
		107.0	42.7	1.45	0.170	
		93.0	52.0	1.56	0.207	
		89.0	54.6	1.66	0.241	
		73.0	65.1	1.90	0.323	
		53.0	77.5	2.28	0.452	
		35.0	87.5	2.71	0.599	
		24.0	92.8	3.03	0.707	
		19.0	94.9	3.20	0.765	
		2.0	99.8	3.89	1.000	

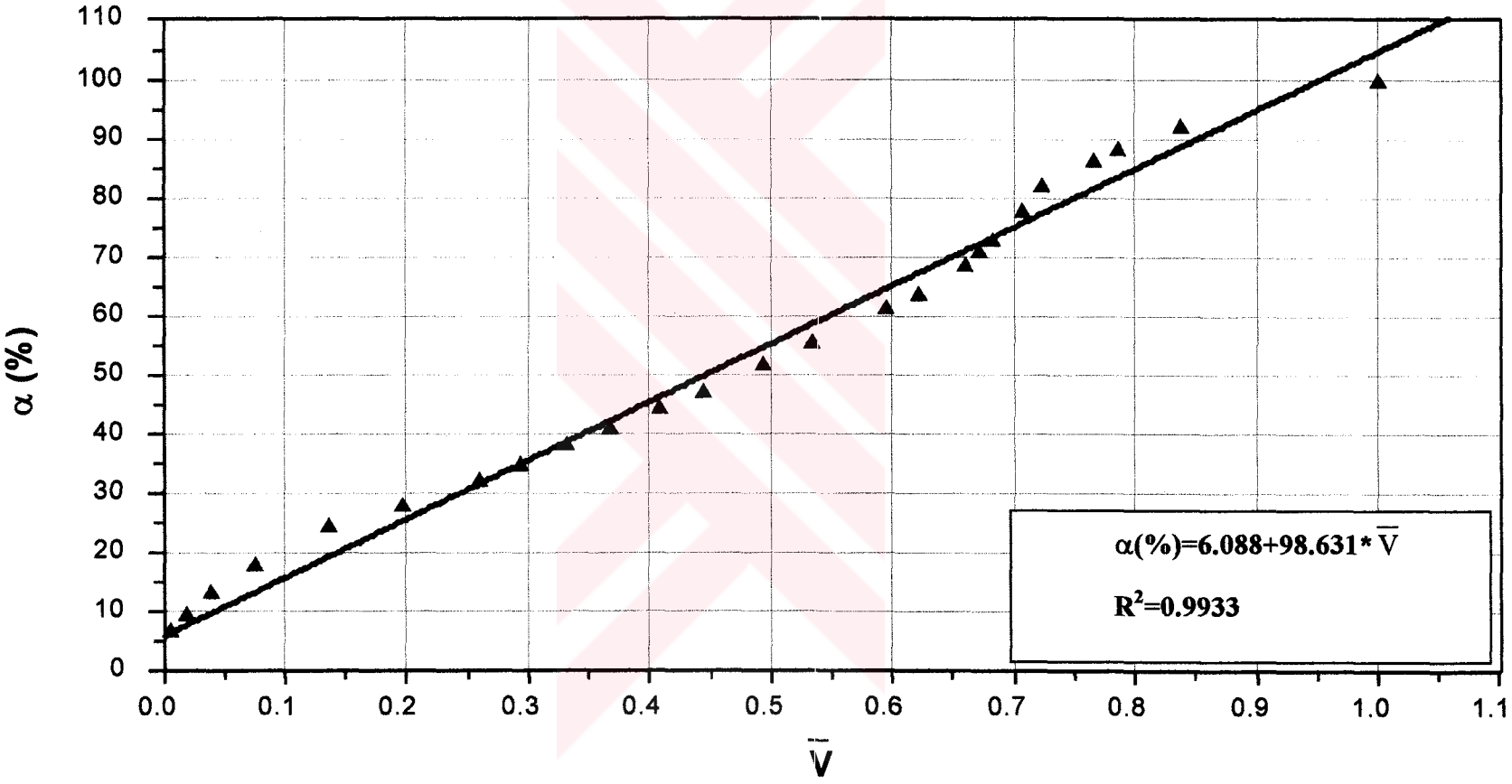

Figure C1: Calibration curve of probe 6

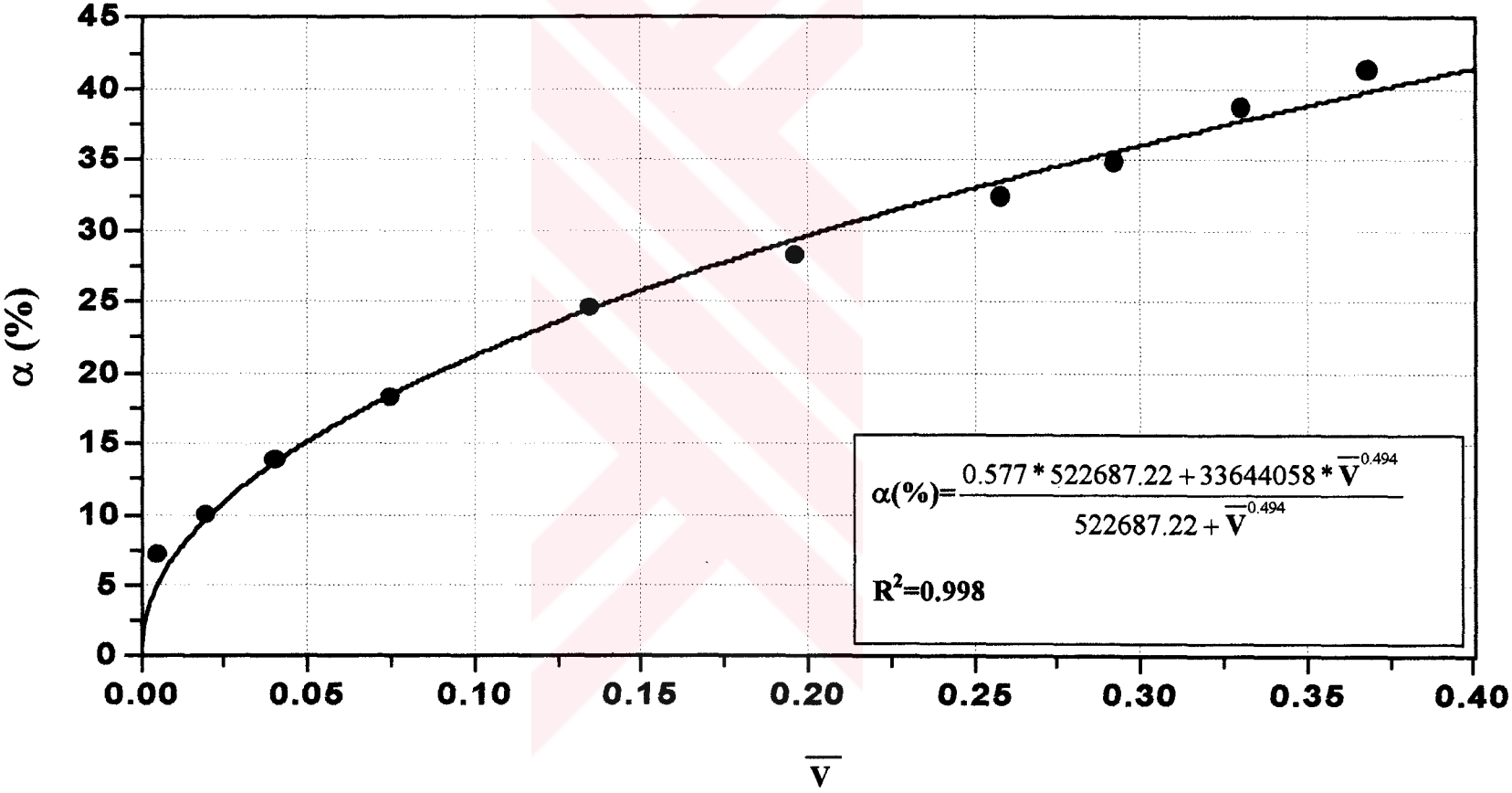

Figure C2: Calibration curve of probe 6 up to 40% void fraction.

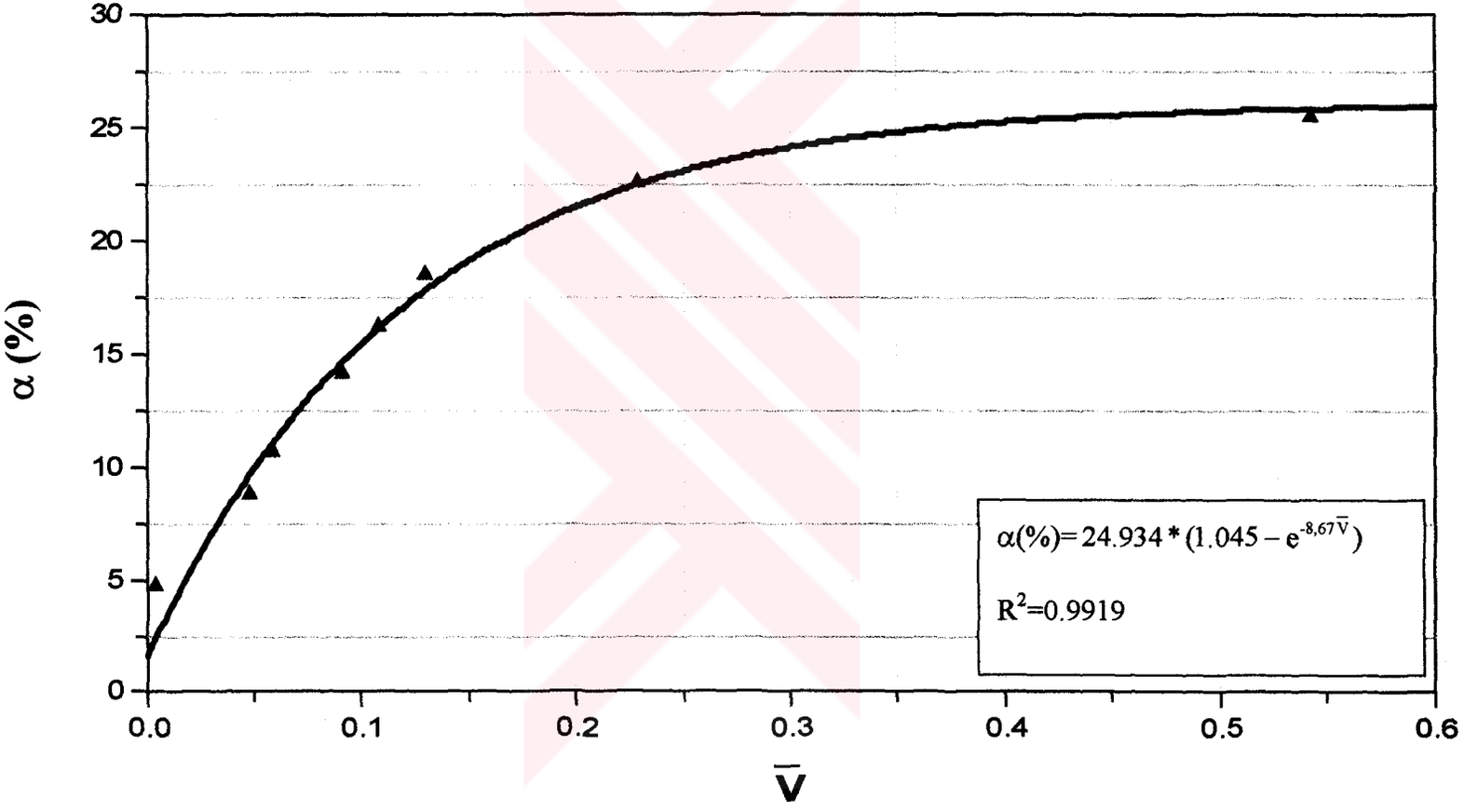

Figure C3: Calibration curve of probe 7 up to 26% void fraction

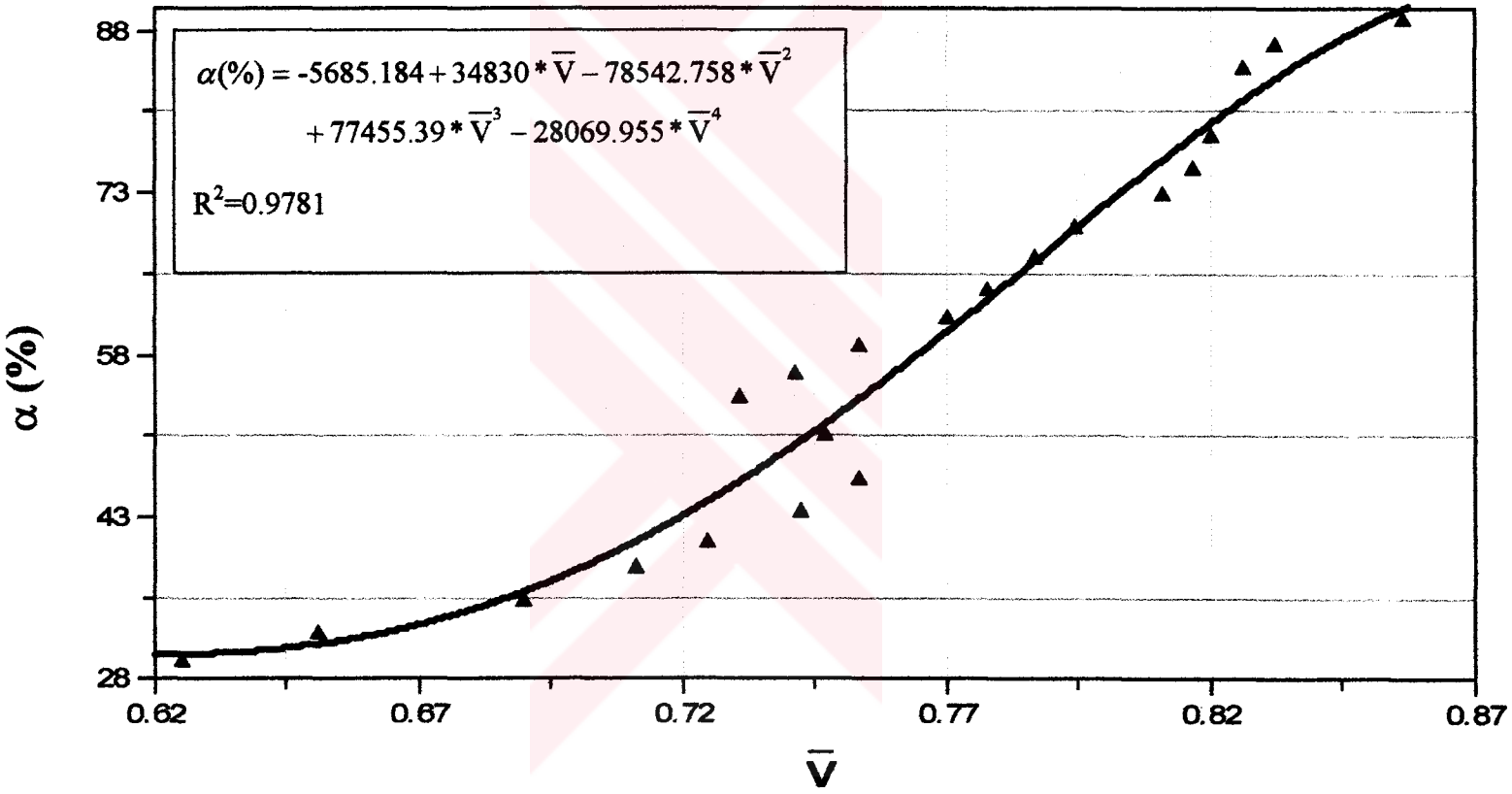

Figure C4: Calibration curve of probe 7 after 26% void fraction

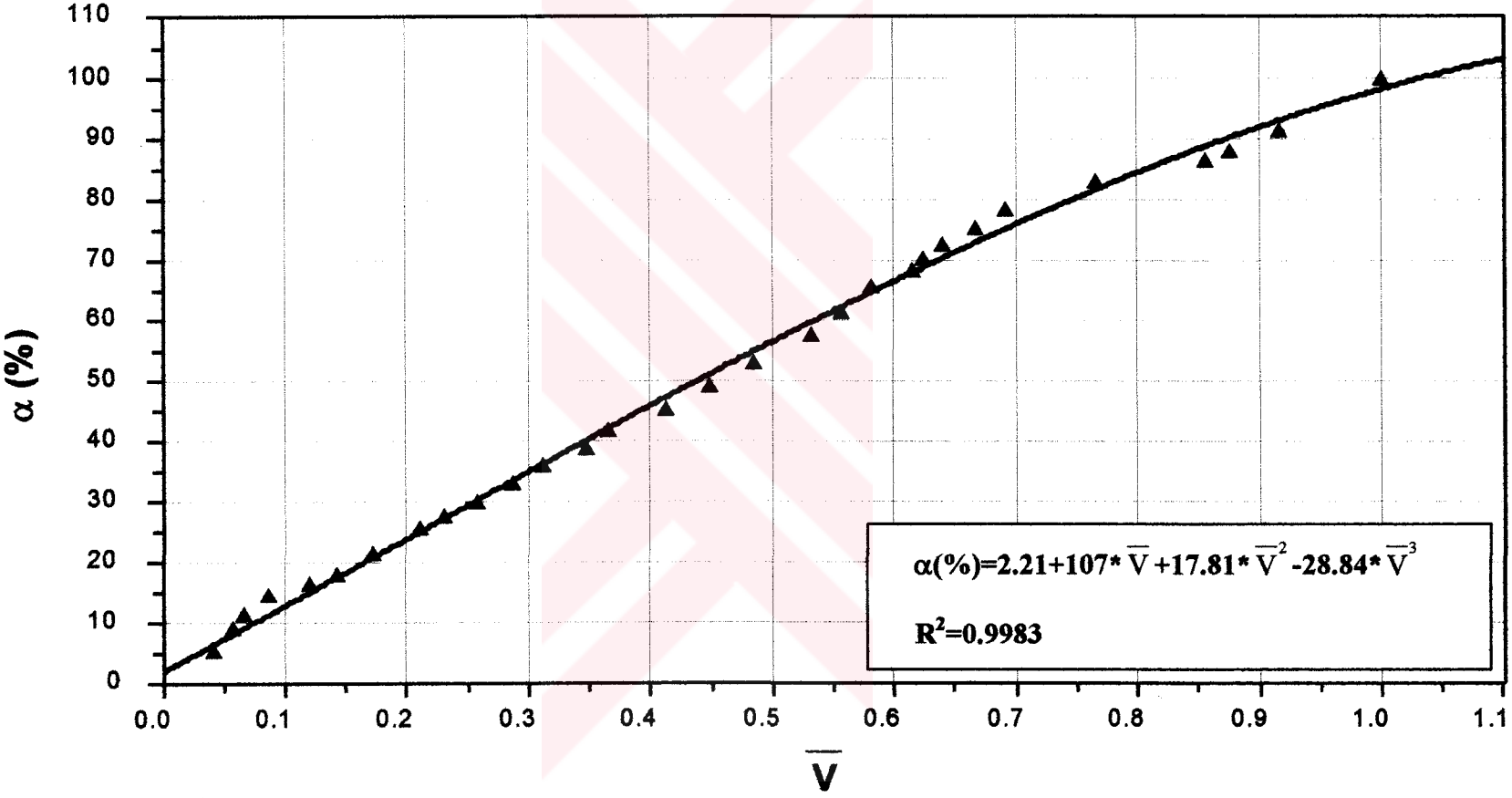

Figure C5: Calibration curve of probe 8

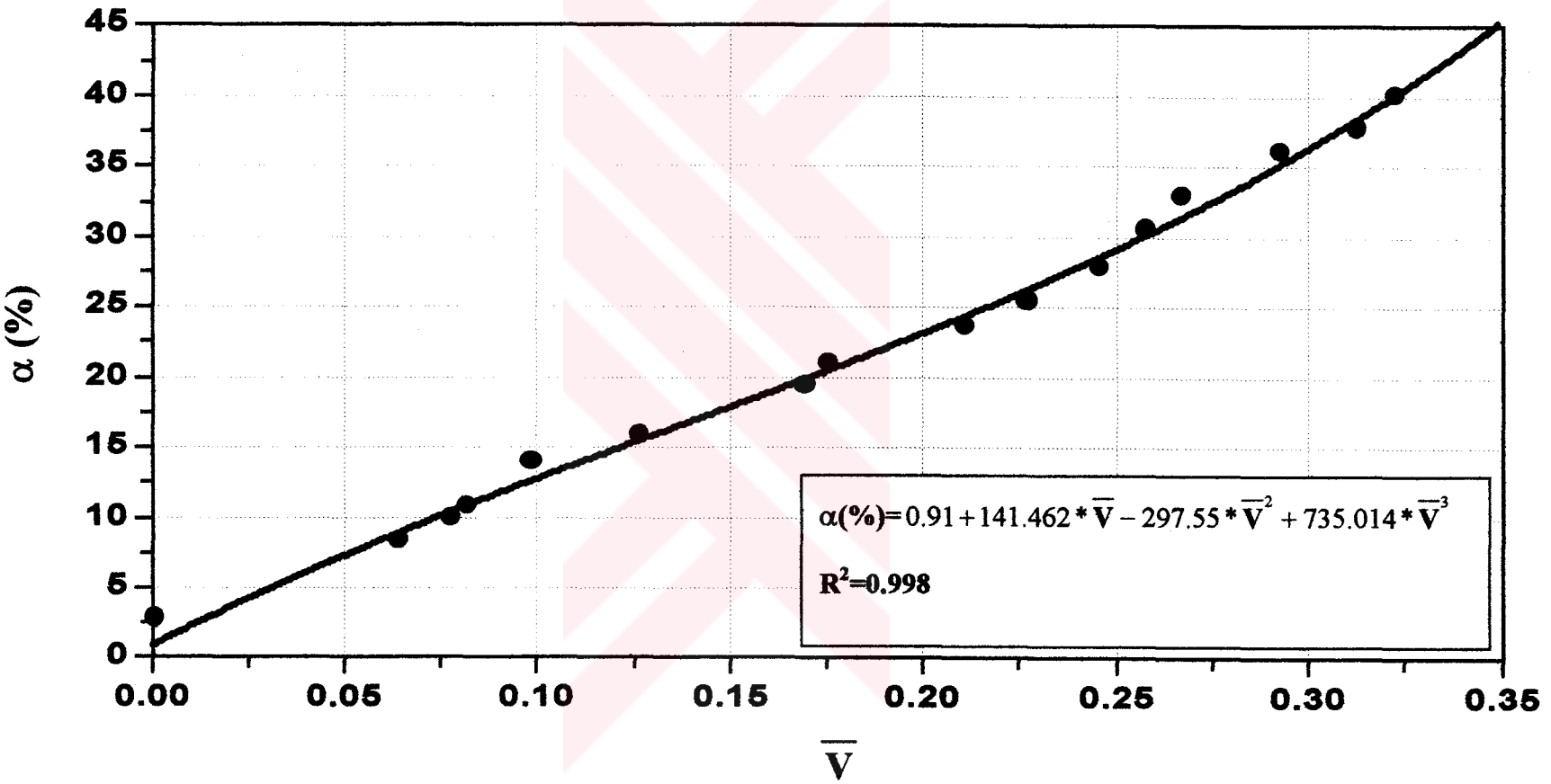

Figure C6: Calibration curve of probe 8 up to 40% void fraction

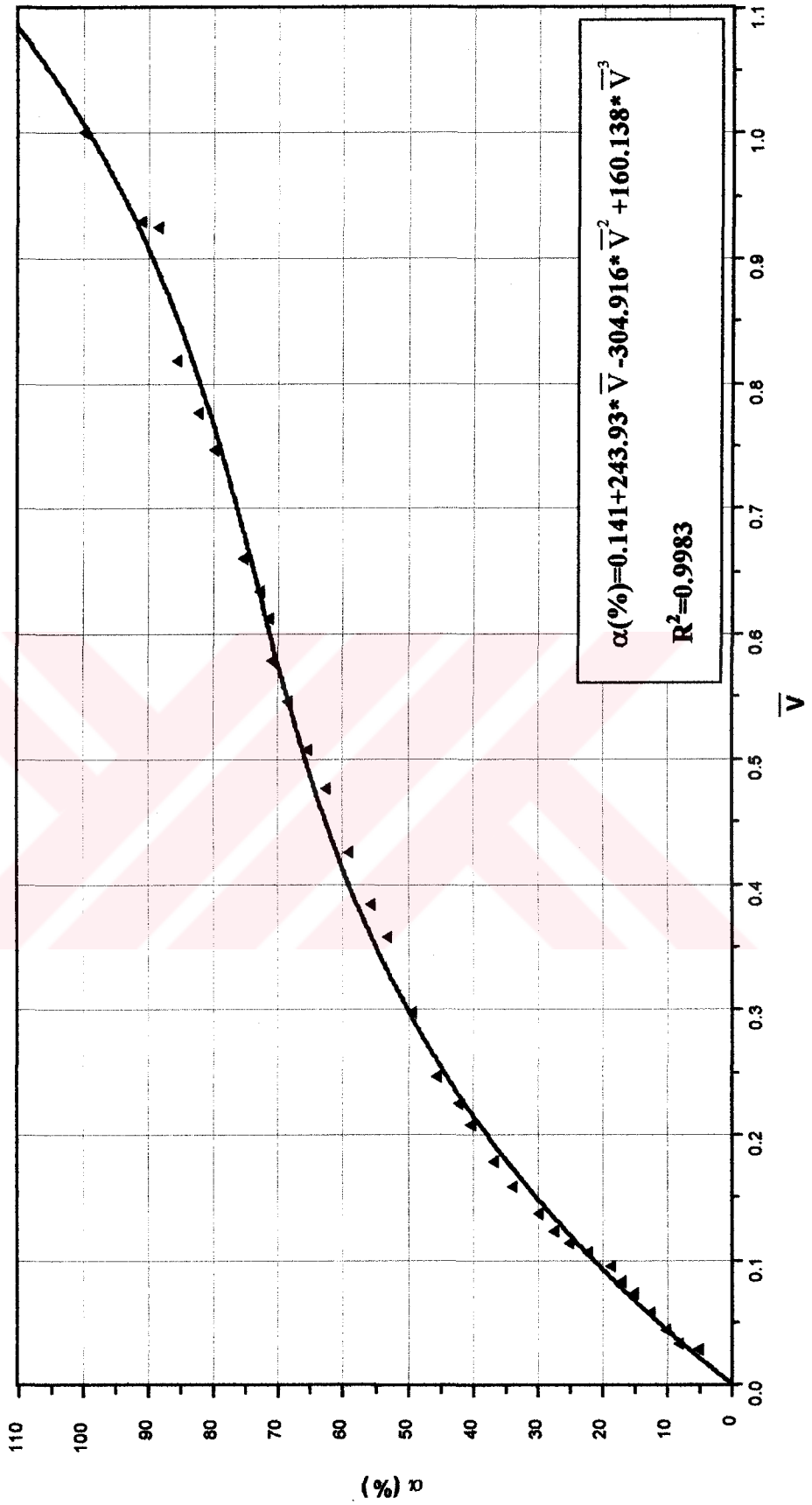

Figure C7: Calibration curve of probe 9

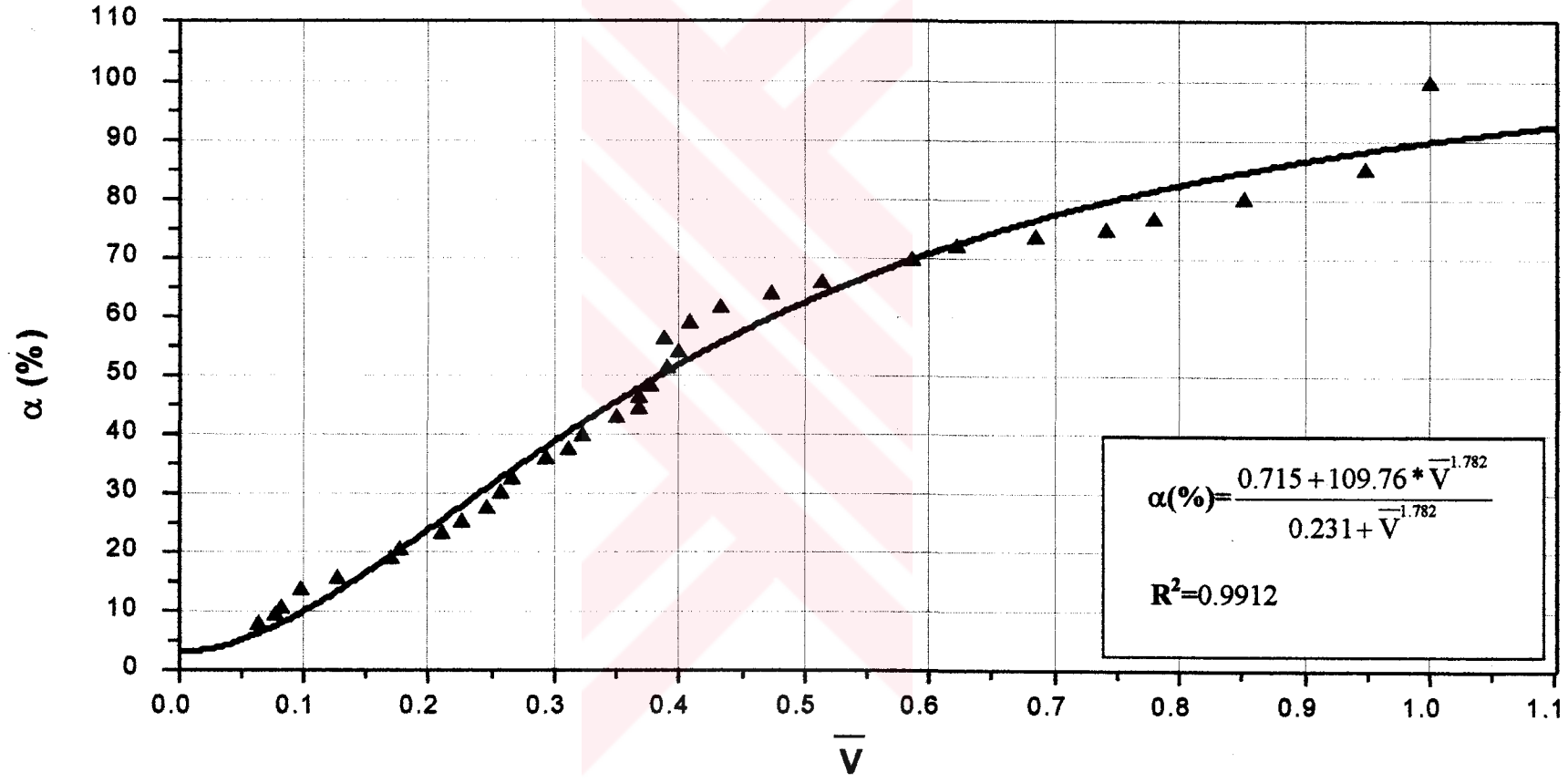

Figure C8: Calibration curve of probe 10

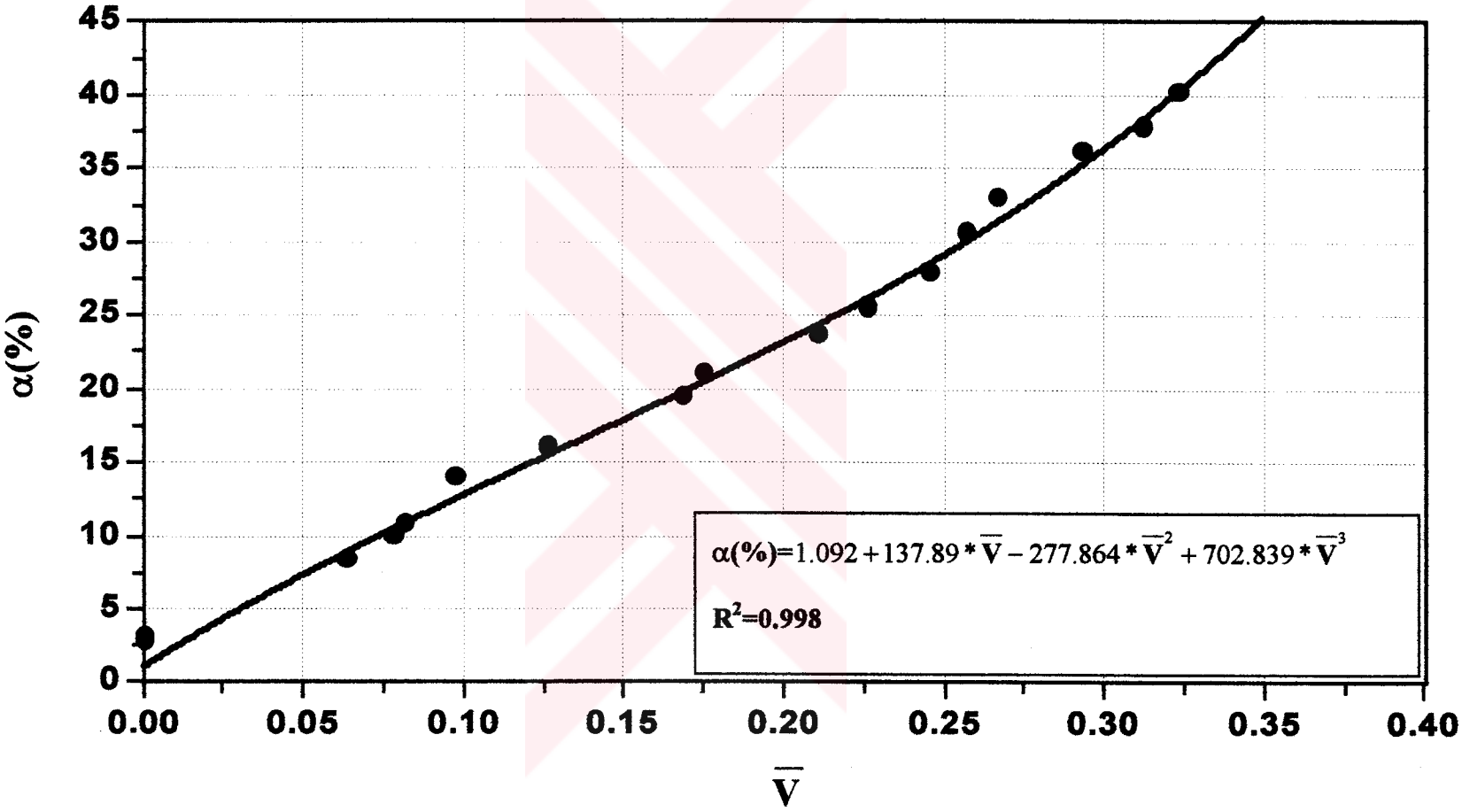

Figure C9: Calibration curve of probe 10 up to 40% void fraction

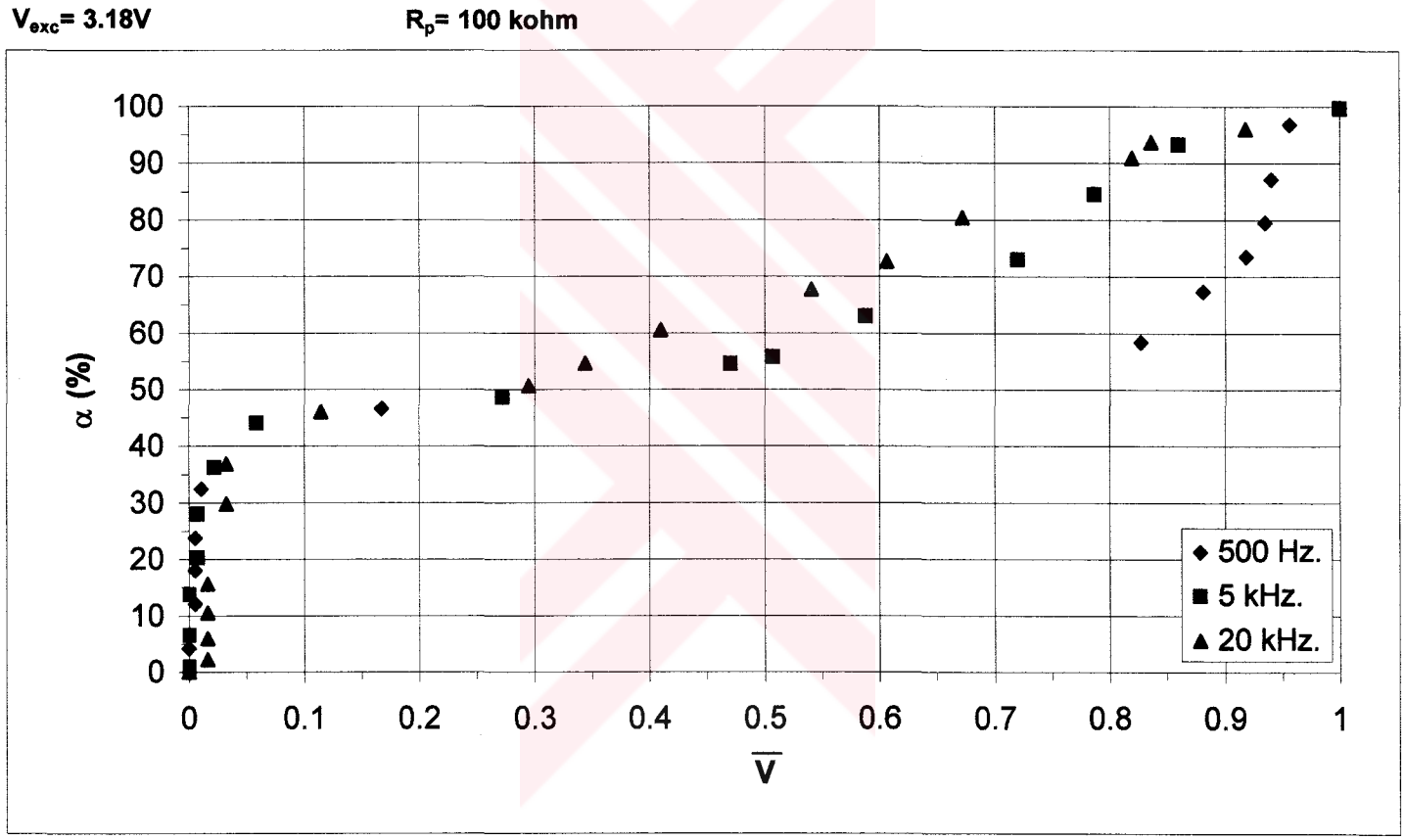

Figure C10: Calibration data of probe 1

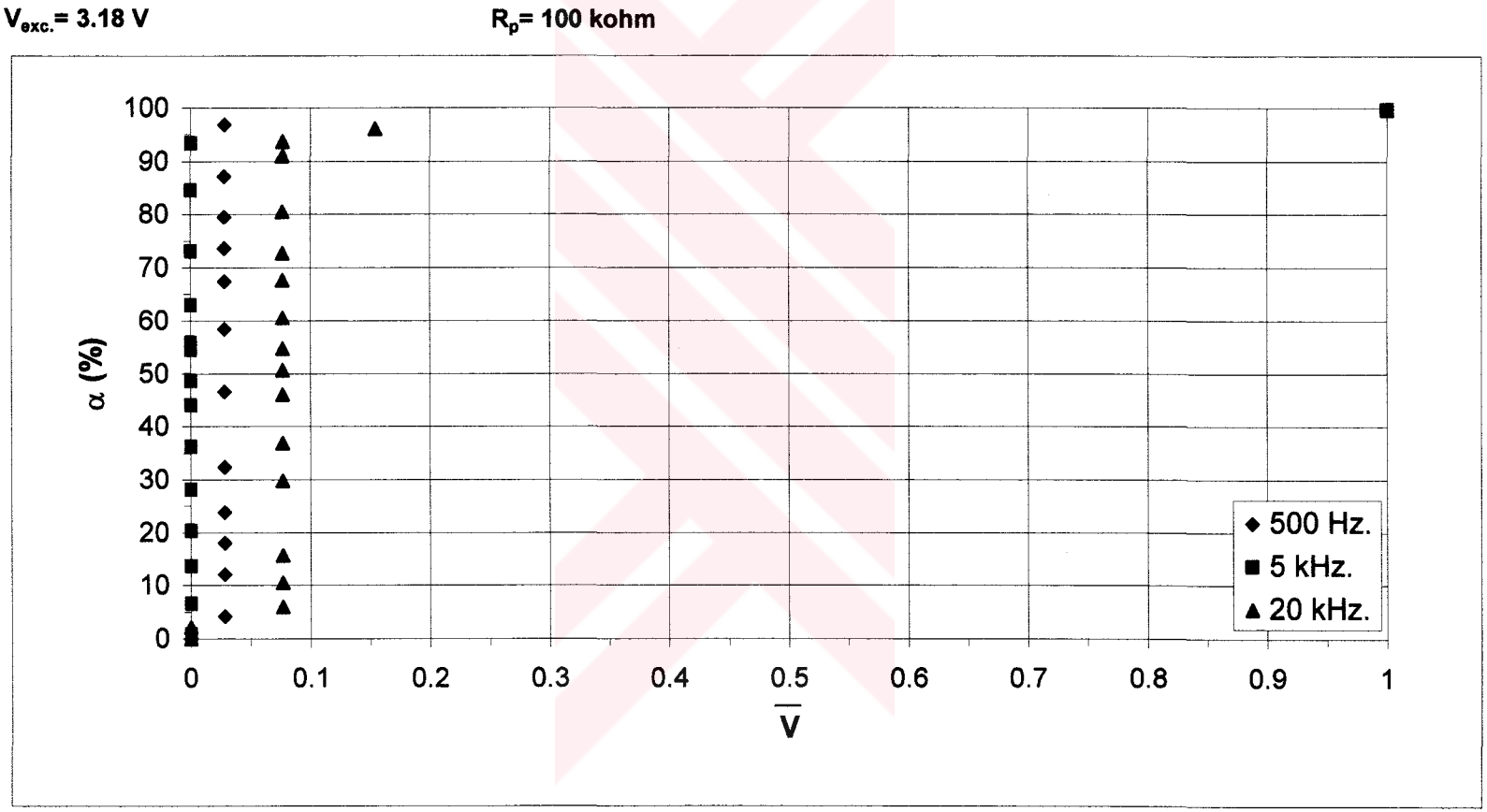

Figure C11: Calibration data of probe 2

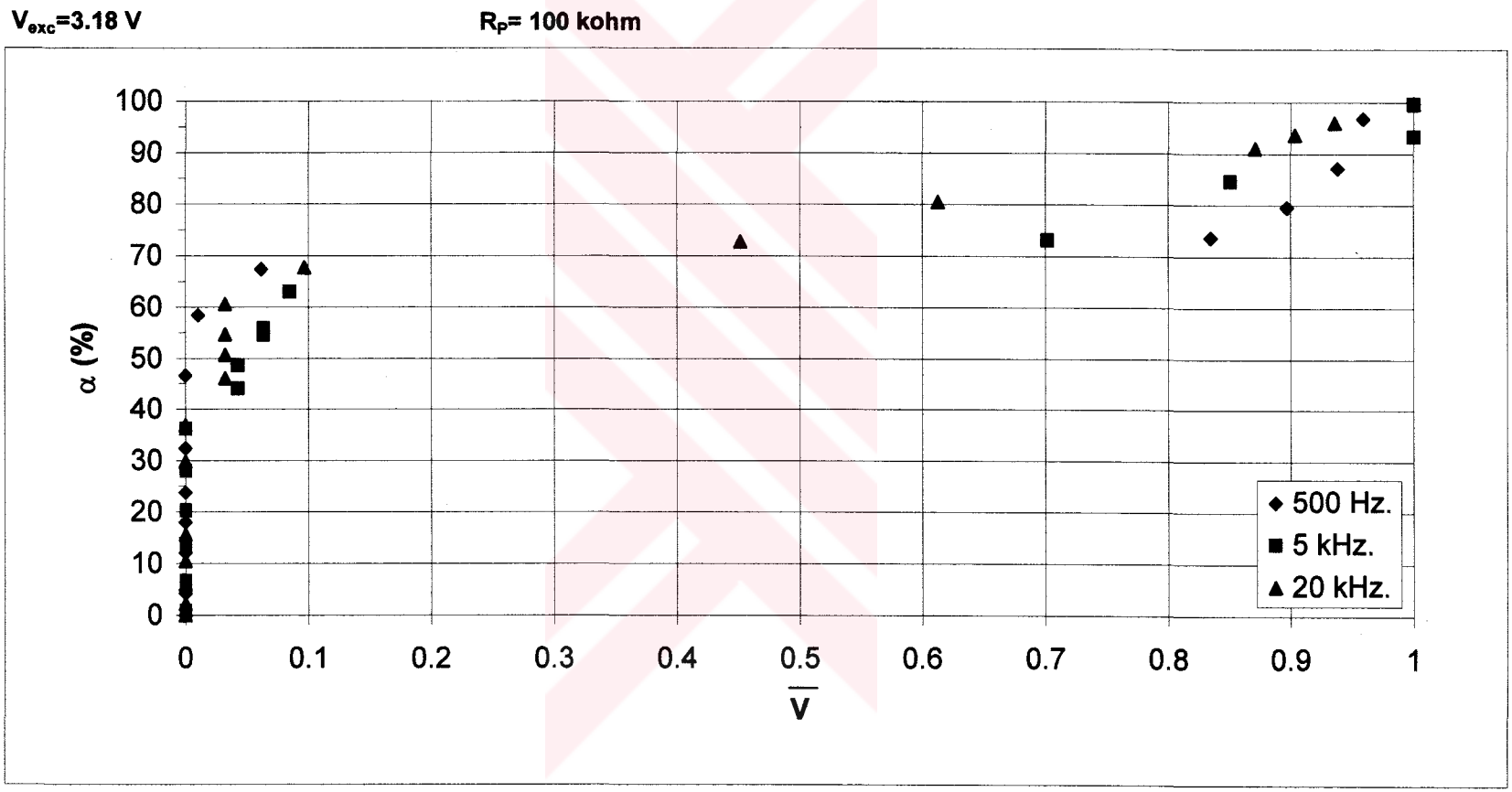

Figure C12: Calibration data of probe 3

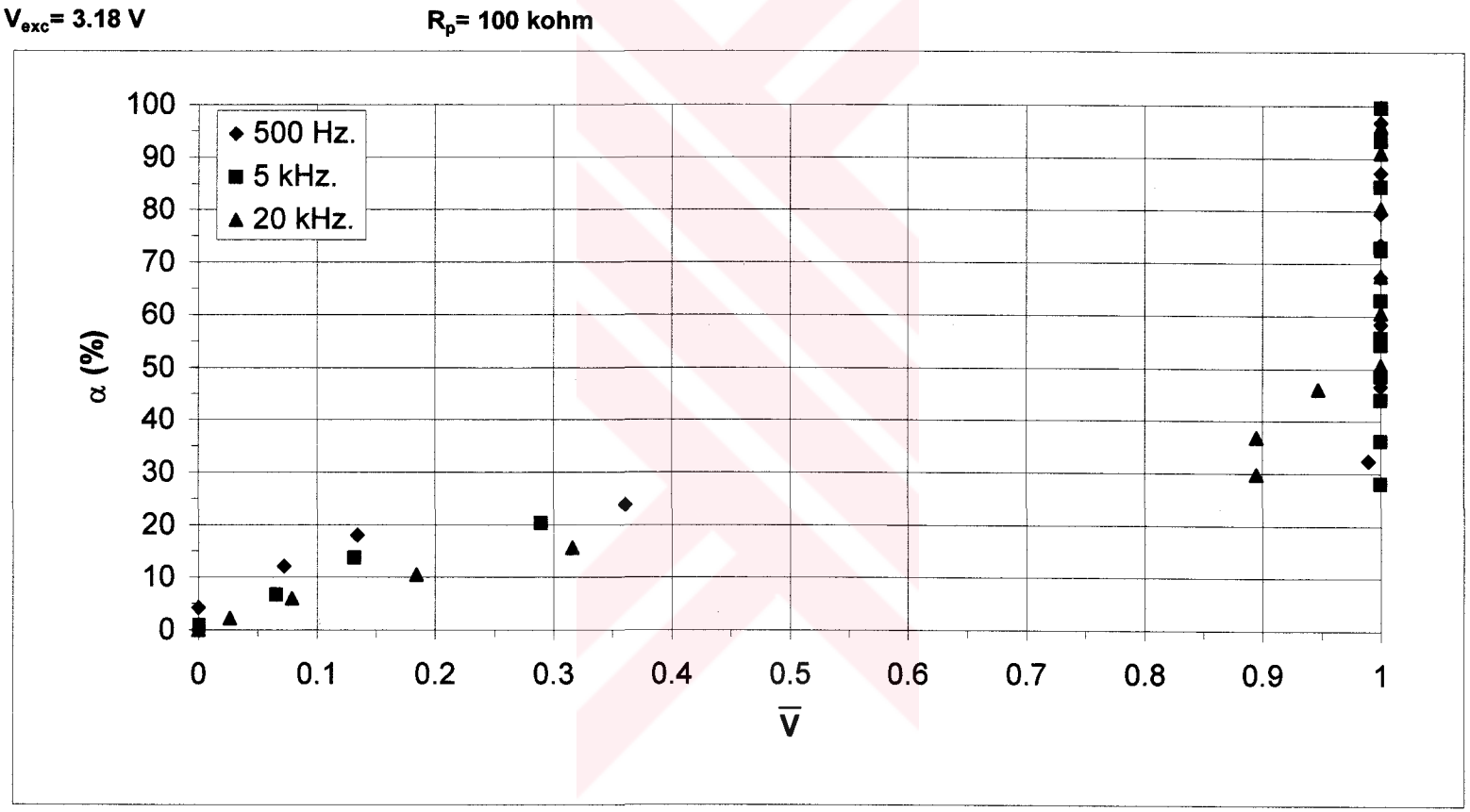

Figure C13: Calibration data of probe 4

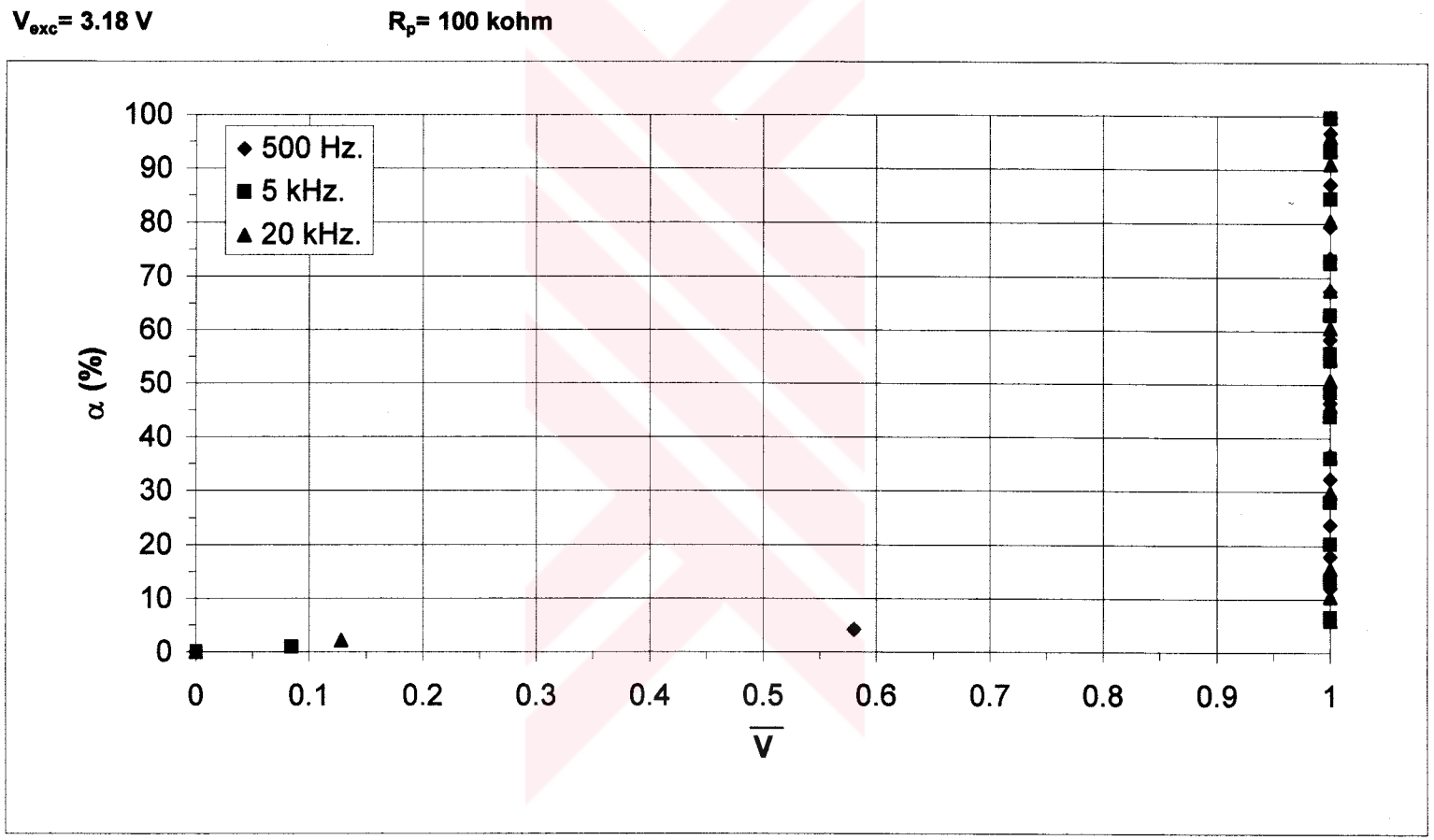

Figure C14: Calibration data of probe 5

$$v = R.[\, I_m \cos(wt + \theta)] \qquad (F.2)$$

where I_m is the peak amplitude of the current in amperes and θ is the phase angle of the current. The phasor transform of this voltage is;

$$V = R.I_m e^{j\theta} = R.I_m \angle\theta \qquad (F.3)$$

$I_m \angle\theta$ is the phasor representation of the sinusoidal current, so we can write equation F.3 as;

$$V = R.I \qquad (F.4)$$

which states that the phasor voltage at the terminals of a resistor is simply the resistance times the phasor current. Equations F.2 and F.3 both contain another important piece of information, namely, that at the terminals of a resistor there is no phase shift between the current and voltage. Figure F.3 depicts this phase relationship.

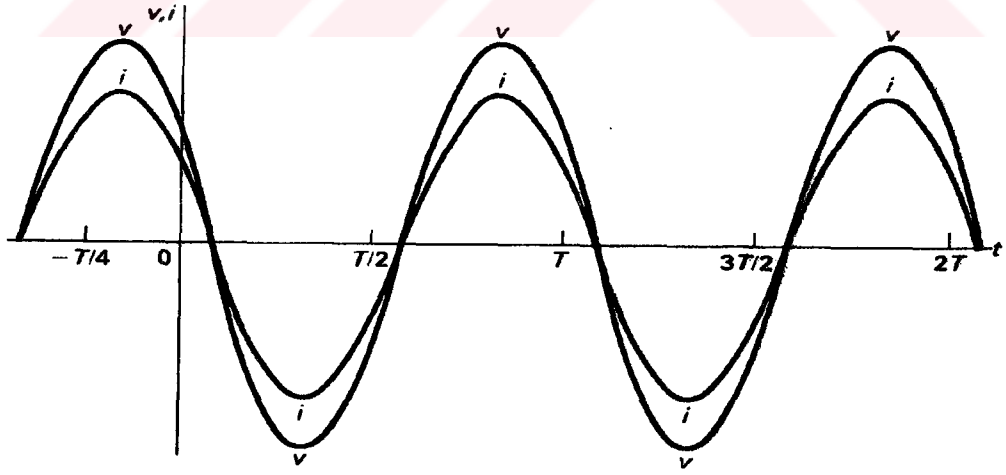

Figure F.3 : A plot showing that the voltage and current at the terminals of a resistor are in phase (θ=60°).

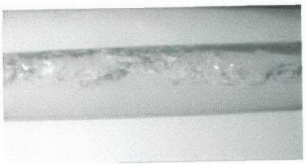

α(%)=35

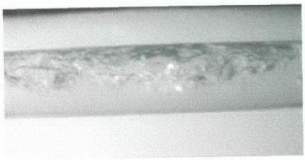

α(%)=40

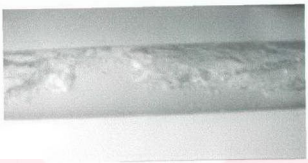

α(%)=45

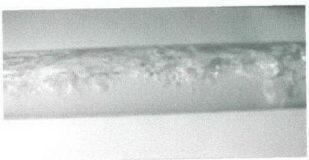

α(%)=50

α(%)=55

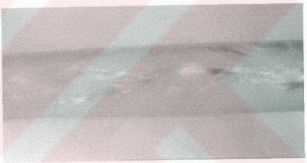

α(%)=60

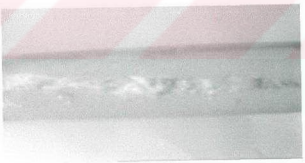

α(%)=65

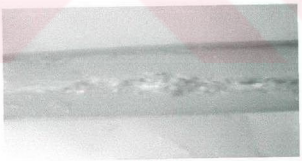

α(%)=70

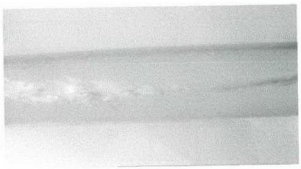

α(%)=75

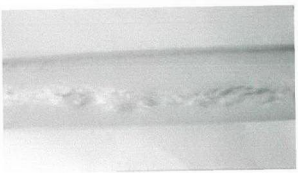

α(%)=80

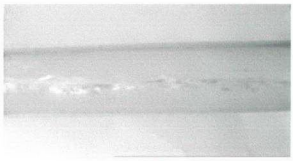

α(%)=85

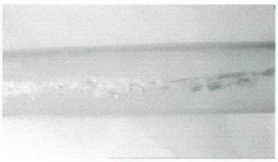

α(%)=90

Figure D.1: Flow visualization data in a horizontal Feeder

D.2 FLOW VISUALIZATION DATA IN A VERTICAL FEEDER

Inner Diameter of the Feeder: 34.5 mm
Inclination : 270 °

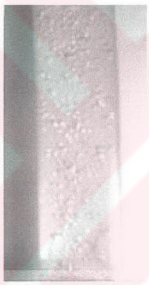

α(%)=5

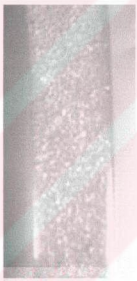

α(%)=10

α(%)=15

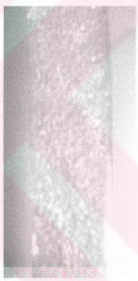

α(%)=20

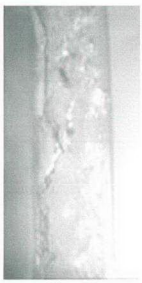

α(%)=25

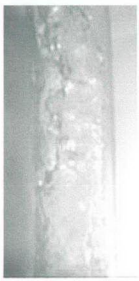

α(%)=30

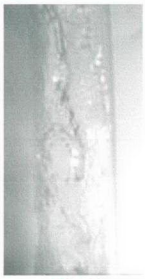

α(%)=35

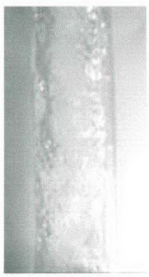

α(%)=40

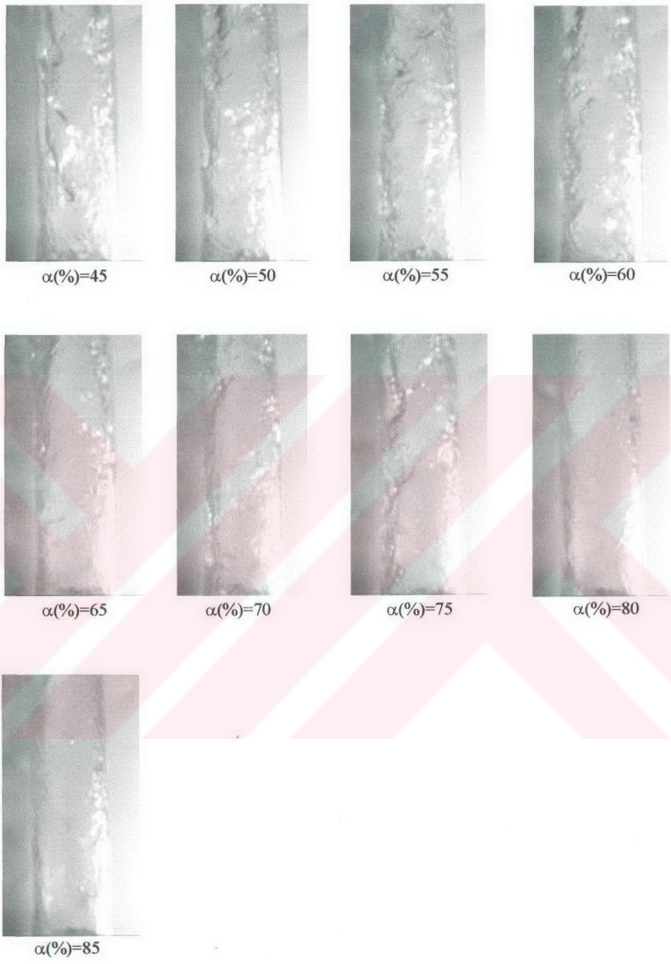

Figure D.2: Flow visualization data in a vertical Feeder

APPENDIX E

COMPUTER CODES

E.1 PRE-RESISTANCE INDICATOR CODE

```
      PROGRAM PRE-RESISTANCE
C.....THIS PROGRAM DETERMINES THE MOST APPROPRIATE
C.....PRE-RESISTANCE VALUE THAT GIVES THE WIDEST VOLTAGE
C.....RANGE DUE TO THE IMPEDANCE VARIATION OF THE PROBE
C.....BETWEEN 0 AND 100 PERCENT OF VOID FRACTION .....
      CHARACTER CEVAP*1
    4 PRINT*, 'ENTER THE IMPEDANCE (Z) OF THE PROBE IN ALL
      WATER MEDIUM (OHM)'
      READ(*, *) A
      PRINT*, 'ENTER THE IMPEDANCE OF THE PROBE IN ALL AIR
      MEDIUM (OHM)?'
      READ *, B
      I=A
      C=(B/(I+B))
      D=(A/(I+A))
      E=C-D
      RMAX=E
      DO 10 I= A+1,B
      C=(B/(I+B))
      D=(A/(I+A))
```

```
      F=C-D
      IF (F .GT. RMAX) THEN
      RMAX=F
      I1=I
     END IF
10 CONTINUE
      WRITE(* ,11)I1
11  FORMAT(' FOR THIS IMPEDANCE VARIATION  APPROPRIATE
     * VALUE OF PRE-RESISTANCE IS',1X ,I4,1X, 'K.OHM .')
      PRINT*, 'CONTINUE TO EVALUATE?(Y/N)'
      READ(*, 13) CEVAP
13  FORMAT(A1)
      IF (CEVAP .EQ. 'Y' .OR. CEVAP .EQ. 'y') THEN
      GO TO 4
      END IF
15  END
```

E.2 VOID FRACTION INDICATOR CODE

```
      PROGRAM LEVEL INDICATOR
C.....THIS PROGRAM CALCULATES THE VOID FRACTION IN THE
C.....HEADER AND FEEDERS IN STRATIFIED FLOW CONDITION...
      CHARACTER CEVAP*1
      PRINT*, 'ENTER THE INNER RADIUS OF THE PIPE(mm)?'
C.....A IS THE INNER RADIUS OF THE HEADER OR FEEDER.....
    4 READ(*, *) A
      PRINT*, 'ENTER THE WATER HEIGHT FROM THE BASE
     *LINE(mm)?'
C.....B IS THE WATER HEIGHT FROM THE BASE LINE.....
      READ *, B
C.....Y IS THE AREA OF CIRCLE (mm2).....
      Y=3.141592654*A**2
```

```
      IF(B .LE. A) THEN
      X=SQRT(A**2-(A-B)**2)
C.....Z IS THE  CENTERAL ANGLE BETWEEN THE LINES FROM..
C..... THE CENTRE OF THE CIRCLE TO THE CONTACT POINTS...
C.....OF THE WATER ON BOTH SIDE OF THE CIRCLE.....
      Z=ASIN(X/A)*180/ 3.141592654
C.....AO IS THE AREA OCCUPIED BY THE WATER .....
      AO=(2*Z/360)*Y-(2*X*(A-B)/2)
C.....XF IS THE VOID FRACTION(%) .....
      XF=(Y-AO)/Y*100
      WRITE(* ,*)XF
      ELSE
C.....IF THE WATER LEVEL FROM THE BASE LINE EXCEEDS THE.
C.....RADIUS OF THE HEADER OR FEEDER , FOLLOWING PART ...
C.....OF THE PROGRAM CALCULATES THE VOID FRACTION(%)...
C.....BY THE SAME PROCEDURE.....
      X=SQRT(A**2-(B-A)**2)
      Z=ASIN(X/A)*180/ 3.141592654
      AO=Y*(1-Z/180)+2*X*(B-A)/2
      XF=(Y-AO)/Y*100
      WRITE(* ,*)XF
      END IF
      PRINT*, 'CONTINUE TO EVALUATE?(Y/N)'
      READ(*, 13) CEVAP
 13   FORMAT(A1)
      IF (CEVAP .EQ. 'Y' .OR. CEVAP .EQ. 'y') THEN
      GO TO 4
      END IF
 15   END
```

APPENDIX F

THEORY OF AC CIRCUIT

F.1 THE SINE WAVE AND ITS PROPERTIES

A sinusoidally varying function can be expressed as either a sine function or a cosine function[20]. There is no clear choice for the use of either function. Cosine function was used in this chapter. The physical representation of a sinusoidal wave developed from a rotating vector is shown in figure F.1. This representation may be for either current or voltage. The instantaneous voltage, v, at a time t is related to the maximum or peak voltage, V_m, by the equation;

$$v = V_m.\cos wt$$

Where w is the angular velocity of the rotating vector in radians per second. (For current, replace v by i and V_m by I_m). The time taken for one revolution or cycle is called the period(T). Hence the frequency, f, in cycles per second is related to the period.

$$f = \frac{1}{T}$$

The unit of frequency is Herzt (Hz).

There are 2π radians in one cycle; hence the following relationship can be written:

$$w = 2\pi f = \frac{2\pi}{T}$$

Several signals having the same frequency and peak amplitude will not necessarily have precisely the same instantaneous amplitude, as illustrated in figure F.1. This difference is the result of the phase angle,θ , which is the angle between the two rotating vectors. When we speak of the phase angle of a sine wave, it is understood that its rotating vector is θ radians counterclockwise from zero (horizontal) at time t=0. When the peak amplitude, frequency and phase angle of a sine wave are given, its instantaneous value at any time t can be calculated by;

$$v = V_m . \cos(wt + \theta)$$

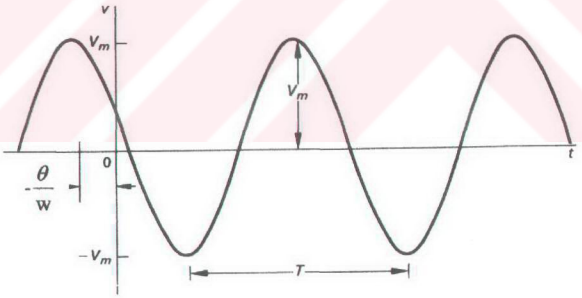

Figure F.1: A sinusoidal voltage

The rms value of a periodic function is defined as the square root of the mean value of the squared function. Hence, if $v = V_m . \cos(wt + \theta)$, the rms value of v is

$$V_{rms} = \sqrt{\frac{1}{T}\int_{t_0}^{t_0+T} V_m^{\,2} \cos^2(wt+\theta)dt} \qquad \text{(F.1)}$$

The mean value of the squared voltage is obtained by integrating v^2 over one period, that is from t_0 to t_0+T, and then dividing by the range of integration, T. The starting point for integration, t_0, is arbitrary. The equation F.1 reduces to

$$V_{rms} = \frac{V_m}{\sqrt{2}}$$

F.2 THE PHASOR

The phasor is a complex number that carries the amplitude and phase angle information of a sinusoidal function.

There are two ways to designate a complex number; the cartesian, or rectangular form , the polar or trigonometric form. In rectangular form, a complex number is written in terms of its real and imaginary components; hence

$$n = a + jb$$

where a is the real component, b is the imaginary component, and j is by definition $\sqrt{-1}$.

In polar form, a complex number is written in terms of its magnitude, or modulus, and angle or argument; hence

$n=ce^{j\theta}$

where c is the magnitude, θ is the angle, e is the base of natural logaritm and as before $j=\sqrt{-1}$. In literature, the symbol $\angle\theta$ is frequently used in place of $e^{j\theta}$; that is the polar form is written

$n=c\angle\theta$

A complex number is represented graphically on a complex number plane, which uses the horizontal axis for plotting the real component and the vertical axis for plotting the imaginary component. The angle of the complex number is measured counterclockwise from the positive real axis. The graphical plot of the complex number $n = a+jb = c\angle\theta$, if we assume that a and b are both positive, is shown in figure F2.

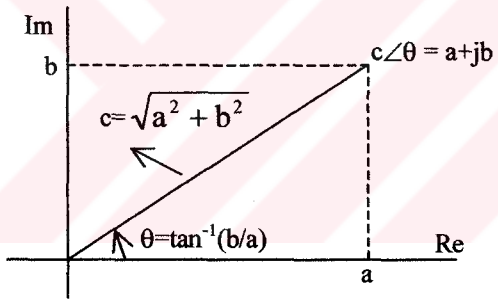

Figure F.2: The graphical representation of a+jb when a and b are both positive

F.3 V-I RELATIONSHIPS FOR A RESISTOR

From Ohm's law, if the current in a resistor varies sinusoidally with time, that is;

$i = I_m \cos(wt + \theta)$, the voltage at the terminals of the resistor;

$$v = R.[\, I_m \cos(wt + \theta)] \qquad (F.2)$$

where I_m is the peak amplitude of the current in amperes and θ is the phase angle of the current. The phasor transform of this voltage is;

$$V = R.I_m e^{j\theta} = R.I_m \angle\theta \qquad (F.3)$$

$I_m \angle\theta$ is the phasor representation of the sinusoidal current, so we can write equation F.3 as;

$$V = R.I \qquad (F.4)$$

which states that the phasor voltage at the terminals of a resistor is simply the resistance times the phasor current. Equations F.2 and F.3 both contain another important piece of information, namely, that at the terminals of a resistor there is no phase shift between the current and voltage. Figure F.3 depicts this phase relationship.

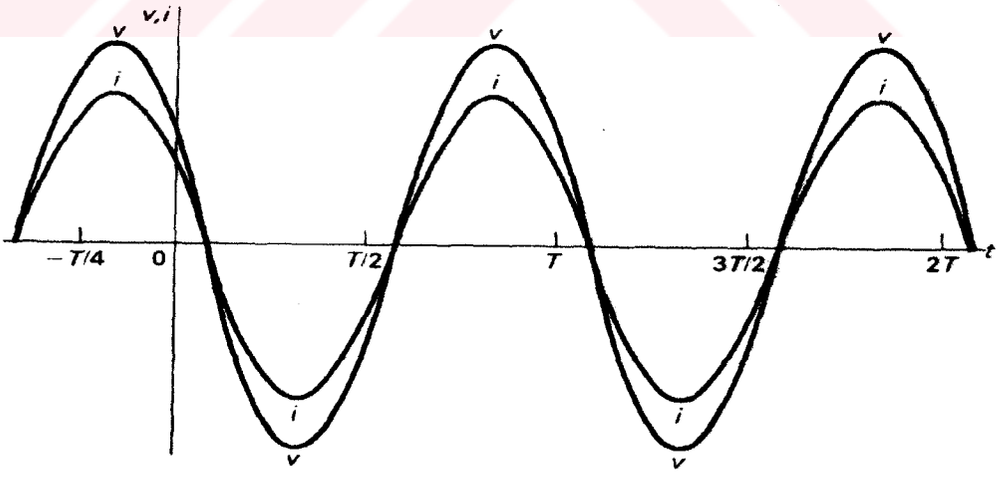

Figure F.3 : A plot showing that the voltage and current at the terminals of a resistor are in phase (θ=60°).

F.4 V-I RELATIONSHIP FOR A CAPACITOR

The amount of stored charge, Q, is proportional to the voltage across the capacitor.

$$Q = C.v$$

This expression may be differentiated on both sides to obtain;

$$\frac{dQ}{dt} = C\frac{dv}{dt}$$

Since the current is defined as i=dQ/dt

$$C\frac{dv}{dt} = i = I_m \cos(wt + \theta) \qquad (F.5)$$

If the equation F.5 rearranged and integrated;

$$v = \frac{I_m}{C}\int \cos(wt + \theta)\, dt = \frac{I_m}{wC}\left(\sin(wt + \theta)\right)$$

Using the trigonometric identity sin x = cos(x-90°), the following expression is obtained;

$$v = \frac{I_m}{wC}\cos\left((wt + \theta) - 90^o\right) \qquad (F.6)$$

This result states that the voltage across the capacitor remains sinusoidal and lags 90° behind the current. The phasor representation of the voltage given by equation F.6 will be;

$$V = \frac{I_m}{wC} e^{j(\theta-90^\circ)} = \frac{I_m}{wC} e^{j\theta} . e^{-j90^\circ}$$

where $e^{-j90^\circ} = \cos 90^\circ - j \sin 90^\circ = -j$

$$V = -\frac{j}{wC} I \qquad \text{(F.7)}$$

This relationship can be rewritten as;

$$V = \frac{I_m}{wC} \angle \theta - 90^\circ$$

This relationship is illustrated in figure F.4

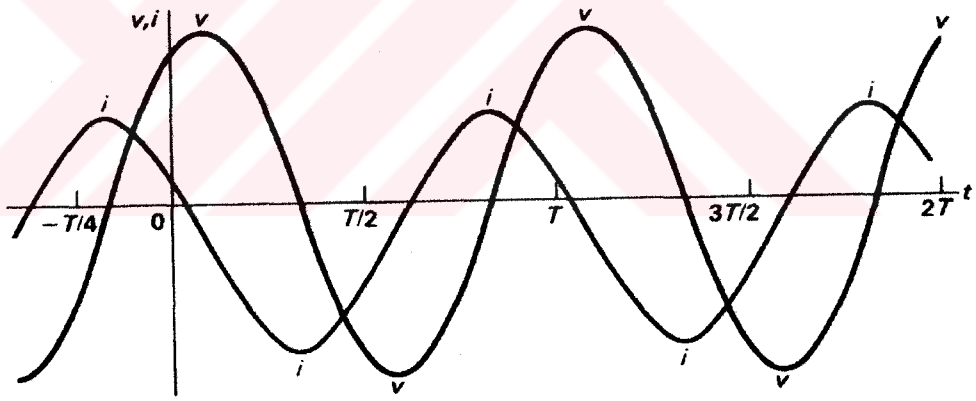

Figure F.4: A plot showing the phase relationship between the current and voltage at the terminals of a capacitor (θ=60°).

It should be noted that, both equation F.4 and equation F.7 are in the same form as;

$V=Z.I$

Where Z represent the impedance of the circuit element. Thus the impedance of a resistor is R and the impedance of a capacitor is 1/jwC. In all cases, impedance is measured in ohms. The term capacitive reactance describes the quantity $-1/wC$ where as the impedance of a capacitor is 1/jwC or $j(-1/wC)(\Omega)$.

APPENDIX G

ERROR ANALYSIS OF DIRECT MEASUREMENTS

Error is defined as the difference between the measured quantity and the true value of the quantity.

The uncertainty , δx, in a measurement of x;

(Measured x)= $x_{best} \mp \delta x$

where x_{best} is defined as best estimate of x, indicates the reliability or precision of the measurement. However the uncertainty δx by itself does not mean much. Obviously the quality of a measurement is indicated not just by the uncertainty, δx, but also by the ratio of δx to x_{best}; and this leads us to consider the fractional uncertainty;

$$\text{fractional uncertainty} = \frac{\delta x}{|x_{best}|}$$

Suppose that x,...,w are measured with uncertanties $\delta x,\ldots,\delta w$ and the measured values are to be used to compute;

$$q = \frac{x \times \ldots \times z}{u \times \ldots \times w}$$

If the uncertainties in x,...,w are independent and random, then the fractional uncertainty in q is the sum in quadrature of the individual fractional uncertainties,

$$\frac{\delta q}{|q|} = \sqrt{\left(\frac{\delta x}{x}\right)^2 + \ldots\ldots + \left(\frac{\delta z}{z}\right)^2 + \left(\frac{\delta u}{u}\right)^2 + \ldots\ldots + \left(\frac{\delta w}{w}\right)^2} \qquad \text{(G.1)}$$

Due to the homogenous flow model, average velocities of gas phase and liquid phase are equal to each other (s=1), and so;

$\alpha=\beta$

$$\alpha = \frac{\text{Volume flow rate of gas phase}}{\text{Total volume flow rate of mixture}} = \frac{Q_A}{Q_W + Q_A} = \frac{1}{1 + \frac{Q_W}{Q_A}}$$

$\alpha = f(Q_W, Q_A)$

According to the equation G.1; the total error in α which is a function of measured independent variables Q_A and Q_W is obtained as;

$$\frac{\delta \alpha}{|\alpha|} = \sqrt{\left(\frac{\delta Q_W}{Q_W}\right)^2 + \left(\frac{\delta Q_A}{Q_A}\right)^2}$$

Volume flow rate of water was measured with a turbine type flowmeter with $\mp 1\%$ accuracy. Flowmeter was calibrated by weighing the collected water in different time durations to its density. Therefore the uncertainty in the volume flow rate of water is a function of mass flow rate and density.

$$Q_w = \frac{\dot{m}}{\rho} = f(\dot{m}, \rho)$$

ρ is assumed as constant and it has no fractional uncertainty.

The uncertainty in the mass flow rate measurement was expected to be different for each experimental run due to the data given in table G.1.

On the otherhand;

$\dot{m} = \frac{m}{t}$; where t is the time duration to collect water mass, m.

$\dot{m} = f(m, t)$

The uncertainty in measuring the weight of collected water depends on the accuracy of electronic balance which has an accuracy of ∓ 20 g in full scale.

The uncertainty associated with the time measurement by a stop-watch is 0.5 second.

The fractional uncertainty in mass flow rate was obtained for each data set (Table G.1) according to the equation G.2.

$$\frac{\delta \dot{m}}{|\dot{m}|} = \sqrt{\left(\frac{\delta m}{m}\right)^2 + \left(\frac{\delta t}{t}\right)^2} \qquad \text{(G.2)}$$

Table G.1 : Fractional uncertainties of water mass, time and the total uncertainty in water mass flow rate.

Collected mass(g) ∓ 20 g	$\frac{\delta m}{m}$	Time(s) ∓ 0.5 (s)	$\frac{\delta t}{t}$	$\frac{\delta \dot{m}}{\dot{m}}$
25535	0.0009	90	0.0056	0.006
35335	0.0006	90	0.0056	0.006
43605	0.0005	90	0.0056	0.006
52420	0.0004	90	0.0056	0.006
63940	0.0003	90	0.0056	0.006
70875	0.0003	90	0.0056	0.006
57215	0.0003	60	0.0083	0.008
65035	0.0003	60	0.0083	0.008
72930	0.0003	60	0.0083	0.008
80345	0.0002	60	0.0083	0.008
67745	0.0003	45	0.0111	0.011
72935	0.0003	45	0.0111	0.011
56435	0.0004	30	0.0167	0.017
			Avg.	**0.008**

The average of the fractional uncertainties, 0.008 is taken as the fractional uncertainty in water mass flow rate measurements.

Volume flow rate of air was measured with a differential pressure transmitter connected to the up and downstream of the orifice . Differential pressure transmitter was calibrated by the help of the gasometer.

Constant cyclindrical volume of gasometer (50 lt) was occupied by the air in different time durations as shown in table G.2.

Table G.2: Occupied volume of air in different flow rates.

Occupied volume of gasometer (lt)	Time(s)
50	66.4
50	69.3
50	73.3
50	74.2
50	77.0
50	81.5
50	88.5
50	98.0
50	103.6
50	105.5
50	125.2
50	187.1

Uncertainty in time measurement by a stop-watch is assumed to be ∓ 0.5 s.

Uncertainties in volume measurement of gasometer were caused by reading the volume scales of gasometer. Since the minimum scale on the level rod of the gasometer is 0.1 lt, it is assumed that the uncertainty is ∓ 0.1 lt.

Since $Q_A = \frac{V}{t} = f(V, t)$

$$\frac{\delta Q_A}{|Q_A|} = \sqrt{\left(\frac{\delta V}{V}\right)^2 + \left(\frac{\delta t}{t}\right)^2}$$

The average of the fractional uncertainties, 0.006 is taken as the fractional uncertainty in air mass flow rate measurements (Table G.3).

Table G.3: Fractional uncertainties of air volume, time and air volume flow rate.

OccupiedVolume(lt.) ∓0.1 (lt.)	$\frac{\delta V}{V}$	**Time (s.) ∓ 0.5(s.)**	$\frac{\delta t}{t}$	$\frac{\delta Q_A}{Q_A}$
50	0.002	66.4	0.008	0.008
50	0.002	69.3	0.007	0.007
50	0.002	73.3	0.007	0.007
50	0.002	74.2	0.007	0.007
50	0.002	77.0	0.006	0.007
50	0.002	81.5	0.006	0.006
50	0.002	88.5	0.006	0.006
50	0.002	98.0	0.005	0.005
50	0.002	103.6	0.005	0.005
50	0.002	105.5	0.005	0.005
50	0.002	125.2	0.004	0.004
50	0.002	187.1	0.003	0.003
			Avg.	**0.006**

The fractional uncertainty in void fraction term, α, is equal to;

$$\frac{\delta\alpha}{|\alpha|} = \sqrt{\left(\frac{\delta Q_W}{Q_W}\right)^2 + \left(\frac{\delta Q_A}{Q_A}\right)^2}$$

$$\frac{\delta\alpha}{|\alpha|} = \sqrt{(0.008)^2 + (0.006)^2} = \mp 0.01 = \mp 1\%$$

APPENDIX H

STUDIES ON ARMAND COEFFICIENT

In 1946 Armand [18] correlated data for the void fraction of air-water flow in a horizontal pipe at pressures close to atmospheric by plotting α against β as shown in figure H.1 and observed that up to a void fraction of about 0.72 (β=0.9),

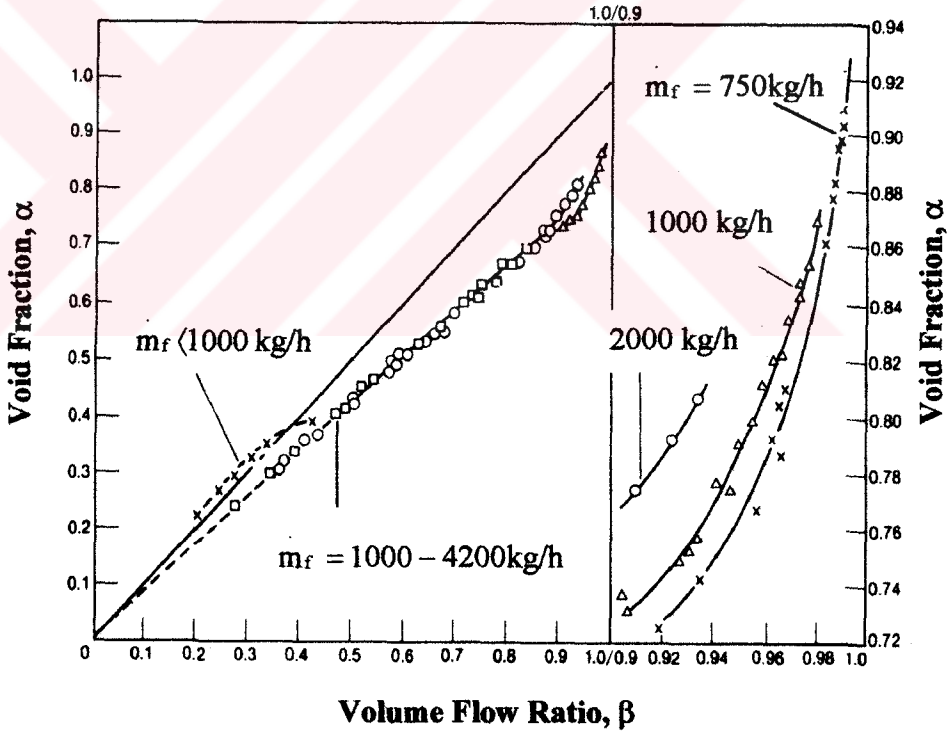

Figure H.1: Void fraction (α) versus volume flow ratio (β). Air-water mixtures in 26 mm bore horizontal pipe at pressure of 1 bar

$$C_A=\frac{\alpha}{\beta} \qquad \text{H.1}$$

where C_A=0.83. C_A is known as the Armand coefficient.

Armand also found similar relationships obtained with air-water mixtures flowing in vertical pipes at pressures close to atmospheric, but in that case there was no tendency as in figure H.1 for the data at low values of β to lie above the line given by equation H.1; this trend is presumably due to a reduction in gas velocity caused by the bubbles rising against the upper pipe surfaces in horizontal flow.

Equation H.1 with a constant coefficient is only applicable up to β=0.9; for values greater than this, Massena has suggested the following appropriate equation.

$$\alpha=[C_A+(1-C_A).x]\beta$$

A number of elementary models exist for the evaluation of the slip ratio (s). Many authors considered the effect of slip ratio (s) on calculating the Armand coefficient [18]. Chisholm found a relationship between volume flow ratio (β) and Armand coefficient (C_A) including the effect of slip ratio (s) which was defined as;

$$s=\frac{1}{\left[1-\beta\left(1-\frac{\rho_g}{\rho_f}\right)\right]^{1/2}}$$

$$\frac{1}{C_A}=\beta+\frac{1-\beta}{\left[1-\beta\left(1-\frac{\rho_g}{\rho_f}\right)\right]^{1/2}} \qquad \text{H.2}$$

when $\rho_g/\rho_f << 1$ then the equation H.2 simplifies to;

$$C_A = \frac{1}{\beta + (1-\beta)^{1/2}} \qquad \text{H.3}$$

and

$$\alpha = \frac{\beta}{\beta + (1-\beta)^{1/2}} \qquad \text{H.4}$$

Figure H.2 compares equation H.4 with Armand's data obtained with air-water mixtures flowing in vertical pipes at pressures close to atmospheric;

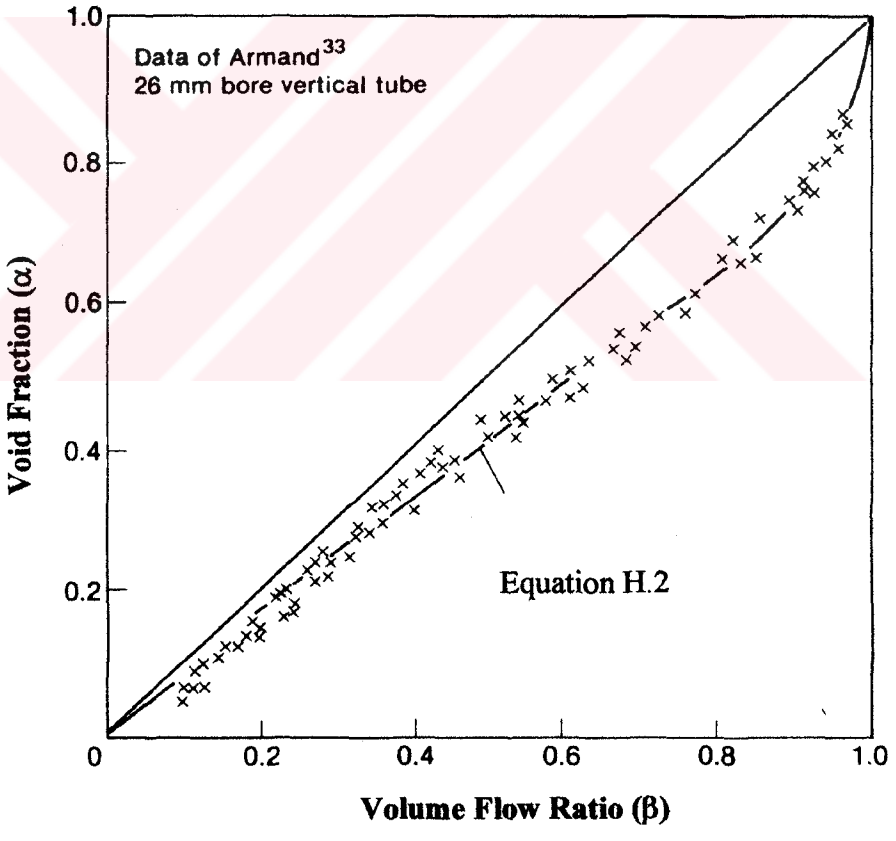

Figure H.2: Void fraction (α) versus volume flow ratio (β) of air-water Mixtures (pressure ≈ 1 bar)

If the graph of equation H.3 is created by assuming $\rho_g/\rho_f << 1$ and compared with the Armand coefficient in horizontal flow (C_A=0.83) for various volume flow ratio between 0 and 1;

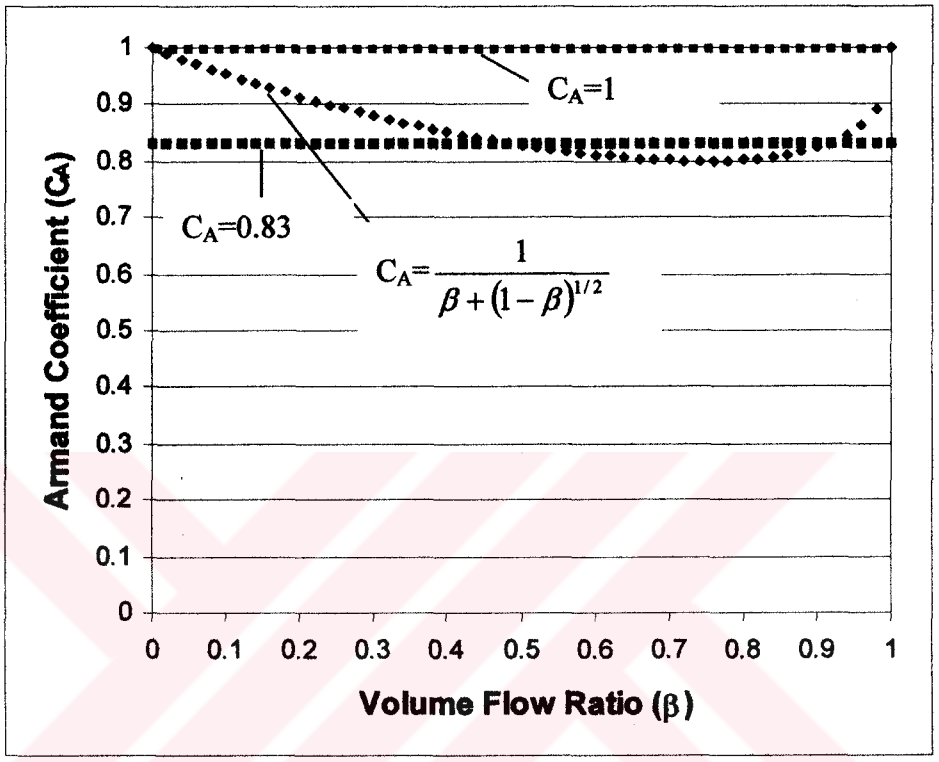

Figure H.3: Comparison of data obtained from equation H.3 with Armand coefficient data of horizontal flows (C_A=0.83)

→ Juri üyelerini belirtmiş??